Synthesis and Characterization of *Stephania abyssinica* leaf extract mediated (Mn, Ni) Co-doped ZnO nanoparticle for Degradation of Methylene Blue

Haileyesus Hatano Haitosa

A thesis Submitted to the Department of Materials science and Engineering,

School of Mechanical, Chemical and Materials engineering

Presented in Partial Fulfillment of the Requirement for the Degree of Master's in Materials science and Engineering

Office of Graduate Studies

Adama Science and Technology University

May, 2022

Adama, Ethiopia

Synthesis and Characterization of *Stephania abyssinica* leaf extract mediated (Mn, Ni) Co-doped ZnO nanoparticle for Methylene Blue

Mr. Haileyesus Hatano Haitosa

Main Advisor: Osman Ahmed zelekew (Asso. Prof.)

Co advisor: Belay Brehane Tesfamariam (Ph.D.)

A thesis Submitted to the Department of Materials science and Engineering,

School of Mechanical, Chemical and Materials engineering

Presented in Partial Fulfillment of the Requirement for the Degree of Master's in Materials Science and Engineering

Office of Graduate Studies

Adama Science and Technology University

May 2022

Adama, Ethiopia

DECLARATION

I hereby declare that this Master Thesis entitled *"*Synthesis and Characterization of *Stephania abyssinica* leaf extract mediated (Mn, Ni) Co-doped ZnO nanoparticle for Degradation of dyes*"* is my own work and it has not been submitted for the award of any academic degree, diploma, or certificate in any other university. All sources of materials that are used for this thesis have been duly acknowledged through citation.

Name of student	Signature	Date

RECOMMENDATION

I/we, the advisor(s) of this thesis, hereby certify that I/we have read the revised version of the thesis entitled "Synthesis and Characterization of *Stephania abyssinica* leaf extract mediated (Mn, Ni) Co-doped ZnO nanoparticle for Degradation of Methylene Blue" prepared under my guidance by Haileyesus Hatano submitted in partial fulfillment of the requirements for the degree of Masters of Science in Materials Science and Engineering, Therefore, I/we recommend the submission of a revised version of the thesis to the department following the applicable procedures.

_____	_____	_____
Major Advisor/Supervisor	Signature	Date
_____	_____	_____
Co-advisor/Co-supervisor	Signature	Date

APPROVAL

I/we hereby certify that the recommendation and suggestion given by the proposal review Committee are appropriately incorporated into the final thesis/dissertation proposal entitled "Synthesis and Characterization of *Stephania* abyssinica leaf extract mediated (Mn, Ni) Co-doped ZnO nanoparticle for Degradation of dyes" by Haileyesus Hatano.

_____	_____	_____
Major Advisor/Supervisor	Signature	Date
_____	_____	_____
Co-advisor/ Co-supervisor	Signature	Date

Approval of Board of Reviewers

We, the undersigned, members of the Board of Reviewers of the proposal open defense by Haileyesus Hatano have read and evaluated the thesis/dissertation proposal entitled "Synthesis and Characterization of *Stephania abyssinica* leaf extract mediated (Mn, Ni) Co-doped ZnO nanoparticle for Degradation of dyes" and assessed the understanding of the candidate about the proposed research. This is, therefore, to certify that the thesis/dissertation proposal is accepted and we recommend the implementation of the proposal.

_____	_____	_____
Chairperson	Signature	Date
_____	_____	_____
Reviewer 1	Signature	Date\
_____	_____	_____
Reviewer 2	Signature	Date

Finally approval and acceptance of the thesis/dissertation proposal is contingent upon submission of its final copy to the Office of Postgraduate Studies (OPGS) through the Department Graduate Council (DGC) and School Graduate Committee (SGC).

_____	_____	_____
Department Head	Signature	Date
_____	_____	_____
School Dean	Signature	Date
_____	_____	_____
Office of Postgraduate Studies,	Dean Signature	Date

ACKNOWLEDGEMENT

First of all, I would like to thanks my almighty God for helping me to realize my long dream. I would like to express my gratitude and sincere to my advisor Asso. Prof. Osman Ahmed Zelekew for encouraged, initiated, guided me, and his patience during my thesis work and his role to finish my work on time. I would like to extend my thanks to my Co. Advisor Dr. Belay Brehane Tesfamariam for him encouraging me, giving me constructive comments and guidance. I would like express my attitude to Asso. Prof. Dinsefa Mensur Andoshe for he encouraged me to join the department, and giving a constructive comments & guiding on my thesis work. Also I would like to extend my thanks to Dr. Gabisa Bekele Fayisa for he appreciating me and encouraging me to follow my attitude toward research. And I would like to express my tanks to Dr. Tadele Hunde, Dr. Temesgen Debelo, and Mr. Sena Tadesse for them giving me a constructive comments and guidance. Following that I would like to extend my gratitude to my family for their unconditional support during this long journey. To all lab assistance and all my friends in our department, thank you for your support, special great thanks to Mr. Demeke for his unlimited support. Lastly, but not least I would like to thanks the Department of Material Science and Engineering, and Adama Science and Technology University in Ethiopia for offering such chance to hold my master's program.

TABLE OF CONTENT

ABSTRACT

The dye from industrial processing makes the water to be contaminated which is toxic and has big problem on health. One of the most basic means of obtaining cleaned water is the removal of dye from wastewater. Employing semiconductors as a photocatalyst is an attractive method for the removal of organic dye pollutants in wastewater. In this study, The ratio of extracted leaf to zinc nitrate in the ratio of 1:2, 1:1, 2:1 v/v are done, and their names are assigned as L1:Z2, L1:Z1, and L2:Z1. ZnO doped with Mn and Ni as $Zn_{0.98}Mn_{0.02}O$ *and* ($Zn_{1-x}Ni_xO$, *x = 0.01, 0.03, 0.05, 0.07) is prepared using the Stephania abyssinica (S. abyssinica) leaf and assigned as 2MZO, 1NZO, 3NZO, 5NZO, and 7NZO respectively. Moreover, the (Mn, Ni) Co-doped ZnO nanostructures using S. abyssinica leaf is synthesized by co-precipitation method as* $Zn_{0.98-x}Mn_{0.02}Ni_xO$ *(x = 0.01, 0.03, 0.05, 0.07, 0.09) and assigned as 1NMZO, 3NMZO, 5NMZO, 7NMZO and 9NMZO respectively. Furthermore, the samples were characterized by different technique. The X-ray powder diffraction (XRD) results confirmed that ZnO is crystalline 3D hexagonal structure with no other impurities peaks, and crystalline sizes varied from* 36.17 *to* 17.32 *nm due to leaf extract and the dopant concentration, and phase shift was occurred due to Ni/Mn dopant concentration. The presence of leaf extract increased the surface area from 14.53* ($m^2\ g^{-1}$) *to 28.256* ($m^2\ g^{-1}$), *prevented aggregation and controls particle size. Due to doping of Ni/Mn, the tuned band gap is tuned from 3.2 eV (Uv light) to 2.62 eV (visible light), PL intensity indicated the recombination rate decreased and charge transfer resistance is well decreased. The photocatalytic activities of pure-ZnO, L2:Z1, L1:Z2, L1:Z1, 2MZO, 1NZO, 3NZO, 5NZO, 7NZO, 1NMZO, 3NMZO, 7NMZO and 9NMZO catalysts were tested towards the degradation of Methylene Blue (MB), and 33.1 %, 69.7 %, 67.4 %, 72.5 %, 76 %, 72.8 %, 74.12%, 79.7%, 78 %, 84 %, 92 %, 97%, and 92% of MB dye was degraded, respectively. Among the catalysts, 5NMZO catalysts had the highest performance and 99.5 % MB dye was degraded within 80 min irradiation. The higher degradation efficiencies could be due to the low recombination, lower electron transfer resistance, high absorption of visible light, low agglomeration, and high surface area. Therefore, preparation of (Mn, Ni) Co-doped ZnO using Stephania abyssinica leaf extract is a good candidate for degradation of MB under visible light.*

Keywords: *photocatalyst, ZnO, Mn/Ni co-doping, Stephania abyssinica leaf, Methylene Blue.*

LIST OF ACRONYMS

AOP	Advanced Oxidation Processes
BET	Brunauer, Emmett, and Teller
CB	Conduction Band
CVD	Chemical Vapor Deposition
C_2H_5OH	Ethanol
EDX	Energy Dispersive X-Ray
EIS	Electrochemical Impedance Spectroscopy
FT-IR	Fourier Transforms Infrared Spectroscopy
HRTEM	Higher Resolution Transmission Electron Microscope
H_2O_2	Hydrogen Peroxide
L:Z	Ratio of Leaf to Zinc Oxide
MB	Methylene Blue
MWWTP	Modern Wastewater Treatment Processes
MZO	Manganese Doped ZnO
NaOH	Sodium Hydroxide
NBD	Nano-Beam Diffraction
NMZO	Nickle and Manganese Doped ZnO
NZO	Nickle Doped ZnO
·OH	Hydroxyl Radicals
PDE	Percent Degradation Efficiency

PL	Photoluminescence-Spectroscopy
PVD	Physical Vapor Deposition
RNS	Reactive Nitrogen Species
ROS	Reactive Oxygen Species
SAED	Selected Area Electron Diffraction
SEM	Scanning Electron Microscopy
TGA	Thermo-Gravimetric Analysis
TEM	Transmission Electron Microscopy
TM	Transition Metals
UV	Ultraviolet-Spectroscopy
VB	Valence Band
XRD	X-Ray Powder Diffraction
XPS	X-Ray Photoelectron Spectroscopy
ZnO	Zinc Oxide

LIST OF FIGURE

LIST OF TABLES

CHAPTER ONE

Introduction

1.1 Background

Water, one of the most inevitable resources for all living beings, is important to protect water resources from pollution (Q. Wang & Yang, 2016). In the past few decades, due to the rapid development of industries and enormous usage of chemicals in agriculture and dying, pollution has become a serious problem and a major concern for immediate action (Dwivedi, 2017). A large amount of untreated wastewater from the industries is being led into the environment (Crini & Lichtfouse, 2019). Typical wastes of concern include volatile organics, dioxins, dibenzofurans, pesticides, nitro-aromatic compounds, polychlorinated biphenyls, chlorophenols, asbestos, heavy metals, arsenic compounds, aviation fuel, solvent, degreasing agents, etc. (Patterson, 1985). The increased amount of water usage would generate an increased amount of wastewater (D. Lv, Zheng, Zhang, & Deng, 2018). So, wastewater treatment must be our goal.

Wastewater treatment is expensive because the contaminants in the wastewater must be thoroughly removed before the water can be safely reused (J. Ma et al., 2019). In 2003, the UN WWAP projected that around 2 million tons of untreated water came from industrial and agricultural runoff (Waste, 2010). Even with traditional approaches such as biological and physical treatments, successful contamination removal would necessitate more modern technology that is less expensive and takes less time (Al-Ghafri, Bora, Sathe, Dobrestov, & Al-Abri, 2018; Q. Wang & Yang, 2016). As a result, academics all around the world are currently focused on decontaminating dirty water supplies. Other wastewater treatment approaches have included adsorption (Grassi, Kaykioglu, Belgiorno, & Lofrano, 2012), catalytic oxidation (Lida & Qingrui, 2020), and photocatalytic degradation (Rauf & Ashraf, 2009). And, the sunlight collecting material is the best for wastewater treatment.

The sunlight collecting material, which is the key portion of just this thesis, is the photo catalyst, which is at the core of solar energy conversion in the artificial process called photosynthesis (El-Khouly, El-Mohsnawy, & Fukuzumi, 2017). The phrase "photo catalyst"

involves a chemical reaction interaction in which light is exploited to activate a chemical component (W. Lv et al., 2012). Photocatalysts have been shown to reduce the harm caused by organic dye environmental contamination and persons by breaking down organic dyes, which are one of the primary classes of pollutants in municipal wastewater, and converting them into less dangerous or even nontoxic substances. And metal oxides are one of the best materials for photocatalytic activities.

Most metal oxides is used as photocatalysts due to the promising arrangement of electronic structure, light absorption qualities, and charge transport characteristics (M. M. Khan, Adil, & Al-Mayouf, 2015). Different nanostructures dictate the use of several conventional metal oxide-based materials (Nunes et al., 2019). Many metal oxides have been used for catalytic activities like TiO_2 (Di Fonzo et al., 2008), ZnO (Di Mauro, Fragala, Privitera, & Impellizzeri, 2017), NiO (Diallo et al., 2018), CuO (Raizada et al., 2020), MnO_2 (Rajrana, Gupta, Mir, & Pandey, 2019), Fe_2O_3 (Mishra & Chun, 2015), CoO (Z. Lin, Du, Yan, & Yang, 2019), Bi_2O_3 (Zhou, Wang, Xu, Sun, & Shang, 2009), Cr_2O_3 (Su, Xue, Gu, Xia, & Pan, 2014), etc. According to Kochetkova et al. (1992), the catalytic activity of metal oxide catalysts during the oxidation of phenol follows the following order: CuO > CoO > Cr_2O_3 > NiO > MnO_2 > Fe_2O_3 > YO_2 > Cd_2O_3 > ZnO > TiO_2 > Bi_2O_3 (Pirkanniemi & Sillanpää, 2002). Zinc oxide nanoparticles (ZnO NPs) are a kind of metal oxide that has been noted as an alternative photocatalyst due to its non-toxicity, excellent catalytic capacity, and low cost (Madathil, Vanaja, & Jayaraj, 2007).

However, because of its high bandgap, ZnO's photocatalytic effectiveness is limited, and its efficient photocatalytic activity to the visible part of the solar spectrum is confined (Chiang & Lin, 2015). It also has a number of drawbacks, including the quick recombination of photo stimulated electron and hole pairs, which reduces photocatalytic performance (Hamid, Teh, & Lai, 2017). To boost the photocatalytic effectiveness, several approaches have been employed, one of which is to dope transition metal into ZnO (Saleh & Djaja, 2014a, 2014b; Siddhapara & Shah, 2014; F. Zhang, Chao, Cui, Zhang, & Zhang, 2015). Doping transition metals into the ZnO lattice can lower bandgap energy and increase charge separation between electrons and holes by producing electron traps, as well as improve ZnO's photocatalytic activity. For doping ZnO, several transitions or noble metals such as Mn

(Achouri et al., 2016), Cr (C.-J. Chang, Yang, & Weng, 2014), Co (Nair, Nirmala, Rekha, & Anukaliani, 2011), Ni (Kant & Kumar, 2012), Fe (K. Kumar, Chitkara, Sandhu, Mehta, & Kumar, 2014), Mg (Samanta, Goswami, & Mahapatra, 2018b), Li (Ajala, Lachheb, Bouazizi, & Houas, 2017), Cu (S. A. Khan, Noreen, Kanwal, Iqbal, & Hussain, 2018), and Ag (R. Singh, Barman, & Sharma, 2017) have been frequently utilized(Barick, Singh, Aslam, & Bahadur, 2010). Furthermore, doped ZnO has better photocatalytic activity than individual doped ZnO (L. Lin, Zheng, Xie, Zhu, & Xie, 2007; Reddy et al., 2020).

When compared to single-element doping, co-doping of semiconductor oxides with two or more distinct materials has the potential to result in higher improvements in performance and attributes (Khanizadeh, Khosravi, Behnajady, Shamel, & Vahid, 2020). Co-dopants can also efficiently reduce recombination centers, which might lead to the development of novel metal-based visible light-driven catalysts (Luo et al., 2004). In this research the green synthesis mediated (Ni, Mn) co-doped ZnO nanostructure was done. Among the transition metals used, Ni offers excellent potential for improving the catalytic activity of ZnO by forming an impurity level in its band gap (Zhao et al., 2011). Ni^{2+} (0.69 Å) have the same valence compared to Zn^{2+} and its radius is close to Zn^{2+} (0.74 Å), so it is very easy for Ni^{2+} sub-lattice to replace Zn^{2+} in ZnO lattice. Mn is easier to incorporate Mn^{2+} in to ZnO lattice due to lower ionic radius(0.67 Å), the same electronegativity and has high solubility with ZnO (R. Sangeetha, Muthukumaran, & Ashokkumar, 2015; L.-w. Wang, Xu, Zhang, Zhao, & Lu, 2010). Hence, Mn is selected as an initial doping element with ZnO, and the doping level is restricted to 2% to avoid the secondary phase formation(Senol, Ozugurlu, & Arda, 2020).

The nanoparticles synthesized by the biosynthesis method are an alternative to conventional methods, which is cheap, non-toxic, and eco-friendly instead of harmful chemical which produces secondary pollution to the environment and less bio-compatible (Mabe, Rapp, Bain, & Nys, 2003) like tri-ethyl amine (Ju et al., 2014), thio-glycerol (Aboulaich et al., 2011) Polyvinylpyrrolidone (PVP) (G. Pandey, Singh, & Hitkari, 2018), Thiodiglycol (TG) (Moritz & Geszke-Moritz, 2013), Bovine Serum Albumin (BSA) (Bai, Wu, Mitra, & Brown, 2016), Chitosan (Javed et al., 2020), Polyethylene glycol (PEG) (Ranjitha et al., 2021), and polyvinyl alcohol (PVA) (Nagvenkar, Deokar, Perelshtein, & Gedanken, 2016)

which is normally employed as a capping and also stabilizing. Green synthesis of ZnO has also been investigated using plant extracts such as *Syzygium Cumini (Sadiq et al., 2021), Synadium grantii (Karthik et al., 2022), Artocarpus gomezianus (Suresh et al., 2015), Eucalyptus globulus (Siripireddy & Mandal, 2017), Moringaoleifera (Archana, Manjunath, Nagaraju, Sekhar, & Kottam, 2017), Laurus nobilis (Chemingui et al., 2019), Hibiscus sabdariffa* (Soto-Robles et al., 2019), *Ulva lactuca (Ishwarya et al., 2018) Carica papaya (Rathnasamy, Thangasamy, Thangamuthu, Sampath, & Alagan, 2017) , Dovyalis caffra (Adeyemi, Elemike, & Onwudiwe, 2019) , Garcinia mangostana (Aminuzzaman, Ying, Goh, & Watanabe, 2018), Trigonella foenum-graecum (Alshehri & Malik, 2019), Azadirachta indica* (Suganya & Vivekanandhan, 2019), and others *(Diallo, Ngom, Park, & Maaza, 2015; Ramesh, Rajendran, & Subramanian, 2014; Senthilkumar & Sivakumar, 2014; Vidya et al., 2013; Vishwakarma, 2013).* However, there is no report on the synthesis of Ni/Mn Co-doped ZnO using *Stephania abyssinica* plant extract for the degradation of MB dye.

In this work, the indigenous plant *(Stephania abyssinica)* leaf which is found in East African species (Beentje, 1994) was used. The plant is commonly found in forest margins, marine, bamboo, and hygienic zone (Beentje, 1994). Stephania abyssinica (Dillon & A. Rich) studied is a twining liana rich in phytochemical bioactive alkaloids, flavonoids, lignans, steroids, terpenoids, and coumarins which are useful for cupping agents. The plant extract was used to synthesize the Ni/Mn co-doped ZnO. The resulting catalysts were characterized by using different techniques and used for the degradation of MB. It is expected that the catalyst could have enhanced catalytic performance due to the low recombination, lower electron transfer resistance, high absorption of visible light, low agglomeration, and high surface area.

1.2 Statement of the Problems

The application of ZnO semiconductor is limited due large band gap (3.2 eV), fast recombination rate of the photogenerated electron–hole pairs, high charge transferring resistance, and lower specific surface area, (Anandan et al., 2007; Uddin et al., 2012). Moreover, agglomeration is other problem (Raha, Mohanta, & Ahmaruzzaman, 2021). The different method has been followed to enhance the photocatalytic performance of ZnO such as doping with metallic and non-metallic, coupling of with other metal. However, photocatalytic

activities of ZnO nanoparticles are not fully efficient and further work is required to resolving those problems. This work focuses on the Stephania abyssinica leaf extract mediated (Mn, Ni) co-doped ZnO for photocatalytic activities. Among the Transition metals (TMs), Mn and Ni have high solubility with ZnO and have approximately equal atomic radius, valence state, and electronegativity**.** so that they can be easily incorporated into ZnO lattice and also possesses many applications in electronics (L.-w. Wang et al., 2010; Zhao et al., 2011). Green synthesis approach of ZnO using plant extract as capping/stabilizing agent to increase specific area and porosity, and to decrease aggregation. is used that provides a low-cost, simple, and environmentally friendly approach instead of using costly and hazardous cupping agents like PEI, PET, PVP, PVA, EDTA, etc. Moreover, to the best of our knowledge, this plant extract has not yet been employed for the synthesis of nanoparticles. Therefore, in this study, the novel method green synthesis using *S. abyssinica* leaf extract is employed as a green surfactant/capping agent for the green synthesis of ZnO nanoparticles for the first time.

1.3 Objectives

1.1.1 General Objectives

Synthesis and Characterization of *Stephania abyssinica* leaf extract mediated (Mn, Ni) Co-doped ZnO nanoparticle for Degradation of Methylene Blue

1.1.2 Specific Objective

- ✓ Extraction of the leaf from Stephania abyssinica.
- ✓ Synthesis of ZnO nanostructures using extracted leaf
- ✓ Synthesis of Mn-doped ZnO and Ni-doped ZnO ($Zn_{1-x}Ni_xO,\ x = 0.01, 0.03, 0.05, 0.07$) nanostructures using extracted leaf
- ✓ Synthesis of (Mn, Ni) Co-doped ZnO nanostructures ($Zn_{0.98-x}Mn_{0.02}Ni_xO,\ x = 0.01, 0.03,\ 0.05, 0.07, 0.09$) using extracted leaf
- ✓ Characterization of prepared catalyst
- ✓ Evaluation of the photocatalytic activity of the synthesized catalyst on dye degradation.

1.4 The Scope of the Research

This research covers the removal of methylene blue dye from wastewater which becomes one of the major ways to get treated water. It started from extraction of indigenous plant extract and synthesis of ZnO by using plant extract as a stabilizing/capping agent. Mn-doped ZnO and Ni-doped ZnO ($Zn_{1-x}Ni_xO,\ x = 0.01, 0.03,\ 0.05, 0.07$) are synthesized. (Mn, Ni) co-doped ZnO ($Zn_{0.98-x}Mn_{0.02}Ni_xO,\ x = 0.00\ 0.01, 0.03,\ 0.05, 0.07, 0.09$) are synthesized. Those samples are characterized by different characterization like XRD, TGA, Uv-Vis, FT-IR, SEM, EDX, TEM, HRTEM, SAED, XPS, BET, PL, and EIS. It also includes how lowering recombination of charge carriers, lowering electron transfer resistance, tanning band gap to visible light, lowering agglomeration, and increasing surface area. The effect of leaf extract concentration and Ni concentration on doping and co-doping, are evaluated. The pH effect, catalytic dosage**,** and reusability of the synthesized catalyst are checked.

1.5 Significance of the Study

This work primarily benefits the industries such as textile, paper, cosmetic and leather processing which release effluent with high concentration of organic dyes. The environmental pollution by these organic dyes will also be reduced. The deterioration of released organic contaminant minimizes the exposure of human being to this contaminant and decrease the amount of oxygen that could be absorbed by this contaminant. From human health point of view, the problem such as cancer, mutation and skin irritation caused by organic dyes could be also minimized.

CHAPTER TWO

2 Literature Review

2.1 Wastewater

Water is one of the most important resources for all living things, and it is also known as the only source of life, so it is very important to protect water resources from pollution (Becerra-Castro et al., 2015). In the past few decades, due to rapid development of industries and enormous usage of chemicals in agriculture and dying, pollution has become a serious problem and a major concern for immediate action. Large amount of untreated wastewater from the industries are being led into the environment (Q. Wang & Yang, 2016). A large number of organic and inorganic harmful environmental pollutants in the aquatic environment have become a serious global problem. Typical wastes of concern include volatile organics, dioxins, dibenzofurans, pesticides, nitro-aromatic compounds, polychlorinated biphenyls, chlorophenols, asbestos, heavy metals, arsenic compounds, aviation fuel, solvent, degreasing agents, etc. More water consumption leads to more waste water. There are various aromatic dyes (e.g. Congo Red, Reactive Black 5, PBS, and Toluidine Blue) (Alhefeiti, Athamneh, Vijayan, & Ashraf, 2021) along with arising contaminants (Squadrone et al., 2015) (e.g. perfluorooctane acid (PFOA) and perfluorooctane sulfonate (PFOS) are created as source of environmental contaminants due to their widespread presence in the environment, living things, and humans. In fact, if water is used for the agriculture, domestic or industrial purpose it will become polluted due to the processes utilize different types of chemical and the exposure of the water the microorganism around there. The water pollutants are classified into radioactive, chemical and microbial contaminants (Q. Wang & Yang, 2016). Higher water consumption will result in more waste water. Wastewater treatment is expensive because the pollutants contained in the wastewater must be effectively removed in order to safely reuse the water(Wiśniewski et al., 2019). Even if traditional methods such as biological and physical processes are used, the effective removal of pollutants requires more complex technology, and the cost and time are lowers (D. Lv et al., 2018). Therefore, the results of good wastewater management practices/strategies are critical to our environment and sustainable development.

Inorganic materials, ozone, etc. (Lou, Yan, & Wang, 2019). Currently available traditional water purification technologies, such as adsorption or coagulation, cannot completely remove or destroy pollutants, which are concentrated on them by transferring another phase in some way**.** Therefore, there is an urgent need to find an alternative water purification technology that can completely remove or destroy these pollutants.

2.2 Wastewater Treatment

Modern wastewater treatment processes (WWTP) and technologies have been developing since the mid-18th century with the initial task to reduce water borne diseases such as cholera and typhoid, which had been caused by the cross contamination between waste and drinking water resources (Prasse, Stalter, Schulte-Oehlmann, Oehlmann, & Ternes, 2015). Wastewater treatment is complicated because the pollutants contained in the wastewater must be effectively removed in order to safely reuse the water (J. Ma et al., 2019). According to the United Nations WWAP data in 2003, about 2 million tons of untreated water came from industrial and agricultural wastewater. The increase in water consumption will lead to an increase in the amount of waste water. Even with traditional methods such as biological and physical treatment, effective removal of pollutants requires better technology with lower cost and shorter time (Al-Ghafri et al., 2018; Q. Wang & Yang, 2016). Therefore, the decontamination of polluted water resources is now the main concern for the researchers in the globe. Although several usual water treatment methods such as filtration , sedimentation , and distillation were pointed out, those methods mostly known by limitations for complete removal of pollutants besides consuming time. Other processes such as adsorption, catalytic oxidation and photocatalytic decomposition have also been used in wastewater treatment. It is known that the adsorption and chemical catalytic oxidation have been the basic approaches for pollutant removal. Because of such methods allow to remove pollutants unselectively than the traditional counterparts do. It is also reported that the photocatalyst is effective and efficient method for treatment of wastewater (Ibhadon & Fitzpatrick, 2013).

2.2.1 Methods of Wastewater Treatment

Many researchers try to find effective and efficient wastewater purification technology methods. These technical treatments mainly focus on the physical chemistry, electrochemistry, biology and advanced oxidation processes as shown in the figure (1). And the process becomes. Under advanced oxidation technology (Chaudhury, Mishra, & Shah, 2019; J. Ma et al., 2019). Conventional wastewater treatment involves a combination of physical, chemical and biological processes and activities to remove particulate matter, organic matter, and sometimes nutrients from wastewater. The general terms used to describe the various degrees of treatment in ascending order are preliminary. , primary, secondary and tertiary wastewater treatment and/or improvement (Sonune & Ghate, 2004). The reusing technologies available now are important, but they are time consuming and costly. Nanotechnologies are excellent in treating wastewater, since they remove contaminants and useful in the recycling process to obtain cleared water. It can also be forwarded to the clarification and uses of unconventional water sources in an economic way (Kanchi, 2014).

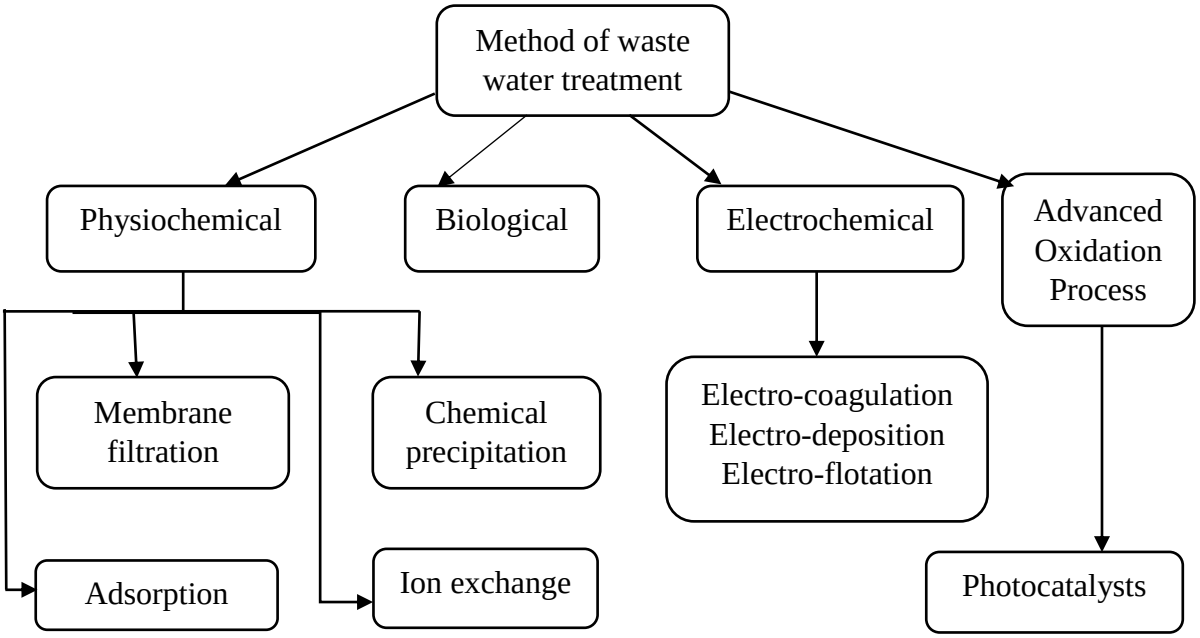

Figure 1 Methods of wastewater treatment (J. Ma et al., 2019)

2.2.1.1 Advanced Oxidation Processes

The Advanced Oxidation Process (AOP) is widely used to remove persistent organic components in industrial and municipal wastewater. The reason why H_2O_2 is mainly used as an oxidant and OH^- free radical generator is that hydrogen peroxide is easy to store, transport and use, and the process is safe and effective. It is determined by the very high oxidation potential of OH^- radicals. Reaction medium through various mechanisms (Pera-Titus, García-Molina, Baños, Giménez, & Esplugas, 2004)

The hydroxyl radicals are the main radicals responsible for oxidation reaction, in addition to a suite of other oxygen based reactive species and radicals. Hydroxyl radicals have a very high reduction potential, 2.70 V (vs. normal hydrogen electrode, NHE), which is much higher than other oxidants such as chlorine or hydrogen peroxide, which have oxidizing potentials of 1.49 and 1.77 V respectively (Kommineni et al., 2000). With most substrates hydroxyl radicals have high reaction rate constants in the order of 10^8-10^{10} $M^{-1}s^{-1}$ along with very short lifetime in water (10^{-6} – 10^{-9}s) (Murcia Mesa et al., 2021). Hydroxyl radicals react with most organic compounds via four basic pathways; electron transfer, hydrogen abstraction, radical addition and radical combination. These reactions, occurring at double bonds and aromatic systems, will trigger a sequence of reactions that break down the molecules (Challis, Hanson, Friesen, & Wong, 2014).

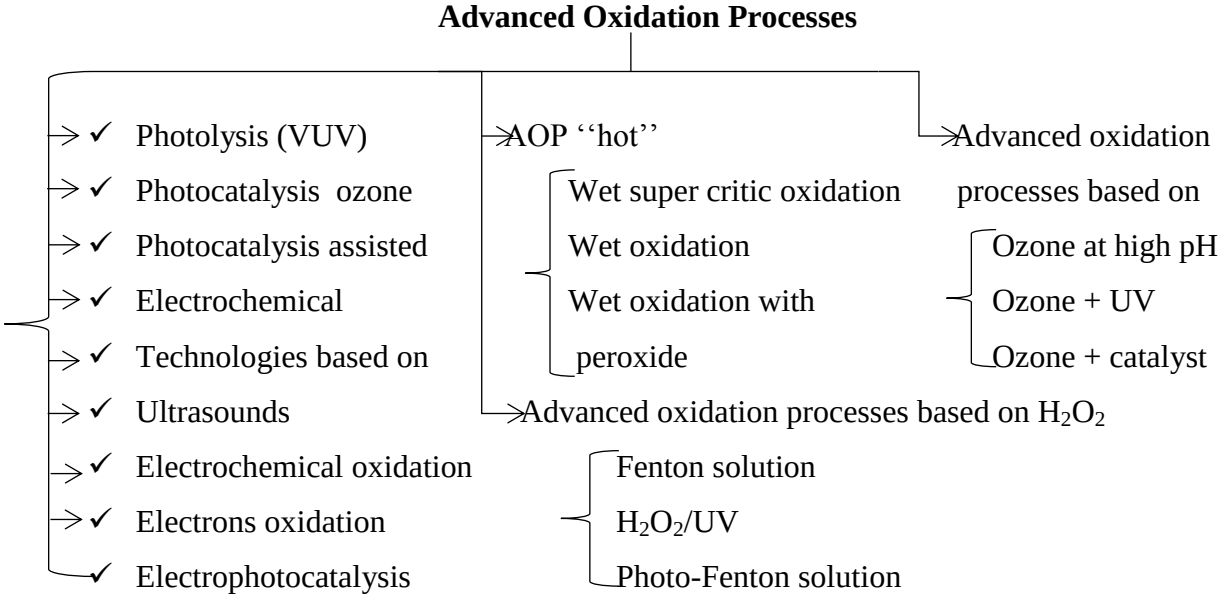

Figure 2 Advanced Oxidation Processes(Parsons, 2004)

2.3 Photocatalyst

Photocatalysts is a reaction which accelerated by light energy in the presence of semiconductor material. The induced light generate the electron and holes from the semiconductor for the oxidation and reduction reaction respectively, holes are farther used to produce hydroxide radical, which degrade the pollutant into carbon dioxide and water (Antonopoulou, Kosma, Albanis, & Konstantinou, 2020). In the presence of semiconductor material, photocatalysts is an event that is promoted by light energy. Induced light produces electron-hole pairs in the semiconductor, which are utilized in the oxidation and reduction reactions, respectively. The holes are then used to form hydroxide radicals, which breakdown the pollutant into carbon dioxide and water (Antonopoulou et al., 2020). Photocatalysts, a novel green technology which is based on advance oxidation processes (AOPs') and is capable of generating different reactive species such as reactive oxygen species (ROS), reactive nitrogen species (RNS), oxygen radicals ($\cdot O^{-2}$), hydroxyl radicals (·OH) have attracted the great attention for their potential application for the degradation of organic and biological wastes (Booshehri, Goh, Hong, Jiang, & Xu, 2014; Nosaka & Nosaka, 2017; Podporska-Carroll et al., 2017). These synthesized semiconductor NPs are energized by light of different wavelengths, include UV, visible, and near-infrared light, depending on their energy band gap (Dreaden, Alkilany, Huang, Murphy, & El-Sayed, 2012). By using a simple photocatalytic redox process, the activated semiconductor degrades organic and microorganisms cells. Over the last year, a lot of work has been conducted on utilizing semiconductor photocatalytic NPs to efficiently remove harmful chemicals and aggressive microorganisms from wastewater.

2.3.1 Mechanism of Photocatalysts

Photocatalysts have similar mechanism with the principles of the photochemical reaction that takes place in semiconductor but with some complexity (Paulos, 2020). In a semiconductor, the chemical reaction could take place due to the electron transferred from the valence band to the conduction band. In the photocatalytic oxidation process, when the light with energy equal or greater than the bandgap energy of the semiconductors photocatalyst hit the surface of the catalyst, the electrons will jump from the valence band to the conduction band by leaving the holes in the valence band (Tun, Wang, Naing, Wang, & Zhang, 2019). The holes left in the valence band have strong ability to oxidize donor molecules and

react with the water molecules to generate free radical species called hydroxyl radicals. These generated hydroxyl radicals have the strong oxidizing potential to degrade the organic pollutants and then leads to the complete mineralization of organic pollutants. Whereas, the electrons excited to the conduction band reacts with the dissolved oxygen to produces Oxygen activated species such as superoxide anions.

2.3.2.1 Oxidation Mechanism

This hydroxyl radical reacts with the organic pollutants present in the dyes (A. Kumar & Lingfa, 2020). During the process, if Oxygen is involved, the oxygen molecules with intermediate radicals in an organic compound can form radical chain reactions and sometimes they consume oxygen. Holes oxidize absorbed water molecules on the photocatalysts surface to produce hydroxyl radicals, a powerful oxidizing agent that fully decomposes the organic pollution. Following that, the produced hydroxyl radicals interact with the organic pollutants in the wastewater, fully mineralizing them into carbon dioxide and water. If oxygen is present in the system, the intermediate radicals can create a radical chain with the oxygen molecules in the organic pollutant in the wastewater, and oxygen is eventually consumed. So, Organic pollutants in wastewater are totally mineralized from wastewater (Rajeshwar et al., 2008)

2.3.2.2 Reduction Mechanism

Since oxygen is easily reducible substances, the reduction of oxygen is used as the best choice for the generation of hydrogen (H. Wang et al., 2017). Superoxide anions are formed when the dissolved oxygen species react with the electrons excited to the conduction band without recombination. These superoxide anions formed are attached to the intermediate products in Oxidative reaction to form peroxide or hydrogen peroxide and finally altered to water (Nakata & Fujishima, 2012)

2.3.3. Working Principle of Photo Catalysis for Water Purification

Advanced oxidation process based on photo catalytic production of hydroxyl radical, which acts as strong oxidizing agents, have emerged as a promising technology for the degradation of organic pollutants (Ibhadon & Fitzpatrick, 2013; Namini, Delbari, Mousavi, & Ghasemi, 2021). This process provides an interesting route for the removal of toxic

pollutants, including ozonolysis or oxidation with H_2O_2 under ultraviolet (UV) light irradiation The photo catalyst absorbs light energy and produces photo generated electrons which in term reduce adsorbed oxygen (O_2) to form superoxide radicals and photo generated holes react with H_2O to form hydroxyl radicals. The superoxide radicals can also generate hydroxyl radicals by reacting with hydrogen peroxide. The generated hydroxyl radicals subsequently oxidize the pollutants resulting in mineralization and complete degradation, these pollutants are broken down into smaller molecules such as CO_2, H_2O and mineral acids, which are not particularly toxic. Electrons in the metal particles absorbing light with energies exceeding the band bending potential can transit to conduction band (CB) of n-type semiconductor (Fig 3). After electrons in the metal particle flow to CB of the semiconductor particle, the metal particle is oxidized from M^0 to M^+. The photo generated electrons are allowed to transfer to the metal particles to produce reduction processes while more holes can transfer to n-type semiconductor surface to produce oxidation processes

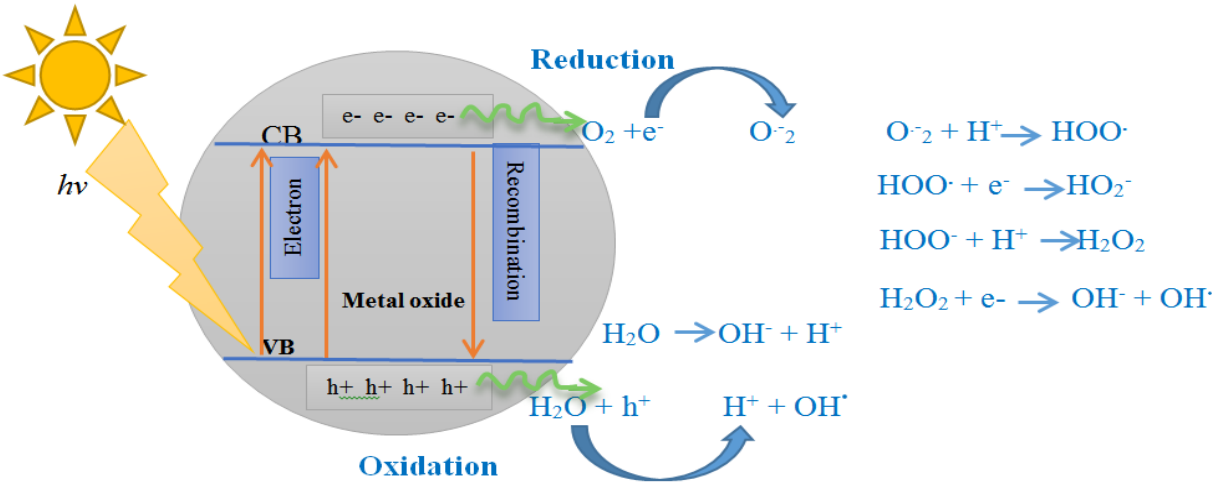

MB) 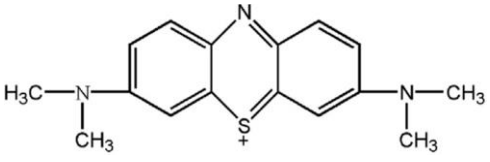 $+ HO_2^{\cdot} + OH_2^{\cdot} + O_2^{\cdot}$

MB degradation ($CO_2 + H_2O + NO_3 + SO_4^{2-}$

Figure 3 Photocatalysts mechanism of metal oxide semiconductor (Ibhadon & Fitzpatrick, 2013)

2.4 Metal Oxide Catalysts

Metal oxides are relevant in a variety of fields, including physics, chemistry, and materials science (Grilli, 2020). Oxide compounds may be formed from a wide range of metallic components. Metal oxides have a wide range of functional characteristics that are impacted by their crystal structure, morphology, composition, intrinsic defects, doping, and other factors that affect their optical, electrical, chemical, and catalytic capabilities. Applications of certain typical metal oxide-based materials, as defined by different nanostructures (Nunes et al., 2019). Large-scale water and soil contamination result from the discharge of hazardous and often difficult to break down compounds from businesses manufacturing medicines, textiles, and paints. For the breakdown of such compounds, metal and metal oxide nanoparticles have been known to have strong photocatalytic activities. Despite their wide bandgaps, metal oxides such as ZnO (3.2 eV) and MgO (7.83 eV) have received the most attention because of their low cost, low toxicity, and mass manufacturing potential (Cuijin et al., 2016; Pei et al., 2016).

Metal oxides can be classified based on their physicochemical properties. One of these characteristics is the stability of metal oxide. Metals with unstable high oxidation state oxides (Ho 298 9.5 kJ/mol of O), such as Pt, Pd, Ru, Au, and Ag, don't really perform stable solid oxides at normal temperatures. The majority of frequently used metal oxide catalysts (Ti, V, Cr, Mn, Zn, and Al) have high oxidation state oxides that are stable (Ho298 > 15.5 kJ/mol of O). Electrical conductivity is another alternative categorization criterion: insulators have limited electron mobility, thus their catalytic activity is typically weak. Furthermore, n-type metal oxides are not catalytically active as oxidation catalysts, with a few exceptions. None conducting metal oxides, on the other hand, are utilized as support in catalytic reactions.

The catalytic activity of metal oxide catalysts during the oxidation of phenol, according to Kochetkova et al. (1992), follows the following order: $CuO > CoO > Cr_2O_3 > NiO > MnO_2 > Fe_2O_3 > YO_2 > Cd_2O_3 > ZnO > TiO_2 > Bi_2O_3$. Photocatalysts may be done using a variety of semiconductors, including TiO_2, ZnO, MgO, WO_3, Fe_2O_3, and CdS. The perfect photocatalyst should have the following characteristics: - Photo activity, biological and chemical inertness, stability toward photo corrosion, suitability towards visible or near uv

light, low cost and lack of toxicity (Al-Rasheed, 2005; Bhatkhande, Pangarkar, & Beenackers, 2002).

Photo - excited electrons are driven from the valence band to conduction band , producing an electron/hole pair (e^-/h^+), whenever the metal oxide is activated with UV radiation, visible light, or a mixture of both. A chemical adsorbed on the photocatalyst surface can be reduced and/or oxidized by the photogenerated pair (e^-/h^+). Metal oxide's photocatalytic activity is derived from two sources: I the creation of OH^- radicals through the oxidation of OH^- anions, and (ii) the production of O_2^- radicals through the reduction of O_2. Contaminants can be degraded or transformed into less hazardous byproducts by both radicals and anions interacting with them.

2.4.1 ZnO Nanoparticles

ZnO nanoparticles have captivated researchers in recent years due to characteristics such as high electron mobility, transparency, and luminescence (Sotiriou et al., 2014). ZnO is a wide-bandgap semiconductor with a hexagonal wurtzite structure. It has a band gap of 3.37 eV, a significant exciton binding energy of 60 meV, strong room-temperature luminescence, and high electron mobility (Fang, 2017; Sze & Ng, 2007). ZnO is used for its optical and physical properties in a various applications, includes rubber and concrete, pharmaceutical additives, pigments, and UV blockers. Pure and doped ZnO nanoparticles have been used in acoustic devices, solar cells, photocatalysis, piezoelectric devices, medicines, transistors, textiles, rubber products, light emitting diodes, laser diodes, food packaging, chemical and biosensors, and as an antibacterial and antifungal agent, among other applications. Its unique properties and diverse applications in antireflection coatings, transparent electrodes in solar cells, ultraviolet (UV) light emitters, diode lasers, visitors, piezoelectric devices, spin-electronics, surface acoustic wave propagator, antibacterial agent [59], photonic material (L. Zhang, Ding, Povey, & York, 2008), photonic material (Xie, Deng, Xu, Li, & Huang, 2006) and gas sensing have attracted intense research efforts. ZnO is "generally recognized as safe" (GRAS) (Liewhiran & Phanichphant, 2007) yet the ZnO nanoparticle system might be hazardous. Among various semiconductor metal oxides used in photocatalysis, zinc oxide (ZnO) have attracted extensive research interests because of its non-toxic nature, being strongly oxidizing, low cost, chemical stability, and physical properties (Du, Chen, Yao, &

Wang, 2013; Duan, Liu, Han, & Wang, 2011; Ismail, El-Midany, Abdel-Aal, & El-Shall, 2005). But, the application of ZnO semiconductor is limited due large band gap, fast recombination rate of the photogenerated electron–hole pairs, high charge transferring resistance, lower specific surface area, charge and instability (Anandan et al., 2007; Uddin et al., 2012). Moreover, agglomeration is other problem (Raha et al., 2021).

2.4.2 Improvement of Photocatalyst Efficiency of ZnO Nanoparticle

Photocatalysis has become promising technology since it applying abundant solar light for the aim of environment protection (degradation of organic pollutants) and energy production (H_2 production, CO_2 reduction). Semiconductor metal oxide such as TiO_2, ZnO, WO_3, CdS, and Cu_2O has been extensively used in photocatalytic degradation of organic pollutants (Aragaw, Sabir, Andoshe, & Zelekew, 2020; Rajabi, Khani, Shamsipur, & Vatanpour, 2013; P. Sathishkumar, Pugazhenthiran, Mangalaraja, Asiri, & Anandan, 2013; Thema, Manikandan, Dhlamini, & Maaza, 2015; Wahab et al., 2011). Among these metal oxide, TiO_2 and ZnO have been widely studied by a researcher in the area of photocatalysts due to their chemical, stability, lower costs, high activity, nontoxicity, optical and electrical properties, and eco-friendly characteristics (Chiang & Lin, 2015; Jiang, Zhang, & Li, 2019; Karimi, Zohoori, & Yazdanshenas, 2014; Saleh & Djaja, 2014b; Shifu, Wei, Wei, Huaye, & Xiaoling, 2009; Sobana & Swaminathan, 2007). ZnO is considered as a promising photocatalyst in the degradation of organic pollutants because of its abundant, cheap, high chemical stability, high quantum efficiency, nontoxicity. Due to its wide bandgap ZnO absorb UV light (~4% of solar spectrum) not the vast potential solar spectrum (~43% of solar spectrum). Wide bandgap and fast recombination limit the applicability and large production of ZnO, therefore, various techniques have been followed to extend its visible light responses and prevent electron-hole pair's recombination such as metal and nonmetal doping, depositing noble metals, constructing heterojunctions with another metal oxide thus, enhance photocatalytic performance of ZnO.

2.4.2.1 Bandgap tuning by Doping on zinc oxide nanoparticle

Doping means intentionally introducing impurities into an extremely pure semiconductor. It is well known that the doping of impurities greatly affects the basic physical properties, (e.g., electrical, optical, and magnetic properties). This introduction of impurities

into an extremely pure intrinsic semiconductor (doping) is an important strategy in optimizing the optical and electrical properties of the ZnO nanostructures (Y.-C. Chang, 2014; Giri et al., 2007; Z. Zhang et al., 2014). Fox example, the presence of copper in ZnO NWs could induce red-shift to lower energy (Lupan, Pauporté, Viana, & Aschehoug, 2011) when the copper ions replace the zinc ions in the lattice parameters of the wurtzite hexagonal ZnO NW. As for ZnO, doping can be divided into two categories as described fig below;

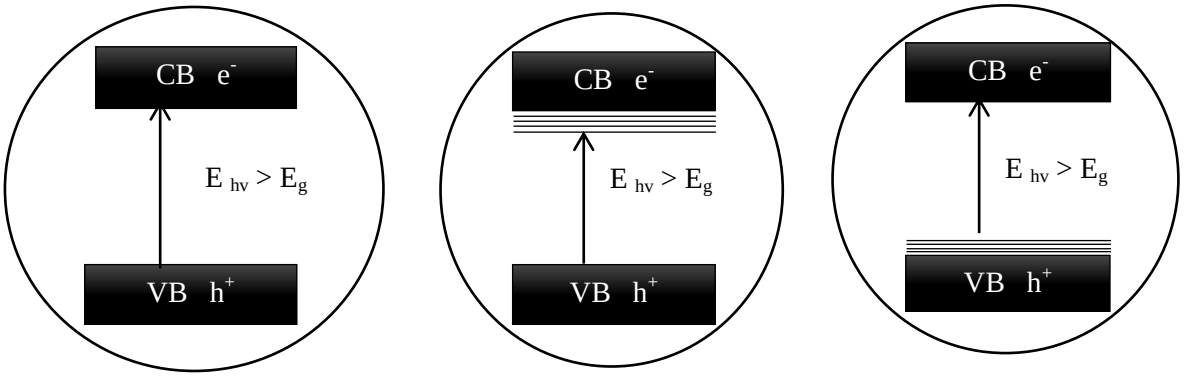

Pure ZnO Metal doped ZnO Nonmetal doped ZnO

Figure 4 Schematic of the comparison of the band structures of pure, metal-doped ZnO, and nonmetal-doped ZnO *(S. G. Kumar, Kavitha, & Sushma, 2020).*

2.4.2.1.1 Bandgap tuning by non-metal

Photocatalytic activity of ZnO_2 under visible light is enhanced by nonmetal (B, C, N, and S) doping due to the synergetic effect of the dopant ions. Shifu et al. reported that Nitrogen-doped ZnO samples show higher photocatalytic activity when compared to pure ZnO samples due to visible light absorption (redshifts) established by nitrogen ions doping which enhanced the photocatalytic activity. Doping elements should not only require lower electro-negativity than oxygen, it should also have a similar atomic radius as the O atom; both conditions are necessary factors for effective doping (Reza, Kurny, & Gulshan, 2017). Dopants, such as C, N, and S, can form intermediate energy levels in the band gap and hence increase visible-light photocatalytic activities

2.4.2.1.2 Bandgap tuning by metal doping

Doping is one of the methods used to improve the photocatalytic activity by bandgap narrowing (Panneerselvam Sathishkumar, Mangalaraja, Anandan, & Ashokkumar, 2013), the formation of oxygen vacancies, impurity energy levels (Cao et al., 2013), electron trapping (Y. Wu, Xing, Tian, Zhang, & Chen, 2010), and unique surface area for the adsorption of organic molecules. Semiconductor metal oxide with smaller bandgap energy is considered effective photocatalyst due to the generation of photo-induced charge carriers (Yousefi, Allahverdi, & Hejazi, 2013). Higher photocatalytic activity is achieved from bandgap narrowing which is accomplished by the introduction of oxygen-deficient sites and impurity energy levels (Cao et al., 2013; Fuerte et al., 2002; Rodríguez-González, Zanella, del Angel, & Gómez, 2008; Shie et al., 2008). Recombination of electrons and holes can be prevented by introducing dopant ions as result the photocatalytic efficiency of the photocatalyst enhanced by trapping the photogenerated electrons (H. Lin, Chen, & Chen, 2007; S. Ma, Li, Lv, Xu, & Gou, 2011; Shifu et al., 2009; Sobana & Swaminathan, 2007). During doping, the dopant ions are entered in to either placed in substitution (replace the lattice ions) or interstitial (if the size of the dopant ions is smaller than the lattice ions). Kanade et al. reported that doping of transition metal ions in the semiconductor metal oxide enhances the visible light absorption of photocatalyst and also photovoltaic devices. Zn ions in ZnO which is coordinated with tetrahedral O can be substituted by transition metal ions (Cu, Co, Mn, and Fe) thus, enabled visible light absorption of ZnO which increase the efficiency of the photocatalytic activity due to the spin exchange interactions. Xiao et al. explained co-doped ZnO which has high surface oxygen defects exhibited more degradation of methylene blue under visible light. Photocatalytic activity can be influenced by the introduction of transition metal having d-electronic configurations with in ZnO lattice. ZnO surface implanting with vanadium ion enhanced its visible light absorption thus, improved the photocatalytic activity of the photocatalyst.

Table1 Summary of works done on metal doping on ZnO

Nanocatalysts	Particle size (nm)	Morphology of NPs	Type of dye carried out	References
Cu-doped ZnO	(16.72-20.73)	Spheroid to rod-like	Acid Black 234 dye	(S. A. Khan et al., 2018)
Ag-doped ZnO	(30.13-35.15)	Bright circular patterns	CR & MO degradation	(Chauhan et al., 2020)
Au-doped ZnO	(21-26)	Monodisperse and uniform	amino compound	(Sohrabnezhad & Seifi, 2016)
Al- doped ZnO	(40-46)	Uniform spherical shape	charge separation	(Srimathi, Hussain, Panigrahi, Subramaniam, & Ahuja, 2020)
Cr-doped ZnO	(19.6-24.3)	Spheroid like	Congo Red	(Shah et al., 2021)
Ce-doped ZnO	(49.98)	Spherical and rod like	Methylene blue	(RR & Rajalaxshmi)
Co-doped ZnO	-	Circular like	Methylene blue	(Zelekew et al., 2021)
Fe-doped ZnO	17	Irregular spherical	of Acid Yellow-3	(Jan, Ullah, Ullah, & Usman, 2021)
Mg-doped ZnO	(37-51)	Spherical	Methylene blue	(Okeke et al., 2021)
Mn-doped ZnO	(43-56)	Spherical like	Methylene blue	(Dhivya & Yadav, 2021)
Se-Doped ZnO	(50-100)	Spherical	Methylene blue	(Dhivya, Yadav, & Powrnika, 2019)
Ud-Doped ZnO	(26.3-73.7)	hexagonal phase	MO and RhB	(Ebrahimian, Mohsennia, & Khayatkashani, 2021)

2.5 Synthesis Methods of ZnO Nanoparticle

Nanoparticle synthesis is divided broadly into two categories: “top-down” and “bottom-up” methods. The top-down approach begins with a bulk piece of starting material and then reduces it to the Nano-sized dimension, whereas the bottom-up approach starts from atomic or molecular levels and assembles them into larger particles. Biological Method using plant and microorganisms is also the best method.

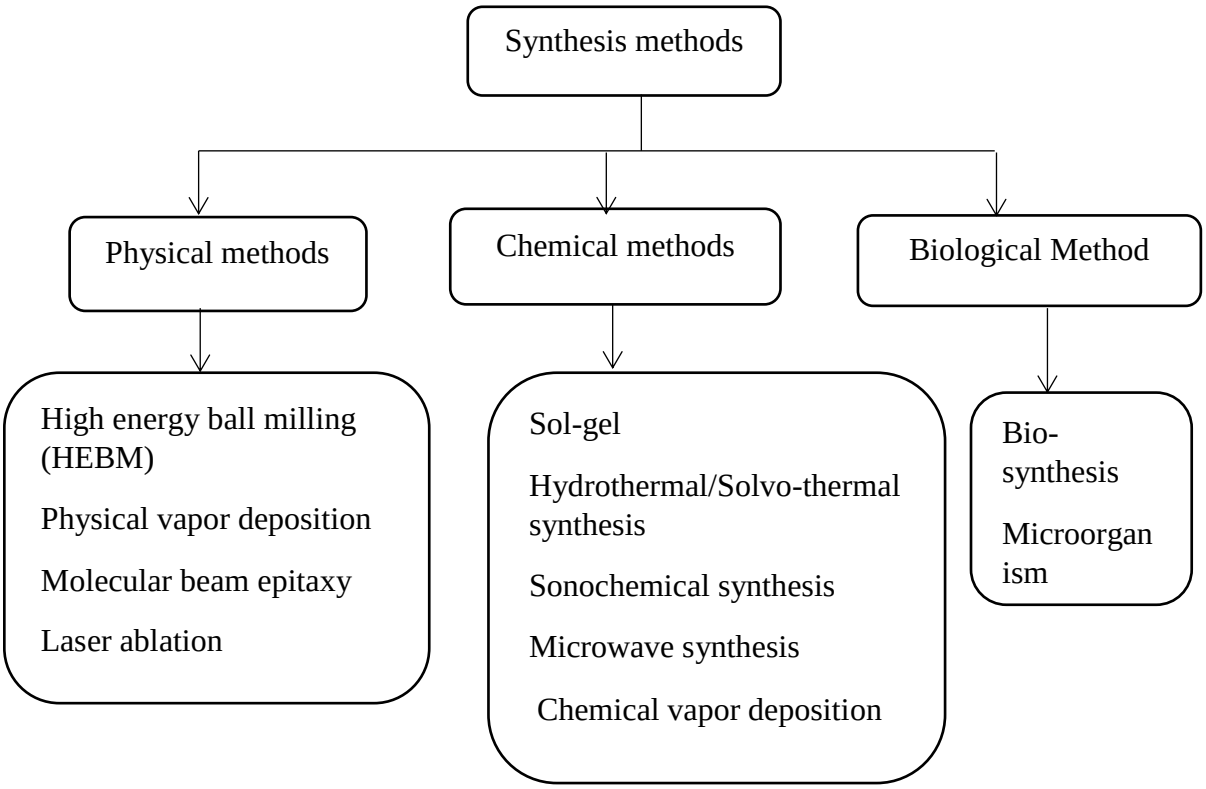

Figure 5 Methods synthesizing nanoparticle (A. K. Pandey, Kumar, Maurya, & Singh, 2015)

2.6 Green Synthesis

The reduction and stabilization of metallic ions into metallic nanoparticles is mostly accomplished by plant extract containing different biomolecules with functional groups such as C=C (alkenyl), C=N (amide), -O-H (phenolic and alcohol), N-H (amine), C-H, and COO- (carboxylic group) (Makarov et al., 2014), to name a few. Because of these interesting properties, plants have been considered a more environment-friendly route for biologically synthesizing metallic nanoparticles and for detoxification applications (Kale, Bao, Zhou, Prevelige, & Gupta, 2013). Plant extracts containing bioactive alkaloids, phenolic acids, polyphenols, proteins, sugars, and terpenoids are believed to have an important role in first reducing the metallic ions and then stabilizing them as seen in Figure 6 (Castro et al., 2011). The variation in composition and concentration of these active biomolecules between different plants and their subsequent interaction with aqueous metal ions is believed to be the main contributing factors to the diversity of nanoparticle sizes and shapes produced. The process begins by mixing a sample of plant extract with a metal salt solution. Biochemical reduction of

the salts starts immediately and the formation of nanoparticles is indicated by a change in the color of the reaction mixture. During synthesis, there is an initial activation period when process metal ions are converted from their mono or divalent oxidation states to zero-valent states and nucleation of the reduced metal atoms takes place (Malik, Shankar, Malik, Sharma, & Mukherjee, 2014). This is immediately followed by a period of growth when smaller neighboring particles amalgamate to form larger nanoparticles that are thermodynamically more stable while further biological reduction of metal ions takes place. As growth progresses nanoparticles aggregate to form a variety of morphologies such as cubes, spheres, triangles, hexagons, pentagons, rods, and wires (Sweeney et al., 2004).

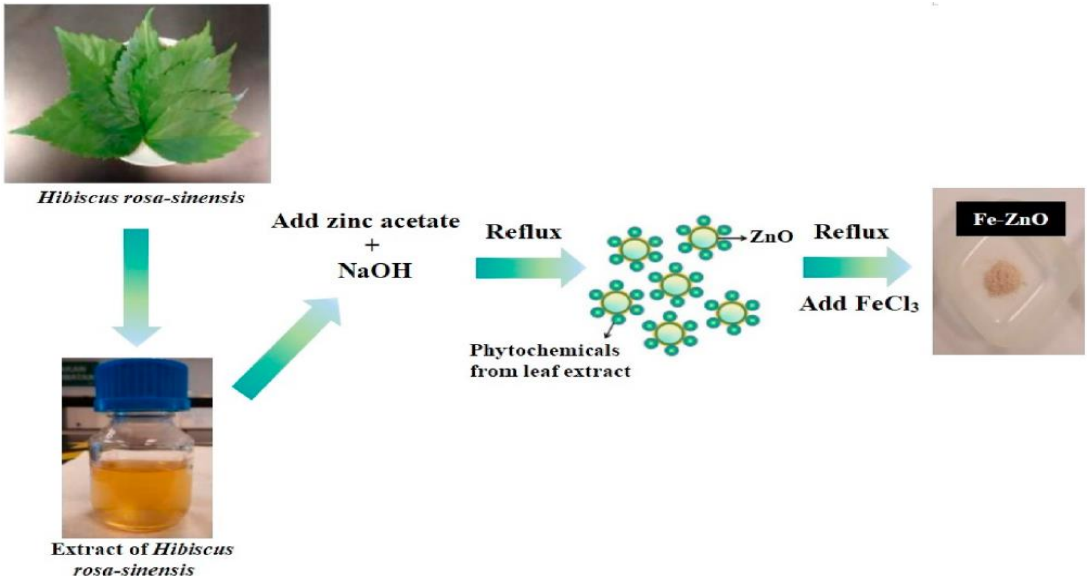

Figure 6 Mechanism of the nanoparticle using the plant extracts (Lam et al., 2021)

Advantages of using the green chemistry method are (Iravani, 2011; Parveen, Banse, & Ledwani, 2016):- Easily scaled up for a large scale synthesis of nanoparticles, metal nanoparticles produced by plants are more stable, rate of synthesis is faster, nanoparticles produced are more various in shape and in sizes : their sizes and morphologies can be controlled by varying some of the critical synthetic conditionssuch as the concentration of the metal salt, contact time, mixing ratio, pH and incubation temperature, cost effective: eliminates the use of expensive chemicals, no need to use high pressure, energy, or temperature, minimizes environmental and human health risks by eliminating the use of harsh ortoxic reagents during synthesis, biodegradable products and by-products (since they come

from either plants), bio-compatible and results in high yield and more stable nanoparticles.

Table 2 Review On different plants used for synthesis of ZnO nanoparticles

Scientific name	Common name	Extract source	Precursor	Size (nm)	Shape	Reference
Abrus precatorius	Rosary pea	seeds	Zn(Ac)	90-500	Irregular	(Vishwakarma, 2013)
Agathosma betulina	Buchu	leaves	$Zn(NO3)2$	~19.4	Spherical	(Thema et al., 2015)
Agathosma betulina	Aloe vera	leaves	$Zn(NO3)2$	25-40	Spherical	(G. Sangeetha, Rajeshwari, & Venckatesh, 2011)
Apalathus linearis	Rooibos	flower	$Zn(NO3)2$	~12.5	Quasi-spherical	(Diallo et al., 2015)
Azadirachtaindica	Neem	leaves	$Zn(NO3)2$	~25	Nanotubes	(Oudhia, Kulkarni, & Sharma, 2015)
Azadirachtaindica	Neem	leaves	Zn(Ac)	9.6-25.5	Spherical	(Bhuyan, Mishra, Khanuja, Prasad, & Varma, 2015)
Calotropis gigantea	Crown flower	leaves	$Zn(NO3)2$	30-35	Spherical	(Vidya et al., 2013)
Calotropis procera	Maddar	latex	Zn(Ac)	5-40	granular	(R. P. Singh et al., 2011)
Camellia sinensis	Green tea	leaves	Zn(Ac)	~16		(Senthilkumar & Sivakumar, 2014)
Cassia auriculata	Tanners cassia	flower	Zn(Ac)	-	Spherical	(Ramesh, Rajendran, & Meenakshisundaram, 2014)
Citrus aurantifolia	Lime	fruit	$Zn(NO3)2$	9-10	Spherical	(Ramesh, Rajendran, & Subramanian, 2014)
Corymbia citriodora	Lemonscented Gum	leaves	$Zn(NO3)2$	~64	Hexagonal	(Zheng et al., 2015)
Euphorbia Jatropa		latex	$Zn(NO3)2$	~15	Hexagonal	(Geetha, Nagabhushana, & Shivananjaiah, 2016)

2.6.1 Reviews on Green mediated Metal Doped ZnO Nanoparticle in Degradation of dye

The green synthesis synthesis of metal doped zinc oxide nanoparticles are the most important for photocatalytic activities. In this review different plants and dopants which are previously studded is included. During doping, the dopant ions are both positioned in substitution (update the lattice ions) or interstitial (if the scale of the dopant ions is smaller than the lattice ions). Kanade et al. mentioned that doping of transition steel ions with inside the semiconductor steel oxide complements the seen mild absorption of photocatalyst and additionally photovoltaic devices.

Green method for synthesizing Zinc Oxide nanoparticles (ZnO NPs) was successfully carried out using unutilized sweet lime *(Okeke, Agwu, Ubachukwu, Maaza, & Ezema, 2020)* .i.e., Citrus Limetta rind pulp (U-CLRP) extract. The structural, morphological and optical studies were elucidated to confirm the crystallinity, size, shape of the synthesized NPs. Copper doping on ZnO NPs (CZnO NPs) was carried out to enhance the optical properties. The as prepared and doped nanoparticle's potential for efficient degradation of a commercial dye, Methylene Blue (MB) was tested under Ultraviolet (UV) and visible light radiation. ZnO NPs showed promising results for dye degradation while improved result was witnessed for CZnO NPs. ZnO NPs showed 74% of degradation of MB dye under UV irradiation and 57% degradation under visible light radiation. CZnO NPs presented 85 and 90% degradation in the UV and visible radiation, respectively.

A hibiscus rosa-sinensis leaf-assisted green approach had been used to make iron-doped ZnO (Fe-ZnO) nanoparticles, which were then used to degrade low density polyethylene (LDPE) plastic under solar irradiation (Lam et al., 2021). The structural, optical, and electrical characteristics of green generated materials were investigated using a variety of characterization methods. The photocatalytic performance of the LDPE/Fe-ZnO film was greater than that of pure LDPE and LDPE/un-doped ZnO films, according to the weight loss data. The Fe-ZnO (2 wt%) nanoparticle demonstrated a greater photocatalytic deterioration of LDPE owing to its boosted optical absorption and the effective suppression of photogenerated charge carriers. The Fe-ZnO (2 wt%) nanoparticle demonstrated a greater photocatalytic deterioration of LDPE owing to its boosted optical absorption and the effective suppression of photogenerated charge carriers. The presence of carbonyl groups as the degradation product of

LDPE was confirmed by Fourier transform infrared (FTIR) analysis. Field-emission scanning electron microscopy (FESEM) images also witnessed the formation of pores at the interface between polymer matrix and Fe-ZnO. The current work put forward the construction of eco-friendly photocatalyst as a green strategy to tackle the challenges of plastic pollution.

Aqueous fresh leaves of Ziziphus mauritiana Lam had been used to successfully dope zinc oxide (ZnO) with copper(cu)and magnesium (mg) (Rahman, Harunsani, et al., 2021). Various approaches were used to investigate the surface morphological, structural, and optical features of ZnO and Mg/Cu-dual doped ZnO. When Mg/Cu dopants were added to the produced ZnO, the particle size and optical band gap energy were lowered. The presence of phytochemicals was also established, which played a crucial role in stabilizing and capping phytogenic produced ZnO. The influence of light on the antibacterial and radical scavenging capabilities of ZnO and Mg/Cu-dual doped ZnO was also investigated. It was observed that the synthesized materials exhibited good antibacterial activities towards *Staphylococcus aureus* compared to *Escherichia coli* in the absence and presence of light. The phytogenic synthesized ZnO and Mg/Cu-dual doped ZnO were also found to exhibit good 2,2-diphenyl-1-picrylhydrazyl free radicals scavenging activity under visible light irradiation.

Cobalt doped ZnO (Co-doped ZnO) was manufactured by accumulating cobalt ions on Eichhornia crassipes plant tissue over various days and combining them with zinc precursor *(A. B. Patil, Patil, & Pardeshi, 2010; Zelekew et al., 2021)*. The resulting catalyst powder samples were characterized by Fourier transform infrared (FTIR) spectroscopy, X-ray diffraction (XRD), X-Ray photoelectron spectroscopy (XPS), field emission scanning electron microscopy (FE-SEM), and Ultraviolet–vis (UV–vis) spectroscopy, and microwave plasma atomic emission spectrometer (MP-AES). The catalysts were also tested for the photocatalytic degradation of methylene blue (MB) in the presence ofH_2O_2 under visible light irradiation. The best catalytic activity was gained by the 8th-days accumulation of cobalt ion onto the Eichhornia crassipes plant tissue and 99.6% of the dye was degraded within 45 min. However, 69.6, 65.7, 73.6, and 94.8% of MB dye was degraded by 1, 2, 4, and 6 days accumulations. Hence, removal of toxic heavy metal by using Eichhornia crassipes plant and recycling in the wastewater treatment gain is highly appreciated. Moreover, the Co-doped ZnO photocatalysts could enhance the photocatalytic activities due to suppressing of the electron-hole

recombination and the porosity of the catalysts resulted from the Eichhornia crassipes plant after calcination.

The preparation of zinc oxide and silver oxide nanoparticles doped with zinc oxide using zinc nitrates and silver nitrates as oxidants and Azadirachta rubber as fuel by the solution combustion method at 500 ° C *(Lam et al., 2021)*. The synthesized nanoparticles were characterized by XRD, FTIR, UVDRS, SEM, and MET studies; these materials were tested for photoluminescence and photocatalytic activity studies. PXRD data indicated that the synthesized nanoparticles were confirmed as a hexagonal phase with average crystallite sizes of 13.33 and 13.34 nm for ZnO and Ag-ZnO, respectively. The SEM data revealed that the material obtained is a very porous and honeycomb structure. In the photocatalytic degradation of methylene blue, Ag-ZnO nanoparticles showed good photocatalytic activity compared to undoped ZnO nanoparticles. This is due to the presence of Ag on the surface of the ZnO catalyst which makes the catalyst more sensitive to light and reduces electron-hole recombination. In addition, we also examined photoluminescence studies for the synthesized materials and gave the green emission for the excitation at 380 nm.

The SEM image shows the morphological characteristics of CZnO NPs. Through the appearance of the microcrystalline structure in the form of rose petals, the morphological changes of ZnO NPs after Cu doping became clear. These crystal structures often change from hexagons to needle-like petals. Confirm the existence of Cu substituted structures (Vanalakar et al., 2015). The CZnO-NP-EDS mapping image also confirmed the presence of Cu in the Zn lattice. The weight percentage of Cu substitution obtained from the EDS spectrum also corresponds to the initial molar concentration used for synthesis. The inclusion of Cu in the ZnO lattice sites obviously affects the surface morphology of CZnO NPs and leads to the formation of crystalline rose petals migrating from the hexagonal shape of ZnO NPs. According to the crystal shape, micro molar doping also plays a decisive role

There is also, the prepared ionic liquid assisted Ag-Au/ZnO NPs, using J.adhatoda leaves extract by hydrothermal method. Ionic liquids performed as a stabilizing and templating agent to improve the surface morphology of the synthesized Ag and Au doped ZnO NPs. The prepared ZnO, Ag-doped ZnO, Au doped ZnO, and Ag-Au doped ZnO NPs exhibit the average crystalline size of 36, 34, 32, and 25 nm and their band gap energy values are 3.36, 3.29, 3.17, and 2.98 eV respectively. The XRD and UV-DRS result shows that after doping of

Au and Ag the ZnO crystalline size and band gap energy was decreased, which leads to enhanced the biomedical (antibacterial and anticancer) properties of AgeAu doped ZnO NPs.

Table 3 review of the important biosynthesized metal doped zinc oxide-based Nano-catalysts in the degradation of pollutants in water

No	**Nanocatalysts**	**Biogenic source**	**Particle size(nm)**	**Morphology of NPs**	**Photocatalytic activities**	**Eficency(%)**	**Refrence**
1	Cu-doped ZnO	Abutilon indicum(Leaf)	(16.72-20.73)	Spheroid to rod-like	Acid Black 234 dye	90%	(S. A. Khan et al., 2018)
2	Cu doping on ZnO	Vernonia amygdalina	(34-39)	Spherical and petal-like	MB	60%	(Okeke et al., 2020)
3	Copper doping on ZnO NPs	Citrus Limetta rind pulp	(14)	Hexagonal to petal shapes	MB	90%	(Narayanan, Begum, Manikandan, & Yuvashree, 2021)
4	Cu-doped ZnO-NPs	Sesamum indicum L	(18.37-64.23)	cylindrical & hexagon	MR and MG	82% &80%	(Das et al., 2017)
5	Cu-doped ZnO	Ziziphus mauritiana	-	Irregular and spherical	2,2-diphenyl-	75%	(Rahman, Tan, et al., 2021)
6	Cu-ZnO nanoparticles	Melia azedarach	(5-17)	Spherical	Organophosphate	91%	(Pathania et al., 2021)
7	Ag doped ZnO	Prunus cerasifera(fruit)	(72.11-100)	spherical, linear and irregular	MO, SO and RB	81.76, 74.11 and 85.52%	(K. S. Ahmad & Jaffri, 2018)
8	Ag-doped ZnO nanoparticles	Rosmarinus officinal(leave	(21.6-28.9)	Hexagonal structure	Degradation of industrial textile	63%	(Noukelag, Razanamahandry, Ntwampe, Arendse, & Maaza, 2021)

9	Ag-doped ZnO nanoparticles	rosemary leaf	(22-40)	quasi-spherical	MB	98%	(Hojjati-Najafabadi, Davar, Enteshari, & Hosseini-Koupaei, 2021)
10	Ag-doped ZnO nanoparticle	Cannabis sativa leaf	(30.13-35.15)	Bright circular patterns	CR & MO degradation	96%&94%	(Chauhan et al., 2020)
11	Ag–ZnO nanomaterials	Azadirachta indica gum	(15)	Porous and honeycomb like	Photocatalytic degradation of MB	98%	(Basavalingiah, Harishkumar, Nagaraju, & Rangappa, 2019)
12	Ag-ZnO nanostructures	Azadirachta indica (Neem)	(10-50)	Hierarchical	Photodegradation of MB	97%	(S. S. Patil et al., 2016)
13	Ag-doped ZnO	Lawsonia inermis (leaf)	(100)	Rod and spherical	Atenolol	-	(Majumder, Saidulu, Gupta, & Ghosal, 2021)
14	Ag-doped ZnO nanoparticles	Vitis vinifera (leaf)	-	Coral rocks	MB	30%	(Saravanadevi, Kavitha, Karpagavinayagam, Saminathan, & Vedhi, 2020)
15	Ag-doped ZnO nanoparticle	Sida rhombifolia	(4.21)	Rod like and spherical	MB and MG	57% & 90%	(Babu & Antony, 2019)
16	Ag-doped ZnO nanoparticle	Pomegranate peel extract	(100)	Collapsed and irregular	MB & TOC	95% &70%	(Kaviya & Prasad, 2015)
17	Ag- ZnO nanoparticle	Oak fruit hull (Jaft)	(19.2)	Spherical	violet 3 dye	79%	(Sorbiun, Mehr, Ramazani, & Fardood, 2018)
18	Au-doped ZnO nanoparti	Imperata cylindrica L	(21.37)	Hexagonal to sphere	Photocatalytic degradatio	-	(Budianto, Yulizar, Saputra, & Sudirman, 2021)

	cles				n		
19	Au-doped ZnO nanoparticles	Carya illinoinensis	(4.9)	Slightly rough	Rhodamine B	95 %	(M. Ahmad et al., 2021)
20	Au-doped ZnO Nanoflowers	Azadirachta indica (neem)	(21-26)	Monodisperse	Degradation of amino compound	94%	(R. Biswas et al., 2021)
21	Aluminum doped ZnO	Cucum sativa fruit pulp	(40-46)	Uniform spherical	Charge Separation	90%	(Srimathi et al., 2020)
22	Cr-doped ZnO nanoparticle	Citrus reticulate(leaf)	(19.6-24.3)	Spheroid Like	CR	92%	(Shah et al., 2021)
23	Cerium ion doped ZnO	Mangifera indica(mango	(49.98	Spherical and rod like	degradation of dye	-	(RR & Rajalaxshmi)
24	Ceion doped ZnO	Sesbania Grandiflora	(43-46.7)	Spherical like	Indigo Carmine dye	70%	(RR & Rajalaxshmi)
25	Co-doped ZnO nanoparticle	Eichhornia crassipes plant	-	Circular like	MB	94%	(Zelekew et al., 2021)
26	Eu3+ doped ZnO	Guizotia abyssinica	(20)	Spherical agglomerated	Photoluminescence studies	79%	(Kavyashree et al., 2015)
27	Fe-ZnO nanoparticles	Hibiscus rosa-sinensis (leaf)	(35-170)	Uniform spherical-like	LDPE	43%	(Lam et al., 2021)
28	Fe-doped ZnO nanoparti	Hibiscus rosa-sinensis (leaf)	(15-170)	Spherical	Photocatalytic of POME	94%	(Chai, Lam, & Sin, 2019)

	cles						
29	Fe-doped ZnO Nps	Amaranthus dubius leaf)	(71-280)	Nearly spherical	Naphthalene	93%	(Muthukumar, Gire, Kumari, & Manickam, 2017)
30	Fe-doped ZnO nanoflower	Platycladus orientalis	-	Flower like	Photocatalytic degradation MO	92.3%	(Liu et al., 2021)
31	Fe-ZnO nanoparticles	Myrtus communis L	17	Irregular Spherical	Acid Yellow-3	74%	(Jan et al., 2021)
32	Mg-doped ZnO nanoparticles	Piperguineense (leaf)	(37-51)	Spherical	photocatalytic activities	94%	(Okeke et al., 2021)
33	Mn doped ZnO nanoparticle	Cassia angustifolia	(43-56)	Spherical like	MB dye	95%	(Dhivya & Yadav, 2021)
34	Se- doped Zinc Oxide	Mangifera indica Leaf	(50-100)	Spherical in shape	Photodegradation of MB	72%	(Dhivya et al., 2019)
35	Se-doped ZnO nanoparticle	Se tolerant isolates	(130-160)	Spherical shaped	4-chloroguaiacol	88%	(Vaishnav, Pal, & Prakash, 2018)
36	Ud-ZnO nanoparticles	Urtica dioica (U. dioica)	(26.3-73.7)	hexagonal phase	MO and RhB	73.4 &75%	(Ebrahimian et al., 2021)
37	Fe- and Ag-doped ZnO	Clitoria ternatea Linn	(30-40)	Spherical shapes	Congo red	94.42%	(Chan et al., 2019)
38	Mg and Cu dual-	Ziziphus mauritiana	(100-1000)	Spherical shaped	Photocatalytic	82%	(Rahman, Harunsani, et al., 2021)

	doping ZnO	Lam(leaf)		particles	scavenging activities		

2.6.1 Research Gap

Therefore, from my literature review different works are discussed and their limitation (like large band gap, fast recombination rate of the photogenerated electron–hole pairs, high charge transferring resistance, lower specific surface area, and instability (Anandan et al., 2007; Uddin et al., 2012; Yang, Li, Chen, & Wang, 2004)) as well as agglomeration (Raha et al., 2021) are seen as the major problem. But no any research is done on (Mn, Ni) co-doped ZnO nanoparticle for degradation of dye. The new plant (Stephania Abyssinica) leaf which is not used before is also introduced in this research. This indigenous plant (S. abyssinica) leaf is extracted and ZnO nanoparticle, Ni-doped ZnO and Mn-doped ZnO are synthesized. Moreover, (Mn, Ni) co-doped ZnO nanoparticles ($Zn_{0.98-x}Mn_{0.02}Ni_xO$) are synthesized. The synthesized samples are characterized by different techniques and the degradation efficiency of the organic dye molecule is evaluated. Finally, the pH effect, catalytic dosage**,** and reusability of the synthesized catalyst are checked.

2.6.2 Background of Selected *(Stephania Abyssinica)* Leaf

Stephania abyssinica is a medicinal plant used in Cameroon alternative medicine to treat arterial hypertension (AHT) (Fodem, Nguelefack-Mbuyo, Ndjenda II, Kamanyi, & Nguelefack, 2021). The leaves are crushed and applied to wounds resulting from tortoise bites. Stephania abyssinica (Dillon & A. Rich) Walp (Menispermaceae) is a twining liana rich in bioactive alkaloids, flavonoids, lignans, steroids, terpenoids, and coumarins (Kupchan, Liepa, & Fujita, 1973). The plant is widely used in African folk medicine for the treatment of various ailments including asthma, hyperglycemia, sleep disturbances, inflammation, men impotence, miscarriage, and liver diseases (Dagne, Gunatilaka, Kingston, & Alemu, 1993). S. abyssinica is also used to treat heart complaints (Schmelzer & Gurib-Fakim, 2008), and in the West region of Cameroon, the aqueous extract from the fresh leaves of S. abyssinica is administered orally for the management of cardiovascular disorders including arterial hypertension. They

also used as S. abyssinica could be useful as food supplement to fight and prevent infant malnutrition as the powder displayed no toxicity on liver.

Greater numbers of medicinal plants are found in the south and southwestern parts of Ethiopia due to the high biological diversity in these regions (Mesfin, Demissew, & Teklehaymanot, 2009). The Stephania abyssinica leaf (as seen in Figure 7) is collected from Shekolo natural forest on Gardula Mountain around Gidole town, south of Arbaminch, (Ethiopia). In S/N/N/P/R around Gidole town, chencha, Arba minch (Kebebew, 2018), and around Hawassa (Tefera & Kim, 2019) (Ethiopia), Peoples uses traditionally s. abyssinica plant leave for medical treatment like of Gadanesa,' eye disease, amoeba, etc. by Grinding the leaf, boiling, liquid form, then drink it.

Phytochemical	Present in
Alkaloids	leaf
Salvadoricine	leaf
flavoides	leaf
Steroids	steam
Saponins	steam
Phenolic	leaf

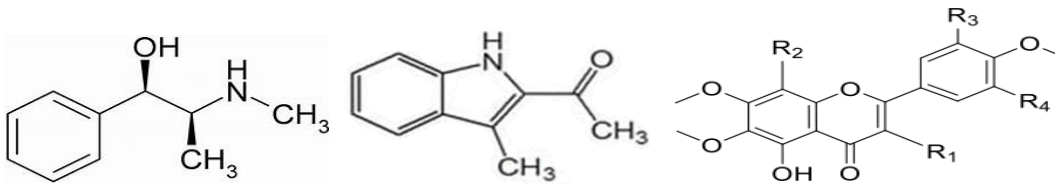

Alkaloids Salvadoricine Flavoides

Figure 7 Photograph of S. abyssinica

CHAPTER THREE

3. Materials and Methods

3.1 Chemicals and Materials

The chemicals and reagents were analytical grade and used without further purification. Zinc nitrate hexahydrate ($Zn(NO_3)_2.6H_2O$) (Loba Chem 98 % purity, India), Manganese acetate tetra hydrate ($Mn(Ac)_2{\cdot}4H_2O$) (98 % purity) and Nickel acetate tetra hydrate (Ni $(Ac)_2{\cdot}4H_2O$) (Loba Chem 99.8 %, India purity) of high-purity, Stephania abyssinica leaf was collected from Shekolo natural forest, Ethiopia. Ethanol (C_2H_5OH) (98 % purity), methylene blue ($C_{16}H_{18}ClN_3S$) (Carelabmed Chem, India), NaOH(97 %, Mumbai, India),, Whatman (No. 40) filter were used distilled water was used throughout the experiment.

3.2 Extraction of Leaf

Stephania abyssinica leaf was collected from Shekolo natural forest, Ethiopia. The same procure other leaf extraction method is used as pervious report with little modification (Aragaw et al., 2020). As seen in Figure 8 the S. abyssinica leaf was first washed with tape water to remove unwanted dusts from the plant followed by distilled water. The leaf was subjected to dry at room temperature and crushed by pestle to powder like. The resulting 10 g of S. abyssinica leaf powder was mixed with 200 mL of distilled water in 250 mL beaker and stirred at 60 °c for 30 min. cooling the mixture in air to room temperature and the solution was filtered using filter paper to remove fibrous impurities. The resulting plant extract was stored for further application.

Figure 8 the schematics on Extraction of Stephania abyssinica leaf

3.3 Green Synthesis of ZnO Nanoparticle

ZnO was prepared as the reported with little modification (Thema et al., 2015). In the particular procedure, 0.336 M (150 mL) of zinc nitrate was mixed with 33.3, 50, and 66.7 mL of plant extract in the ratio of 1:2, 1:1, 2:1 v/v, respectively, and stirred at 60 °C for 30 min. The pH was adjusted 10.5 by adding NaOH with continuous stirring for 2 h The resulting samples were abbreviated as L1:Z2, L1:Z1, and L2:Z1. The precipitates were washed with distilled H_2O repeatedly and centrifuged at 1000 rpm for 10 min and subsequently dried in an oven at 100^0c. The dried precipitate was annealed in an open furnace at $400\ ^0C$ for 2 hr.

3.4 Green Synthesis of Ni doped ZnO Nanoparticle

The Green synthesis of Ni doped ZnO nanoparticle ($Zn_{1-x}Ni_xO$, x = 0.01, 0.03, 0.05, 0.07) were synthesized according to literature report with some modifications (Gnanamozhi et al., 2020) and assigned as 1NZO, 3NZO, 5NZO, and 7NZO respectively. The addition of stoichiometric dopant solution of Ni $(CH_3CO_2)_2{\cdot}4H_2O$ was added drop wise in to Zn $(NO_3)_2{\cdot}6H_2O$ solution and the mixture solution was immediately added drop wise into the 50 mL of leaf extracted solution under continues stirring. For all samples, the same procedure

was performed. The Figure 9 shows the schematics on preparation of Ni-doped ZnO nanoparticle using *S. abyssinica* leaf

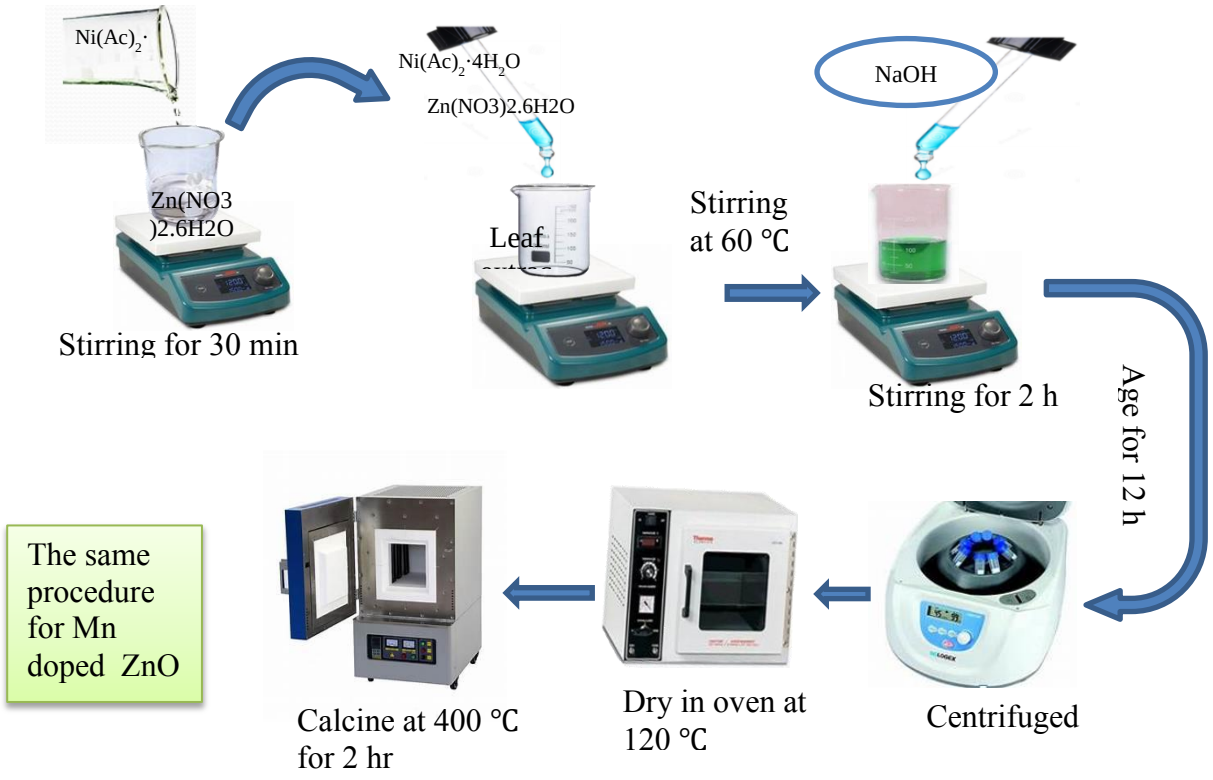

Figure 9 the schematics representation on preparation of Ni-doped ZnO nanoparticle using S. abyssinica leaf

3.5 Green Synthesis of Mn doped ZnO Nanoparticle

In the case of Mn doped ZnO nanocrystals, the amount of dopant was limited as $Zn_{0.98}Mn_{0.02}O$ to prevent phase segregation (Senol et al., 2020) and is assigned as 2MZO. The addition of stoichiometric dopant solution of Mn $(CH_3CO_2)_2{\cdot}4H_2O$ was added drop wise in to Zn $(NO_3)_2{\cdot}6H_2O$ solution. The mixed solution was added immediately by drop wise into 50 mL of the leaf extract solution under continues stirring. Then, the same procedure was carried out throughout the experiment.

3.6 Green Synthesis of (Mn, Ni) co-doped ZnO Nanoparticle

The (Mn, Ni) co-doped ZnO NRs ($Zn_{0.98-x}Mn_{0.02}Ni_xO$, x = 0.01, 0.03, 0.05, 0.07, 0.09) was synthesized co-precipitation method, and assigned as 1NMZO, 3NMZO, 5NMZO, 7NMZO

and 9NMZO, respectively. The preparation was according to the literature report with modification(Senol et al., 2020). In a particular procedure, 0.33 M of Zn $(NO_3)_2.6H_2O$ was dissolved in to 50 mL of ethanol to form solution and stirred for 30 min. The resulting solution was added to zinc solution and stirred for 30 min. Then, the mixed solution was immediately added drop wise into the 50 mL of leaf extracted solution under continues stirring. After 20 min stirring, the required amount of NaOH solution was added drop by drop to the mixed solution under magnetic stirring to adjust pH to 10.5. The solution was continually stirred for 2 hr and age for 12 hr after reaction. The aged precipitates was centrifuged until pH to be neutral and dried in oven at 80 ^0c . The powder was calcined at 400 ^0c for 2 hr. to obtain (Mn, Ni) co-doped ZnO powder. Figure 10 shows the schematics on preparation of (Mn, Ni) co-doped ZnO nanoparticle using S. abyssinica leaf

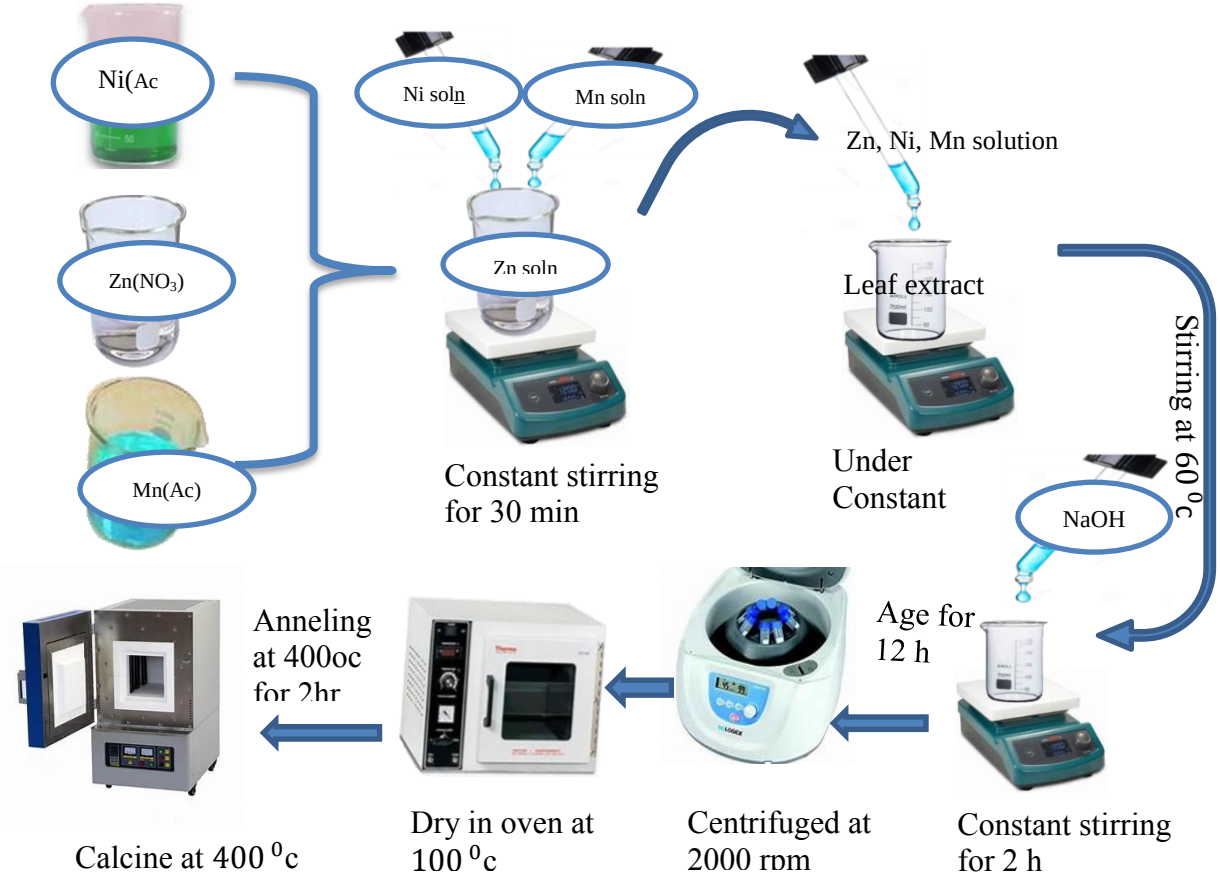

Figure 10 the schematics representation on preparation of (Mn, Ni) co-doped ZnO nanoparticle using *S. abyssinica* leaf

3.7 Characterization

The crystallinity, crystalline size, and phase of the catalyst was characterized by X-Ray Powder Diffraction (XRD) (Shimadzu XRD-7000). Fourier Transform Infrared Spectroscopy (FT-IR) with Spectrum 65 FT-IR (PerkinElmer) was performed using KBr pellets for the chemical functional group analysis. Differential Thermal Gravimetric (DTG) (Shimadzu DTG-60H) was used to now the thermal stability. X-ray photoelectron spectroscopy (XPS) ESCALAB 250 was used to elucidate the elemental composition. Energy Dispersive X-Ray (EDX) using JEOL Japan was used for quick examination–elemental composition and percentage weight of nanoparticles. Absorption properties of nanoparticles were measured by Ultraviolet-Visible Absorption Spectrum (Uv-Vis) using a JASCO V-670UV-Vis at room temperature. Photoluminescence (PL)-Spectroscopy of a JASCD FB-8500 was used to investigate the recombination at a certain excitation wave length. Electrochemical impedance spectroscopy (EIS) for study of charge transfer resistance was performed by Bio logic SP-300. Scanning Electron Microscopy (SEM) using JSM 6500F JEOL and Transmission Electron Microscopy (TEM) using (TEM, Tecnai G2 F20) was used for morphology, analysis. Higher Resolution Transmission Electron Microscope **(**HRTEM) was allowed for direct imaging of the atomic structure of the sample & know the exact d-spacing in between crystalline. Brunauer, Emmett, and Teller (BET) by Micromeritics ASAP 2020 was served for measuring surface area and pore size distribution directly. A Shimadzu–3600 Plus UV–vis spectrophotometer was used to assess the MB dye degradation.

3.8 Photocatalytic Activities

Photocatalytic activities of the as-synthesized samples were evaluated by the degradation of MB dye according to the method report with modification (Uddin et al., 2012). All of the trials were carried out in the open room temperature. In each experiment, 0.025 g of metal oxide catalyst was added in to 100 mL of MB solution (10 mg/L), followed by stirring for 20 minutes in the dark to validate the catalyst-pollutant adsorption-desorption equilibrium. Throughout the experiments, the mixture was constantly stirred. After 20 minutes of stirring in the dark, the light was turned on, and a 150 W halogen bulb was employed as the visible light source. 4 mL of the suspension was collected at predetermined irradiation times and centrifuged (4000 rpm, 10 min) to separate the photocatalyst particles. The MB concentration

was evaluated by UV−visible Spectrophotometer (Shimadzu, UV-1650 pc) monitoring the absorption maximum at λmax = 664 nm. The reusability of the (Mn, Ni) Co-doped ZnO catalyst was also checked by dispersing 0.125 g of catalyst in 500 mL MB (10 mg/l) solution. Then, the same process is used and the remaining solution was separated from the catalyst and the supernatant solution was removed by decantation. The catalyst that remained in the bottom of the beaker left was reused for the next photocatalytic reaction run with a similar procedure five times as mentioned above.

3.9 Electrochemical Studies

The electrochemical characteristics of the samples were studied using three-electrode quartz cells on an Electrochemical Potentiostate (Gamry Interface 1000) with 0.5 M Na_2SO_4 as electrolyte solution (Lam et al., 2021). The counter electrode was platinum wire, while the reference electrode was Ag/AgCl. The following process was used to make the working electrodes: The 10 mg of powdered sample was added to 1 mL of ethanol and mixed well together by ultrasonography for 40 min. The 20 microliters of generated suspension were then spread out on fluorine-doped tin oxide (FTO) glass plat which have 2 mm thick and area of 2x2 cm, and dried at 80 degrees Celsius for three hours. The EIS was obtained with a10 mV AC voltage amplitude in the frequency range of 100 kHz to 0.1 Hz.

CHAPTER FOUR

4. Results and Discussion

4.1. Structural Characterization by XRD

To study the crystalline structure, crystallinity, and crystalline size of different ZnO samples prepared with different concentration Stephania abyssinica leaf extract, XRD was used. The diffraction peaks pure-ZnO as shown in Figure 11 a located at 31.79°, 34.45°, 36.27°, 47.57°, 56.61°, 62.91°, 66.41°, 68.01, 69.17°, 72.74°, and 77.12°, belong to the (100), (002), (101), (102), (110), (103), (200), (112),(201), (004), and (202) planes of ZnO which is match with card number (JCPDS File No. 36-1451). It has hexagonal space group of P63mmc with unit cell parameters a = 3.2435 Å and c = 5.212 Å (Yadav, Raghavendra, Manjunath, & Nagaraju, 2018). Figure 11a depicts the patterns of reflection of various concentration of leaf to ZnO (L2:Z1, 1L: Z1, L1:Z2).

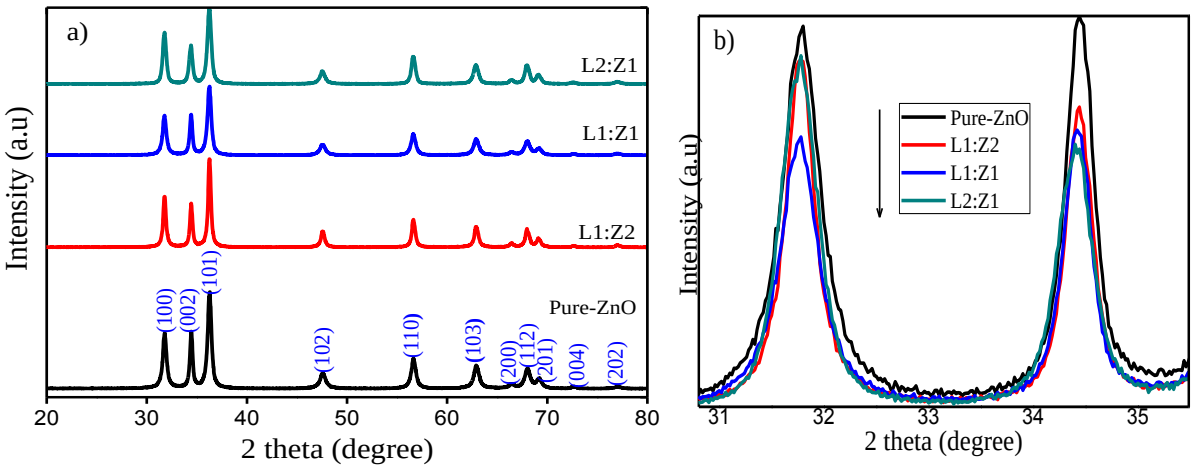

Figure 11 a) XRD pattern of pure ZnO, L1:Z2, L1:Z1, L2:Z1 nanostructures derived from S. abyssinica leaf extract and b) the variation of XRD peak intensity along (100) and (002) plane.

The size can be calculated by using Debye–Scherrer strategy: $D = \frac{0{,}9\lambda}{\beta \cos\theta}$ (1)

Where the crystal size is D, the X-ray wavelength is (1.5418), the full-width half maximum of the diffraction peak is the β and the scattering angle is the θ. The average

crystalline size of pure-ZnO, L1:Z2, L1:Z1 and L2:Z1 are 36.17 nm, 22.9 nm, 20.88 nm, and 15.49 nm respectively. It is clear from Figure 11b, that a decrease in the intensity and crystalline size of ZnO nanoparticles as the concentration of leaf increases which influences the crystallinity and the size of the crystals (Soto-Robles et al., 2019; Suresh et al., 2015).

Moreover, the XRD pattern of pure ZnO, 1-NZO, 3-NZO, 5-NZO, and 7-NZO is indicated in Figure 12 a. As it is indicated, there is no new phase observed resulted from Ni in ZnO, indicating that the dopant has been successfully doped into the ZnO lattice. Furthermore, as it is observed in Figure 12 b, the characteristic peak of (100) and (002) planes with dopant samples shifts toward a greater angle as compared to undoped (pure) ZnO NPs. This is due to the introduction of impurities (Ni^{2+}) and caused distortion in a host ZnO lattice, as well as the reduction of grain size and the existence of strain in the ZnO lattice due to the introduction of Ni dopant atom in the host ZnO matrix. (Rana & Singh, 2016)

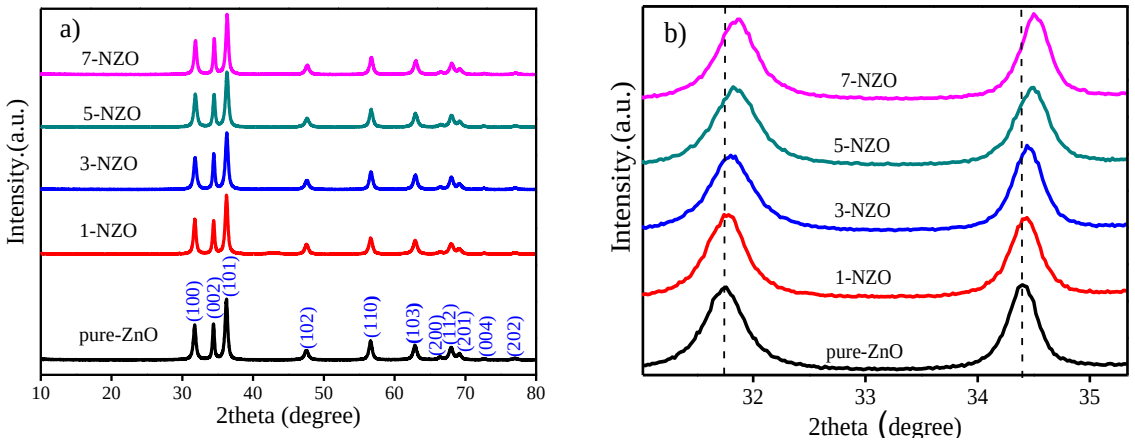

Figure 12 a) XRD pattern of pure ZnO, 1-NZO, 3-NZO, 5-NZO, and 7-NZO nanostructures derived from S. abyssinica leaf extract and b) the variation of XRD peak intensity along (100) and (002) plane.

The micro-strain (ε) is derived from the relation: Micro strain originates due to the presence of defects such as vacancies in the lattice, excess fraction of grain boundaries, etc., and causes broadening of the XRD peaks.

$$\varepsilon = \left(\frac{\beta}{4\tan\theta}\right) \quad (2)$$

Dislocation is a crystallographic defect or irregularity, within a crystal structure. The presence of dislocations strongly influences many of the properties of materials. Where Dislocation densities are calculated using the formula, Where D is the crystallite size and δ is the dislocation density, $\delta = 1/D^2$ (3)

From the XRD peak intensities, d-value, cell parameters "a" and "c," and c/a ratio, of all the three samples are presented in Table 4. The d-value was derived from Bragg's law, 2d sin θ = nλ. The unit cell parameters "a" and "c" have been calculated using the formula for the hexagonal system.

$d_{hkl} = \frac{\lambda}{2\sin\theta}$, Where λ is the wavelength of the X-ray beam (0.154nm) (4)

$\frac{1}{a^2} = \frac{4}{3}\left(\frac{h^2+hk+k^2}{a^2}\right) + \frac{l^2}{c^2}$ (5)

Table 4 Shows the average crystallite size, cell parameter, Dislocation density, lattice spacing, and micro-strain of Ni-doped ZnO from XRD pattern

Samples	Average crystalline size by sher rer's formula (nm)	Cell parameter(Å)		c/a ratio	Dislocation density ($x10^{-4}$) δ	Lattice spacing (Å) d	Micro strain ($x10^{-3}$) ε
		a = b	c				
1-NZO	20.37	3.2435	5.212	1.6069	24.103	1.89	0.764
3-NZO	19.98	3.2446	5.214	1.6069	25.051	1.88	1.052
5-NZO	19.84	3.2432	5.212	1.6070	25.404	1.86	1.103
7-NZO	18.49	3.2415	5.210	1.6073	29.251	1.83	1.182

The study of the crystalline structure and phase of Stephania abyssinica leaf extract-mediated pure-ZnO, 5NZO, 2MZO, 1NMZO, 3NMZO, 5NMZO, 7NMZO, and 9NMZO nanostructures are also done as seen in Figure 13 a. When we see the XRD peaks corresponding to co-dopants of Mn/Ni less than 7% Ni, their oxides were not observed that which justifies the phase purity of the samples**.** But, for the doping level of nickel at 9%, the NiO (200) diffraction peak is observed as seen in Figure 13 b. Therefore, the saturation solubility of Ni in Mn/Ni doping is limited to 7% of Ni. An enlarged view of the XRD peak along the (100) and (002) plane Table 13 (c-d) shows significant variation in peak position and intensity due to the incorporation of Mn^{2+} and Ni^{2+} which have small ionic radius (0.67 Å and 0.69 Å, respectively) than Zn^{2+} (0.74Å) in to ZnO. A decrease in peak intensity indicates the sensible decrease in the crystallinity of doped samples when compared to un-doped ZnO due to the distortion in the Zn–O lattice by Mn/Ni addition (Subbiah, Muthukumaran, & Raja, 2021). Moreover, the peak position is shifted slightly to the higher 2θ side due to Mn and Ni doping respectively, which suggesting the successful incorporation of Mn^{2+}/Ni^{2+} in the ZnO crystal

lattice or replacement of Zn^{2+} ions by $Mn^{2+/}Ni^{2+}$ ions (Naskar, Lee, & Kim, 2020). As seen in Table 5, the doping of Mn into ZnO and co-doping of Ni/Mn to ZnO significantly reduced the size to 17.32 nm. The reduction in crystalline size of samples as the dopant increase is due to incorporation of smaller ionic radius Ni^{2+} (0.69 Å) and Mn^{2+} (0.67 Å) in the place of Zn^{2+} (0.74 Å) (W. Yu et al., 2008).

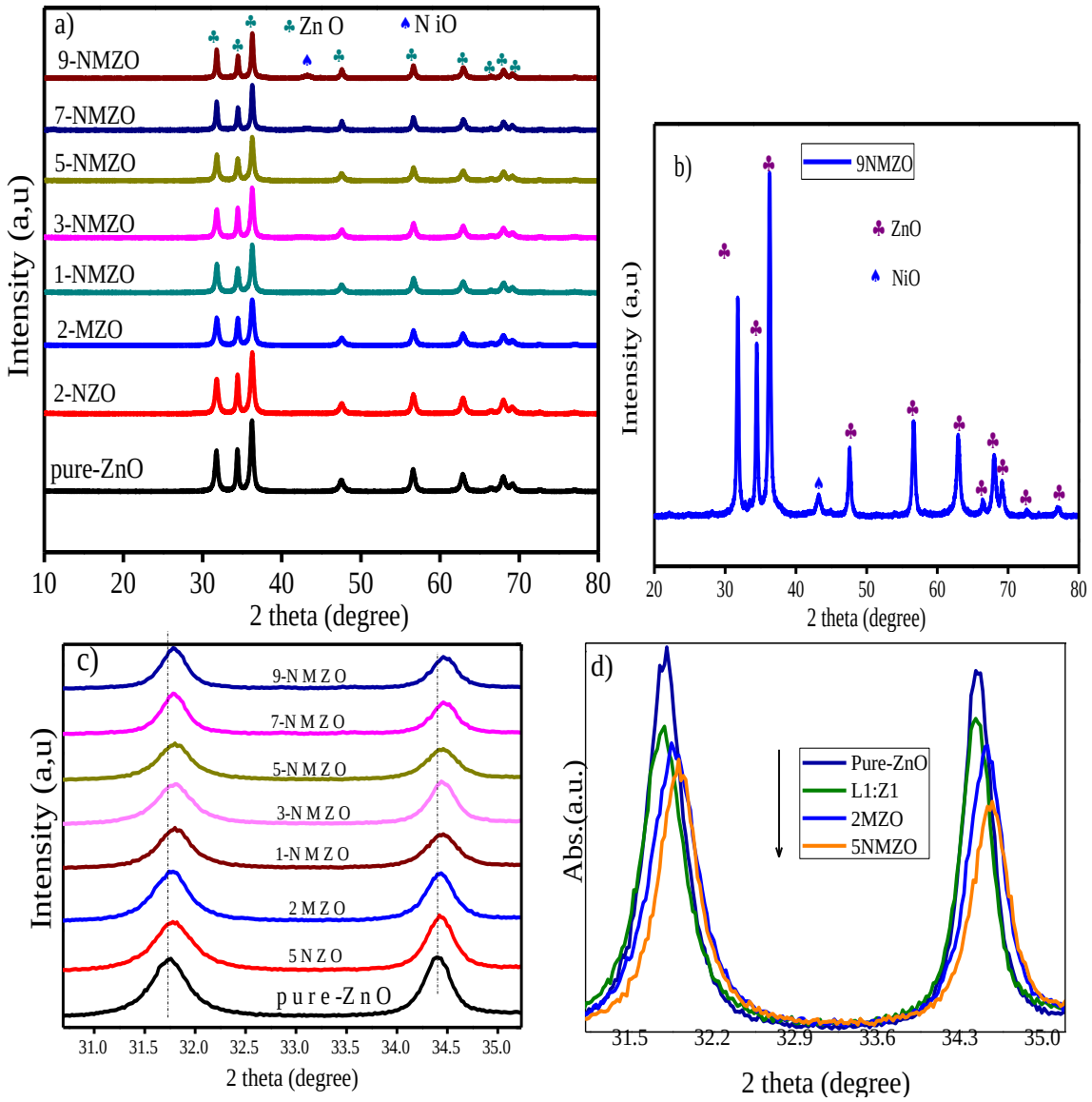

Figure 13 a) XRD pattern of green synthesized pure-ZnO, 5NZO, 2MZO,1NMZO, 3NMZO, 5NMZO, 7NMZO, and 9NMZO nanostructures b) the XRD pattern of 9NMZO nanostructures c) the variation of XRD peak position d) intensity along (100) and (002)

Table 5 shows the average crystallite size, cell parameter, Dislocation density, lattice spacing, and micro-strain of S. abyssinica -mediated of pure, doped, and co-doped ZnO from XRD pattern.

Samples	Crystalline size by sherrer's formula (nm)	Cell parameter(Å)		c/a ratio	Dislocation density ($x10^{-4}$) δ	Lattice spacing ($x10^{-10}$) Å	Micro strain ($x10^{-3}$) ε
		a = b	c				
1L:1Z	20.88	3.2426	5.209	1.6064	22.93	2.55	1.175
5NZO	19.84	3.2432	5.212	1.6070	25.423	2.01	1.203
2MZO	19.23	3.2447	5.216	1.6075	27.038	2.08	1.373
1NMZO	18.75	3.2428	5.211	1.6069	28.442	2.35	1.108
3NMZO	18.61	3.2428	5.211	1.6069	28.871	2.26	1.202
5NMZO	18.55	3.2422	5.209	1.6066	29.060	2.43	1.127
7NMZO	18.11	3.2424	5.210	1.6068	30.490	2.61	1.203
9NMZO	17.32	3.2431	5.212	1.6072	33.375	2.38	1.153

4.2. Thermo-Gravimetric Analysis (TGA).

The most extensively used approach for analyzing the thermal degradation of synthesized samples is Thermo-Gravimetric Analysis (TGA). Figure 14(a, b, c) shows the TGA and DSC traces of pure- ZnO, 2MZO, and 5NMZO samples which was heated at a rate of 10 °C/min from 0 to 1000 °C. The DTA and TG curves reveal that the heat breakdown of the precursor occurs in two stages**.** The endothermic peak for the first step of the TGA curve revealed a significant weight loss around 35 -147 °C due to water evaporation (Lakshmi, Mathusalini, Arasakumar, Kadirvelu, & Mohan, 2017). The weight loss of pure- ZnO, 2MZO, and 5NMZO in this range are, -2 %, -1.38 %, and -3.24 % respectively. The main weight loss occurred due to other endothermic peaks around the temperature range of 147–350 °C, in which the breakdown of intermediate molecules that may remain in the powder. The weight loss of pure-ZnO, 2MZO, and 5NMZO in this range are, -3.74%, -7.92%, and -13.38% respectively. This TGA indicated the thermal stability of crystalline structure, as confirmed by the XRD examination. There is no considerable weight loss after 400°C (Kayani, Anjum, Riaz, Naseem, & Zeeshan, 2020). In Figure 15 d**,** the TGA of those three samples are taken at about 355 ^{0}C

for comparison of thermal stability and it shows the weight loss -17.04%, -9.66%, and -5.80% of pure- ZnO, 2MZO, and 5NMZO respectively, in which 5NMZO has high thermal stability. This might be due to introduction of manganese and nickels in to ZnO which have different thermal decomposition (Xiao & Ouyang, 2009).

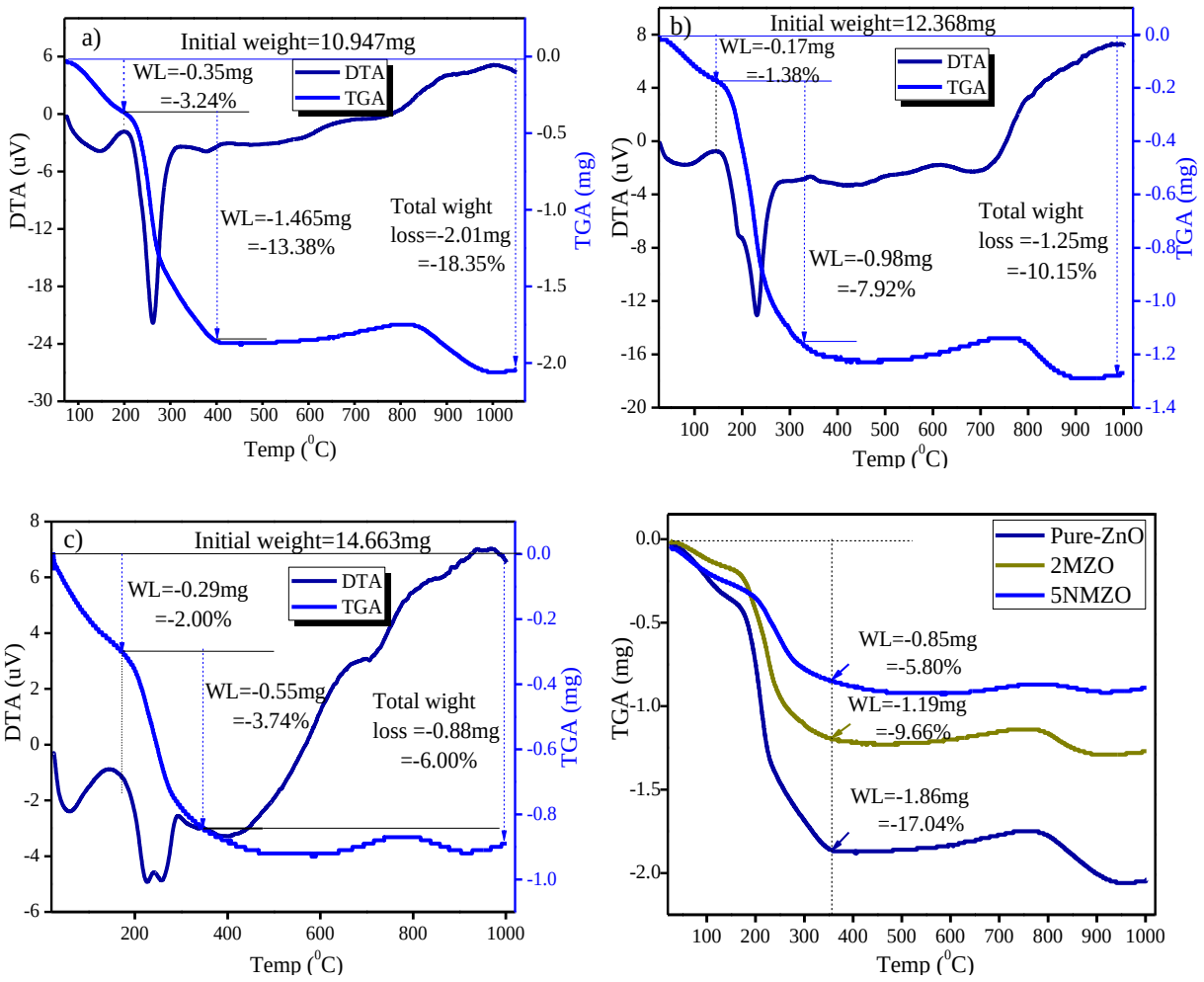

Figure 14 the TGA-DTA graph of synthesized zinc (a) pure-ZnO, (b) 2MZO, (c) 5NMZO, and (d) the thermal stability comparison

4.3. Uv-Vis Absorption Spectra and Optical Properties

The absorption properties of pure- ZnO, 5NZO, 2MZO, 5NMZO and 9NMZO nanoparticles were measured by ultraviolet-visible (Uv-Vis) absorption spectrum nanoparticles within the wavelength range of 200 nm to 800 nm at room temperature. The absorbance spectra of different samples are shown in Figure 15 (a). The band edge for the pure-ZnO sample was

appeared at about 387 nm while the band edges of the 5NZO, 2MZO, and 5NMZO samples shifted to longer wavelength regions with higher absorption wavelengths after doping as well as the absorption intensity also increase respectively due to incorporation of nickel and manganese in to lattice. The light absorption extended to the highest value of 475 nm when incorporation of Ni into ZnO lattice was increased to 5% in weight (at 5NMZO). The absorbance coefficient was calculated from the raw absorbance data to obtain the optical band gap (Eg). Tauc's relationship is used to compute the energy gap values (Eg) of the synthesized samples. The band gap values were thus determined by the extrapolation of the linear portion of the $(\alpha hv)^2$ curve versus the photon energy (eV) as shown in Figure 15 b. With variation, as pure-ZnO, 5NZO, 2MZO and 5NMZO, the band gap energies decreased in the range of 3.2 eV, 2.93 eV, 2.89 eV, and 2.62 eV respectively. But at 9NMZO, this slight increases of band gap energy to 2.79 eV that may be due to doping induced band edge bending (C. Yu et al., 2012) which means, the formation of new phase (NiO) made junction with ZnO, thus will have new properties of composite. Since Ni is not fully dissolved into ZnO matrix, that's why some of the Ni atoms may be located at the surface of ZnO in the form of NiO. Similar results were reported in Sn-doped ZnO and In-doped ZnO where the oxides appeared on the surfaces of doped ZnO as SnO_2 and In_2O_3 respectively (C. Wu, Shen, Yu, Huang, & Zhang, 2011).

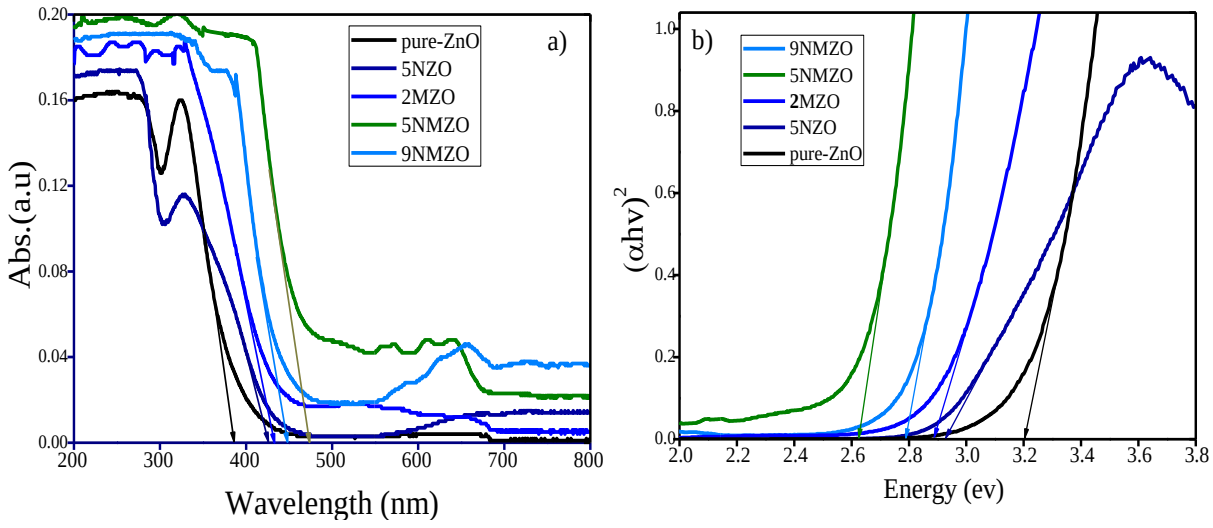

Figure 15 a) UV–visible absorption spectra of pure-ZnO, 5NZO, 2MZO, 5NMZO and 9NMZO nanoparticles the, b) Talc plots for the optical energy gap calculation of those nanoparticles.

4.4. Fourier Transform Infrared Spectroscopy (FT-IR) Analysis

Fourier transform infrared spectroscopy has been used to determine the presence of vibrational bands in the prepared samples. The FTIR of Stephania abyssinica leaf is done in Figure 16 a. and the peaks observed at 499, 1424, 2844, 2924, 3408, and 3822 cm^{-1} were attributed to stretching C–H vibration (S. Kumar, Kumar, Sahu, & Kumar, 2020). The absorption peak at 3416 cm^{-1} parallel to the O–H stretching vibration of the water molecule, the additional bands are observed at 1073 and 1632 cm^{-1} correspond to C-O (ester) stretching vibrations, and the band at 1429,1736 cm^{-1} stretching vibrations corresponds to C=C (carbon-carbon bonding) (Ashokkumar & Ramaswamy, 2014). FTIR spectra of pure ZnO, leaf, ZnO-leaf, 2MZO, and 5NMZO nanoparticles are shown in Figure 16 b. FTIR spectra typically reveal the existence of functional groups. The observation of a strong peak at 450 cm^{-1} may be assigned to the stretching vibration of Zn-O which confirmed the wurtzite structure of the prepared samples (Guo et al., 2008). The Presence of the weak absorption band found around 645 cm^{-1} corresponds to the asymmetric stretching of the Mn–O bond (B. D. Biswas et al., 2021) . The band at ∼1385 cm^{-1} may be due to O–C=O asymmetric stretching. The sharp stretching bands observed at 856 cm^{-1} and 1378 cm^{-1} were due to the Ni–O vibrational frequency and Zn–O–Ni bonding respectively, because of the presence of Nickel in the ZnO lattice structure, Ni^{2+} ions occupy Zn^{2+} sites of host lattice of ZnO NPs (Mullani et al., 2020). The observed band at 1047 and 1630 cm^{-1} can be attributed to C–O (stretching), and the peaks at 1514 and 1742 cm^{-1} was corresponding to C=O (asymmetric stretching). The peaks observed at 2245 and 2352 cm−1 are the stretching O=C=O vibrations due to the presence of CO2 molecules in acetate, and C–H stretching mode, respectively (Dhanalakshmi, Natarajan, Ramadas, Palanimurugan, & Thanikaikarasan, 2016). The O–H group of H_2O is observed to be responsible for the formation of a large absorption peak at 3451 cm^{-1}, showing the presence of water absorbed on the surface of monocrystalline powders.

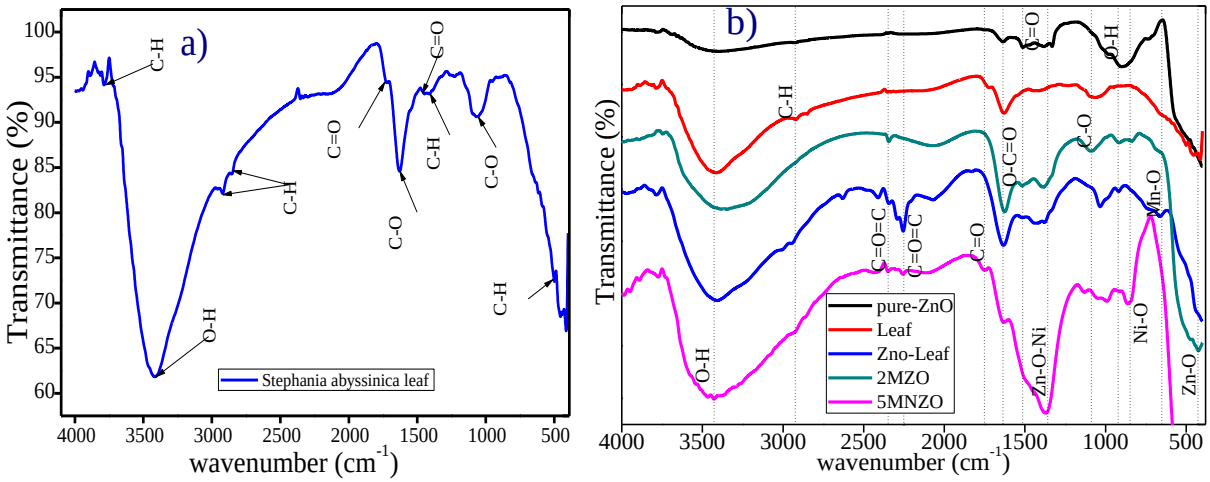

Figure 16 a) the FTIR spectra of S. abyssinica leaf b) pure-ZnO, ZnO-leaf, 2MZO, 5NMZO and 9NMZO nanoparticles.

4.5. Scanning Electron Microscope (SEM) Analysis

To study the surface morphology, Scanning Electron Microscopy (SEM) was taken for pure-ZnO, ZnO with leaf and the green synthesized sample of 5NMZO nanoparticles. SEM images are appropriate for demonstrating the nanoparticles' surface morphology, size and shape. As we see in Figure 17 a-b, the shape of pure- ZnO spherical like, agglomerated than the particle of ZnO with leaf, and have high particle size (around 122 n m). This may be due to the absence of cupping agent in the particle. The nanoparticles of ZnO with leaf in Figure 17 c-d are well dispersed, less aggregated and low particle size (around 101 m) than pure ZnO, and its shape is elliptical like which have the same shape with the previous report (Samanta, Goswami, & Mahapatra, 2018a). Due to the introduction of leaf extract and Ni/Mn dopants, the shapes of green synthesized sample of 5NMZO in Figure 17 e are seems elliptical like, some rode like and some flower like. Image J software has been utilized to calculate the particle size of the nanoparticles from SEM images, and the average particle size is around 86 nm as we seen in Figure 17 f. The change in shape from elliptical like to same rode like and some flower like structures confirming the presence of Mn and Ni substitutions. The grains are packed homogeneous and uniformly distributed or highly dispersed throughout the structure with good crystallinity. This could be beneficial for photocatalysts since they aid not only to adsorb organic contaminants on the surface of photocatalysts, but also to allow light to pass through during illumination.

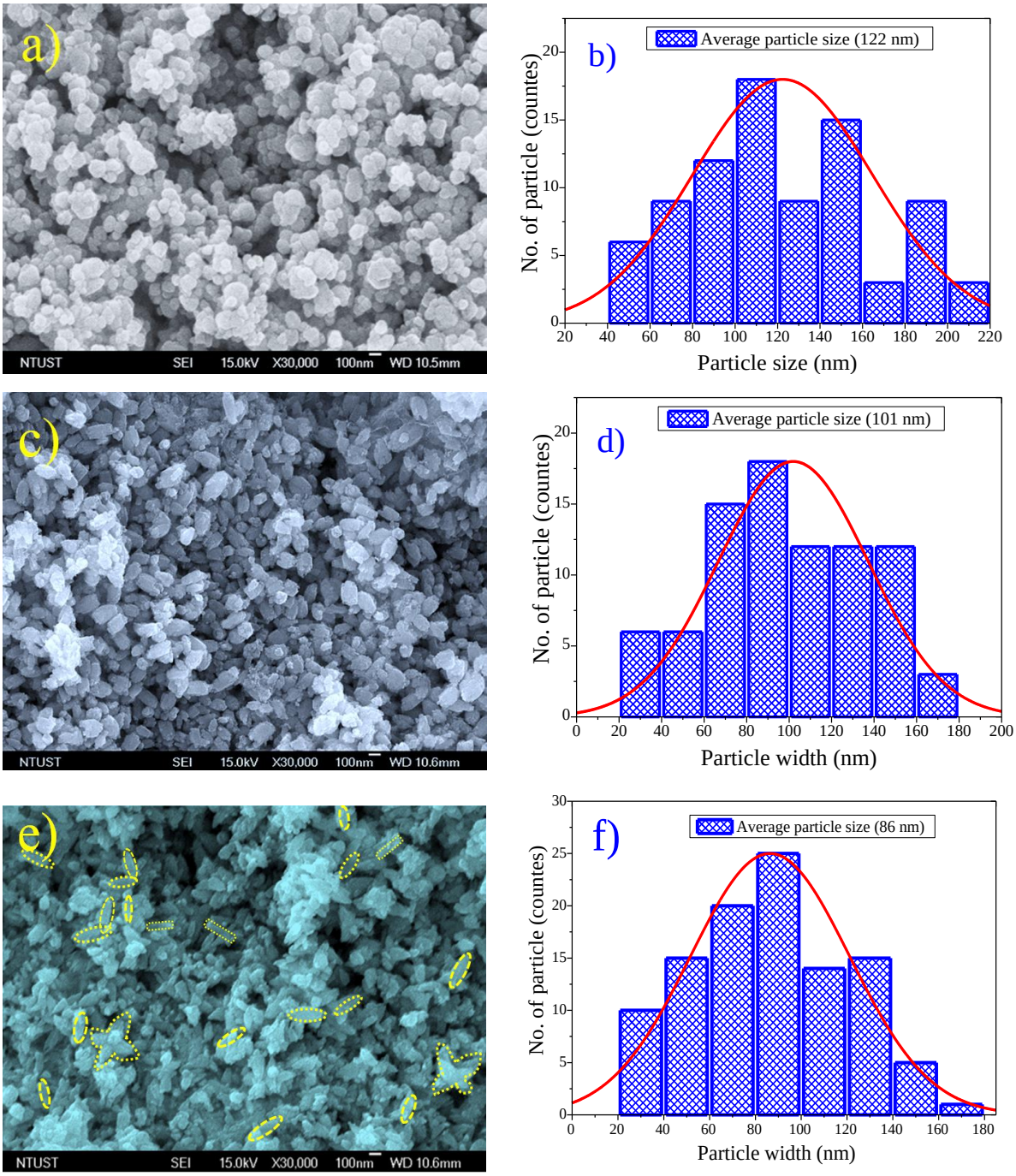

Figure 17, i) The SEM image for nanoparticle of (a) pure-ZnO without leaf extract, (c) ZnO with leaf extract, (e) 5NMZO nanoparticle with leaf extract, ii) the nanoparticle average particle size of (b) pure-ZnO without leaf extract, (d) ZnO with leaf extract, (f) 5NMZO nanoparticle with leaf extract

4.6 Energy-Dispersive X-Ray (EDX) Analysis

The chemical compositions of the elements created are evaluated by Energy-Dispersive X-Ray (EDX) spectroscopy analysis. One of the most important confirmation procedures for elemental identification is elemental mapping. The EDX spectra of six samples are shown in Figure 18 (a-f) Pure ZnO, 2MZO, 5NZO, 1NMZO, 3MNZO, and 5NMZO are among them. All of the samples contain the spectra elements that are expected to be happen. As a result, the purity of all synthesized samples was validated, with all predicted elements present and no unexpected elements identified. The weight and atomic ratio of the elements as found in EDX spectroscopy analyses are specified in the outcome to know how much weight of each element is there. To know the appropriate amount of dopant into the Zn lattice, the weight percentage of Ni, Mn, Zn to total(Ni + Mn+ Zn), are Calculated by weight percentage composition formula which created by Sal Khan (Anandan & Muthukumaran, 2015).

$$\text{Weight \% of X(in Zn lattice)} = \frac{\text{Weight percentage of X(in ZnO)}}{\text{Total Weight percentage (Mn+Ni+Zn) in ZnO}} \text{X100} \ldots\ldots\ldots\ldots \quad (6)$$

Where, X is Mn, Ni, and Zn elements. And the resulted weight % is presented in Table (6) and it confirms the doped value and the expected values are very close to each other. This shows there is the appropriate amount of doped element.

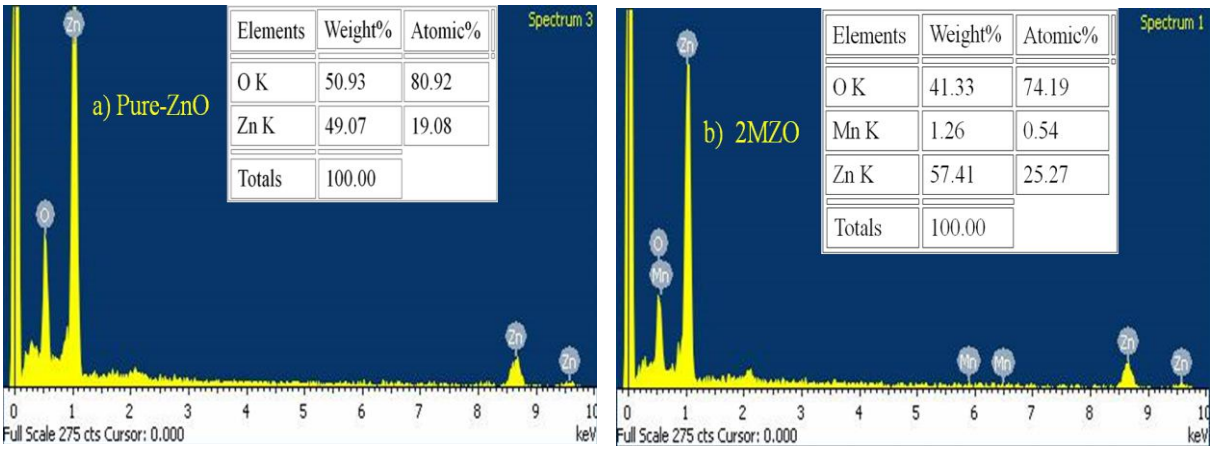

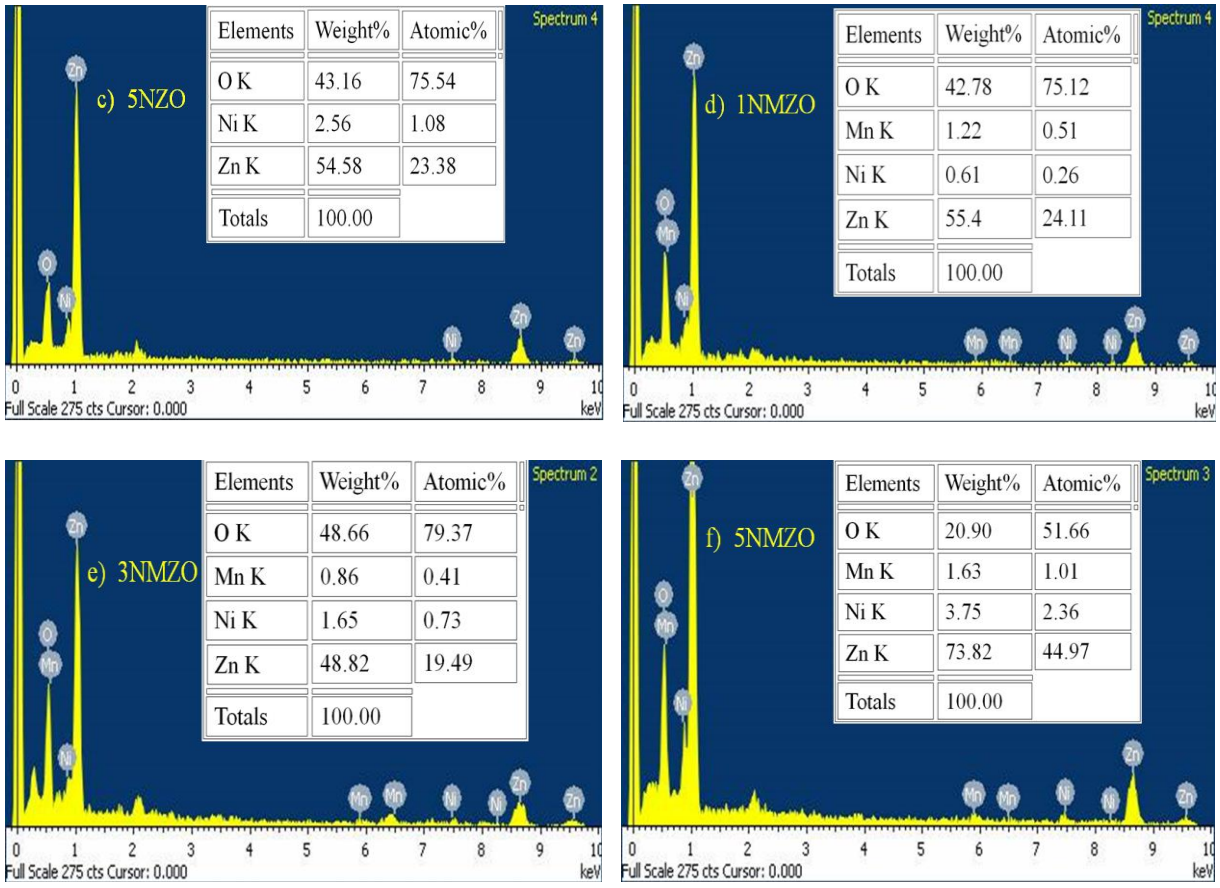

Figure 18 EDX analysis spectra of a) pure - ZnO b) 2MZO c) 5NZO d) 1NMZO e) 3NMZO f) 5NMZO nanoparticles

Table 6 the calculated outcome from EDX data, the expected weight percent, and percentage difference on weight percentage of Ni, Mn, and Zn to (Ni + Mn+ Zn) elements

Sample names	Expected weight %			The result weight%			Difference (% error)		
	Mn	Ni	Zn	Mn	Ni	Zn	Mn	Ni	Zn
Pure-ZnO	0	0	100	0	0	100	0	0	0
2MZO	2	0	98	2.19	0	97.81	+0.19	0	-0.19
5NZO	0	5	95	0	4.72	95.28	0	-0.28	+0.28
1NMZO	2	1	97	2.13	1.07	96.80	+0.13	+0.07	-0.20
3NMZO	2	3	95	1.70	3.15	95.15	-0.3	+0.15	+0.15
5NMZO	2	5	93	2.06	4.74	93.20	+0.06	-0.26	+0.20

4.7 Transmission Electron Microscopy (TEM) Analysis

The morphology and the exact particle size of as prepared 5NMZO nanoparticles have been investigated by Transmission Electron Microscopy (TEM), which confirms the particle size that studded in SEM images. The Figure 19 (a) Shows the TEM image confirms the shape tend to flower like structure of the 5NMZO nanoparticles. Image J software has been utilized to calculate the particle size of the nanoparticles from TEM images (J. Singh, Sharma, Soni, Sharma, & Singh, 2019). The TEM image in Figure 19 (b) confirms the exact particle size 94.23nm and 72.14nm of which is found in range that calculated from SEM image. Higher Resolution Transmission Electron Microscope **(**HRTEM) images of the samples are shown in Figure 19 (c). These images confirm the uniform structural growth at the surface of the nanoparticles (Samanta et al., 2018a)**.** The planar distance as seen in the HRTEM images is around 0.259 nm which matches well with the spacing between (002) crystal planes of ZnO. This finding of (002) plane oriented growth of ZnO much well with the earlier XRD results 0.2602 as mentioned in Table-7 below. From Selected Area Electron Diffraction (SAED) pattern in Figure 19 (d) shows the diffraction rings pattern of plans which confirms the crystalline nature of the samples. The indexing of diffraction rings of SAED pattern has been done using Image J software (J. Singh et al., 2019). From this pattern, (101), (102) (110), (112), and (202) planes of the ZnO nanoparticles were identified.

Table 7 similarity of d-spacing on expected, calculated, and HRTEM of 5NMZO nanoparticle

Name of sample	Plane index (hkl)	2θ	d(hkl) expected(Å)	d(hkl) calculated (Å) from XRD	d(hkl) from HRTEM (Å)
5NMZO	(002)	34.412˚	2.604	2.602	2.590

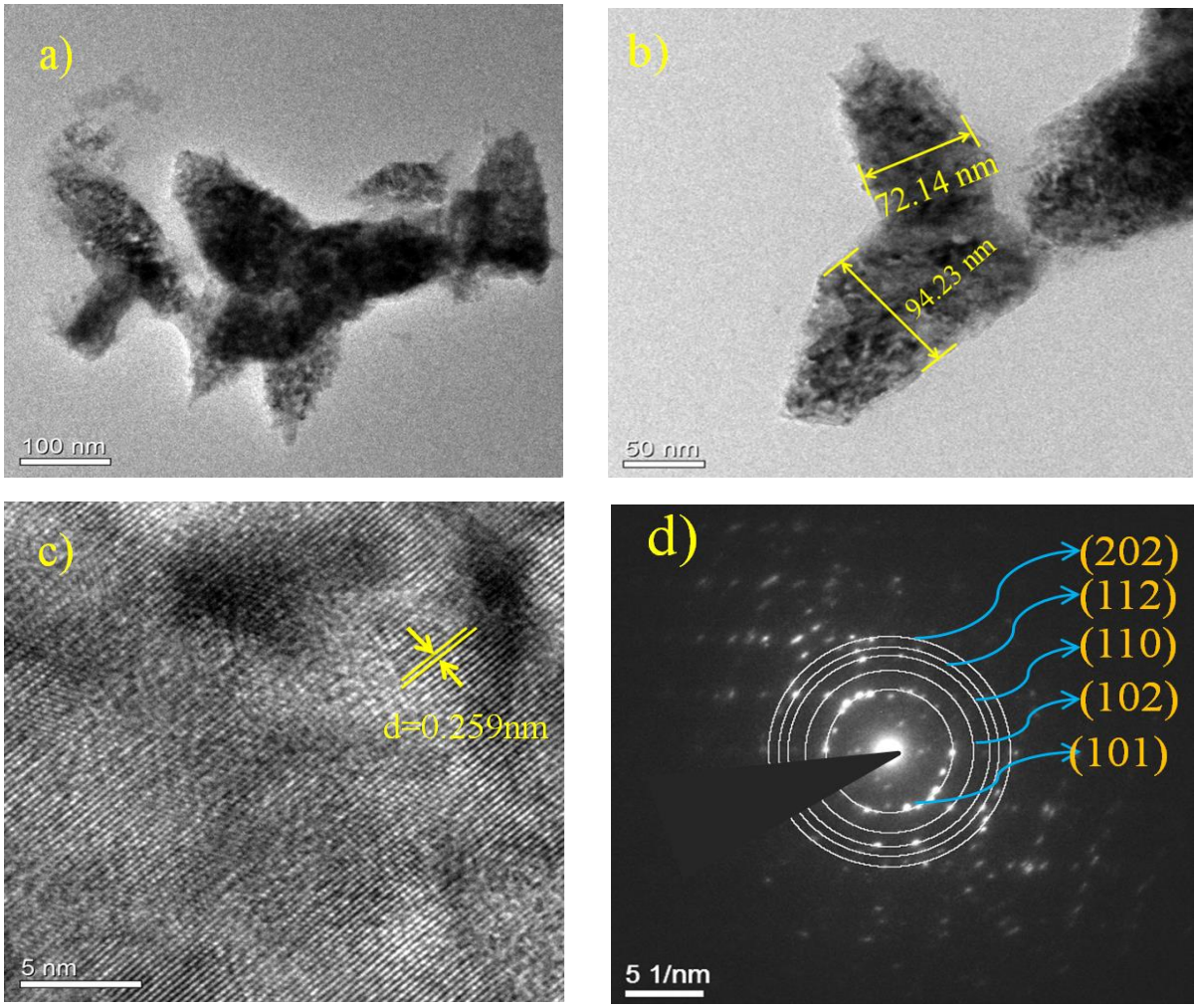

Figure 19 Those images are:- (a-b) the TEM images, (c) the HRTEM images, (d) the SAED pattern

4.8. X-Ray Photoelectron Spectroscopy (XPS) Analysis

The oxidation status of chemical components included in the 5MNZO sample was determined using XPS. The binding energy signatures of Zn 2p and Ni 2p from 5MNZO are seen in XPS spectra Figure 20 (c). The binding energy signals of Zn 2p are shown with strong signals at 1022.1 and 1045.2 eV, which correspond to the binding energies of Zn $2p_{3/2}$ and Zn $2p_{1/2}$, respectively. The energy difference between the binding energy levels of zinc $2p_{3/2}$ and zinc $2p_{1/2}$ can be calculated to be 23.1 eV, confirming the presence of zinc as Zn^{2+} in the nanomaterial (Naskar et al., 2020).

The Mn 2p spectrum is shown in Figure 20 (a), with two peaks at binding energies of 641.8 eV and 653.4 eV, corresponding to the Mn^{2+} $2p_{3/2}$ and Mn^{2+} $2p_{1/2}$, respectively. The binding energy of the Mn 2p1/2 peak is 641.8 eV, indicating that manganese ions are in the Mn^{2+} valence state (M. M. Khan et al., 2020; Prabhakar et al., 2012). As a result, these findings suggest that the doped Mn ions are in the divalent state, implying that Mn functions as a dopant to replace a significant portion of the Zn in the ZnO lattice. The binding energy between $2p_{3/2}$ and $2p_{1/2}$ has a spin-orbit double splitting value of roughly 11.6 eV, which is within the normal binding energy distance of the Mn^{2+} orbital level.

The Ni 2p spectra of the 5MNZO sample was fitted into four peaks at 855.4, 861.5, 872.8, and 879.8 eV, as shown in Figure 20 b. As a result, the Ni $2p_{3/2}$ and Ni $2p_{1/2}$ had eV values of 855.4 and 872.8. They differ from Ni at 852.3 eV and Ni $2p_{3/2}$ of Ni_2O_3 at 856.7 eV, but they are extremely similar to Ni $2p_{3/2}$ of NiO at 855.4 eV (Yin et al., 2005). The computed value (17.4 eV) from the energy gap between the Ni $2p_{3/2}$ (855.4 eV) and Ni $2p_{1/2}$ (872.8 eV) peaks differs significantly from NiO (18.4 eV), indicating that nickel is not present in the form of NiO in ZnO lattice sites in the sample. Furthermore, the satellite peaks of Ni $2p_{3/2}$ (861.5 eV) and Ni $2p_{1/2}$ (879.8 eV) reveal the presence of Ni^{2+} , indicating that the Ni^{2+} ion has been successfully doped in the ZnO lattice (Ganesh et al., 2017).

Three types of oxygen energy levels centered at 529.7, 531.3, and 532.8 eV may deconvolution the O 1s peaks of ZnO Nano particle with varying concentrations of Ni as show in in Figure 20 d. The chemisorbed oxygen of the surface hydroxyl group is responsible for the high binding energy component centered at 532.8 eV (Li et al., 2006), which cannot be easily removed. The O^{2-} ions in the ZnO lattice could be responsible for the component with low binding energy centered at 529.7 eV. The intensity of this peak would represent the number of oxygen atoms in the hexagonal Zn^{2+} ion array's wurtzite structure. The O^{2-} ions in the oxygen-deficient regions within the matrix of ZnO, whose intensity partly represents the variation in the concentration of oxygen vacancies, could be related to the medium binding energy peak centered at 531.3 eV, which could be related to the O^{2-} ions in the oxygen-deficient regions within the matrix of ZnO (Gayen, Majumder, Varma, & Pal, 2010).

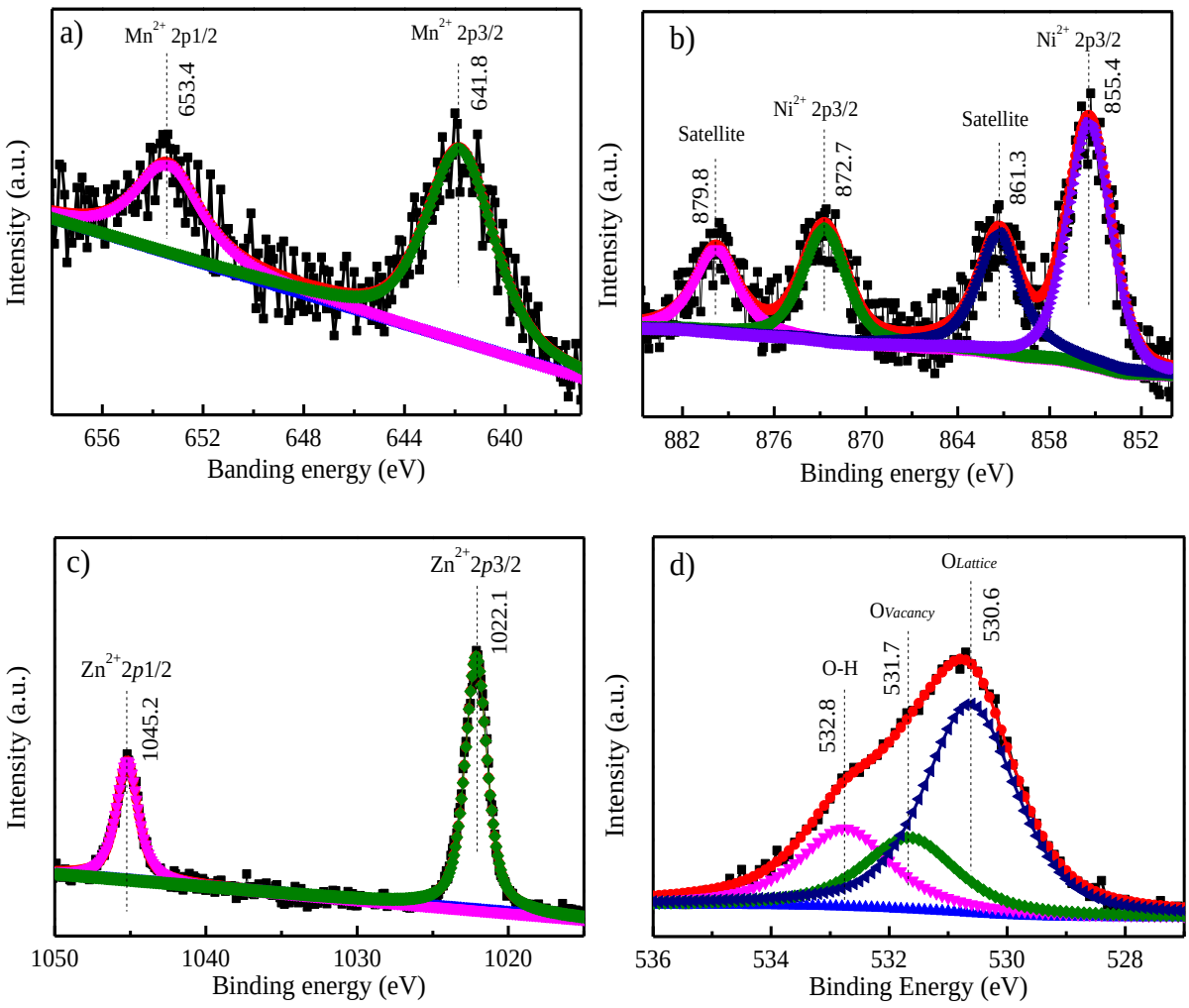

Figure 20 XPS survey of (a) Mn^{2+} 2p (b) Ni^{2+} 2p, (c) Zn^{2+} 2p, and (d) O 1s for 5NMZO prepared catalyst with leaf extract

4.9. Brunauer, Emmett, and Teller (BET) Analysis

The specific surface area of the 5NMZO powder prepared with *Stephania abyssinica* plant extract was 28.256 m^2/g, while the specific surface area of the 5NMZO prepared without leaf extracts was 14.53 m^2/ g. The results revealed that the presence of leaf extract increases the surface area of the catalyst which is similar with the reported value by Tarafdar et al. (Ebadi, Soltan Mohammadzadeh, & Khudiev, 2009). The ability of surface area improved to enable many active locations and to adsorb organic pollutants on the surface of catalysts. The greater surface area of the catalyst may allow organic contaminants to adsorb on its surface; these designs ultimately enable the catalyst to achieve efficient degradation of MB in a shorter time.

Table 8 shows the measured BET data of 5NMZO nanoparticle with leaf and without leaf

	5MNZO Without plant leaf extract	5MNZO with plant leaf extract
Specific surface area ($\boldsymbol{a_s}$)	14.53 ($m^2 g^{-1}$)	28.256 ($m^2 g^{-1}$)
Total pore volume ($\frac{\boldsymbol{P}}{\boldsymbol{P_o}}$)	0.0074369 ($cm^3 g^{-1}$)	0.014276 ($cm^3 g^{-1}$)
Mean pore diameter	2.0474 (nm)	2.021 (nm)

4.10. Photoluminescence (PL) Analysis

The PL emission spectra of pure-ZnO, 5NZO, 2MZO, 5MNZO, and 9MNZO photocatalysts were measured at room temperature at the excitation wavelength of 325 nm to investigate the effect of Mn/Ni doping on the Photoluminescence of ZnO. The pure ZnO photocatalyst had a significant UV emission peak at 387nm and several somewhat mild visible emissions around 407nm. The visible emissions are caused by many types of defect states transitioning (Sagar et al., 2007). The decreased recombination rate of the charge carriers in the Mn/Ni-doped ZnO samples was evidenced by the lower emission intensity. It is widely acknowledged that Mn/Ni ion doping can result in doping levels/ electron trapping level below the conduction band. These doping levels were advantageous for trapping electron due to photogenerated electrons and holes, which could improve charge separation efficiency and hence limit recombination. As a result, as seen in Figure 21a of pure-ZnO, 5NZO, 2MZO, and 5MNZO, the PL intensity decreased respectively. On the other hand, the PL intensity of the prepared 5MNZO samples was lower than that of pure-ZnO, 5NZO and 2MZO. However, the intensity of the PL increases as the farther increase of doping concentration to 9MNZO on which the new phase (NiO) is formed as seen from XRD. There are two probable explanations: (1) when the dopant concentration surpasses a particular threshold, these doping levels may operate as a recombination center rather than a charge separation center, facilitating the recombination process. (2) Photogenerated electrons may pass from the CB of ZnO to the CB of NiO because the composite of ZnO/NiO would have their own properties when forming composite. Too many photogenerated electrons were collected in the NiO conduction band too quickly, leading some photogenerated electrons to recombine indirectly to hole. The intensity peaks in the higher wavelength region revels the presence of vacancy's due to integration of Ni/Mn into

ZnO nanoscale material (Mondal et al., 2020). It also confirmed in XPS like oxygen vacancies.

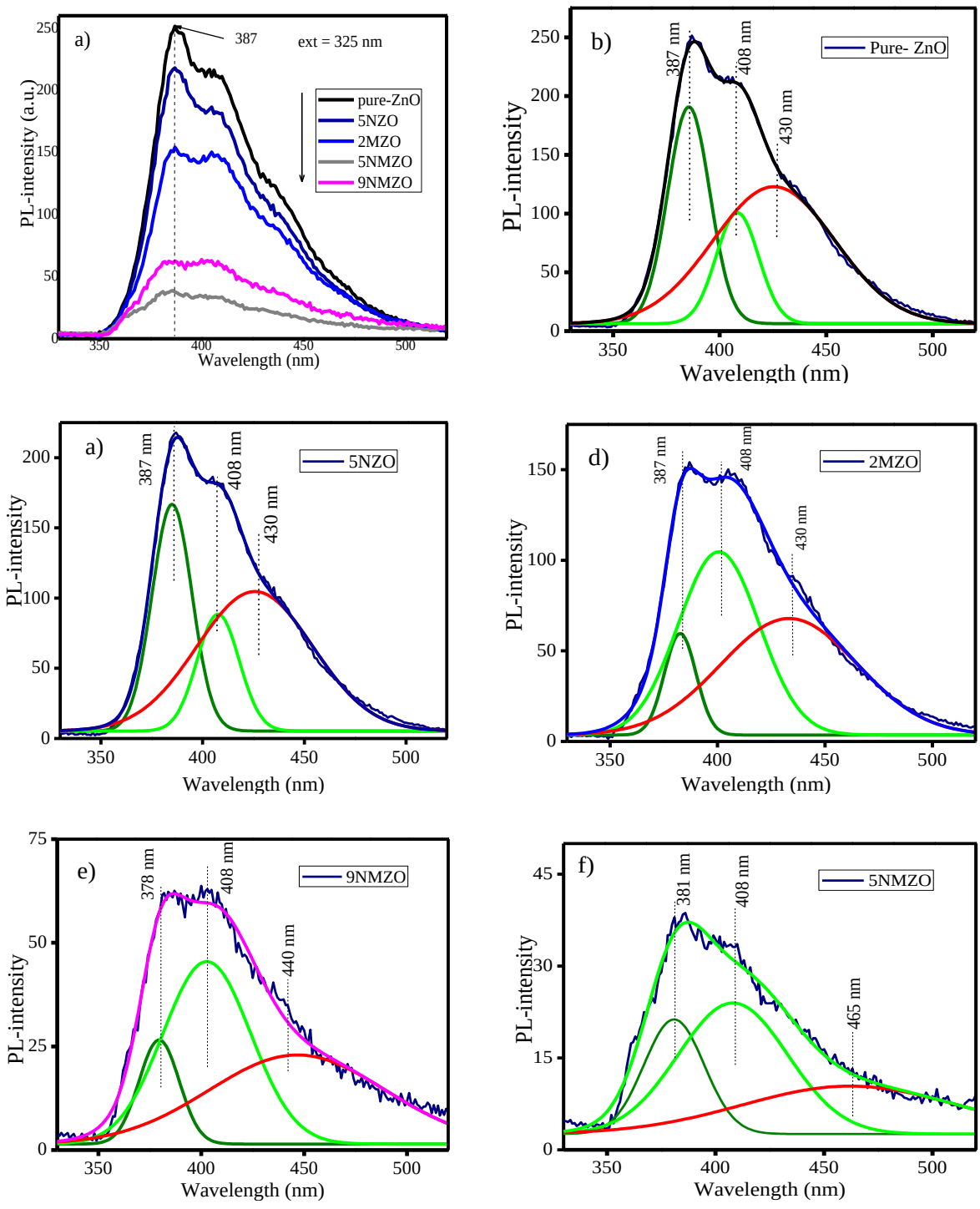

Figure 21 Room temperature PL spectra of a) pure-ZnO, 5NZO, 2MZO, 5NMZO and 9NMZO samples, and (b-f) the deconvolutions of each sample.

4.11. Electrochemical Impedance Spectroscopy (EIS) Study

The interfacial charge transfer dynamics in the photocatalyst were further investigated using Electrochemical Impedance Spectroscopy (EIS). To better understand the effect of doping on the separation of photogenerated electron-hole pairs, the Nyquist plot EIS of pure ZnO, 2MZO, 5NZO, 5NMZO, and 9NMZO samples was performed as shown in Figure 22. The a lower arc radius indicates effective charge carrier separation (Qiao et al., 2020). The arc radius of the impedance curve related to the 5NMZO electrode was much smaller than that of pure ZnO 2MZO, 5NZO, and 9NMZO electrodes. Their charge transfer resistances (R_{ct}) are 5705 Ω, 4712 Ω, 3387 Ω, and 1360 Ω and their serious resistance (Rs) of the solution are 121 Ω, 107 Ω, 70 Ω, and 37 Ω respectively as fitted circuit shown below. However, the photogenerated electron-hole pairs were separated and moved more easily in the 5NMZO structure due to the lower charge transfer resistance (R_{ct}) which is 979 Ω. The EIS results matched the photocatalytic activity of the as-prepared photocatalyst, which is compatible with the photoluminescence (PL) tests, which show that lowering the recombination probability of photogenerated electrons and holes, and increases the photocatalytic activity. The PL spectra and EIS experiments revealed that to prevent photogenerated electron-hole pair recombination.

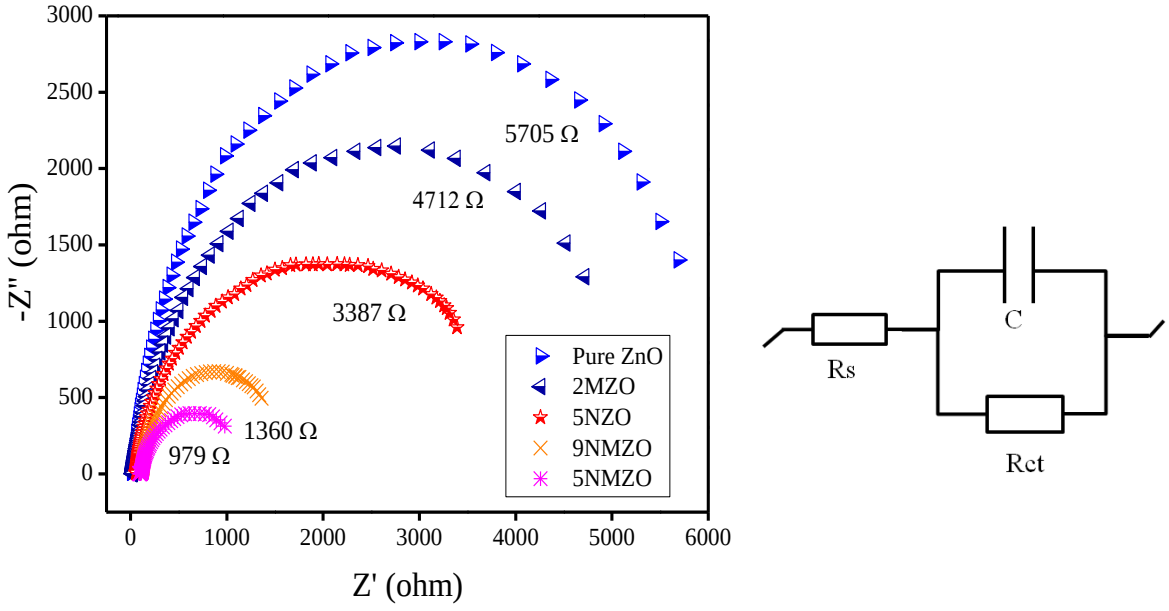

Figure 22 the Nyquist plot EIS of pure-ZnO, 5NZO, 2MZO, 5NMZO and 9NMZO nanoparticles derived from S. abyssinica leaf extract.

4.12. Photocatalytic Activity Evaluation

To check the photocatalytic degradation efficiencies of pure ZnO and different concentrations of Stephania abyssinica leaf extract-mediated ZnO, Methylene blue (MB) dye, which is a major pollutant in water discharged by factories in the textile industry, was chosen as the model of organic pollutant while doing the experiment under visible light irradiation. The molecular formula and molecular weight of MB are C16H18ClN3S and 319.851 g/mole respectively. Figure 23 (a, b, c, d) shows the UV-vis adsorption changes in the absence of leaf and the presence of leaf concentration (pure-ZnO, L1:Z1, L2:Z1, and L1:Z2) photocatalysts, where a peak of absorbance at 664 nm of the UV-vis of the MB solution. This presence of the peak is attributed to the absorbance of the transitions of the MB. The degradation was divided into two phases: The dye/catalyst solution was kept under continual sonication for 20 minutes in the first phase (without turning on the visible light). While in the second stage (the visible light on), the degradation efficiency (η) of the bio-synthesized sample can be achieved by the following equation:

$$\eta = \frac{C_0 - C_t}{C_0} x\ 100\ \% \qquad (6)$$

Where, C_0 and C_t are the concentration of the dye at the irradiation for time, "0" and "t" minutes, respectively. And it is observed that the Z1:1Lsample exhibits the highest photocatalytic activity (72.5 %), compared to the pure-ZnO, Z2:1L, and Z1:2L samples (33.1 %, 69.7 %, and 67.4 %, respectively), during 80 minute reaction time. These results are attributed according to previous studied (Angasa, Jamarun, & Arief, 2020). As if the leaf concentration is to law, the particles were still agglomerated in shape, and if the leaf concentration high, leads the particles too small and tends to agglomerated. But if their enough concentration, this can effectively act as a capping agent in the synthesis (Angasa et al., 2020). It also needs SEM for farther confirmation.

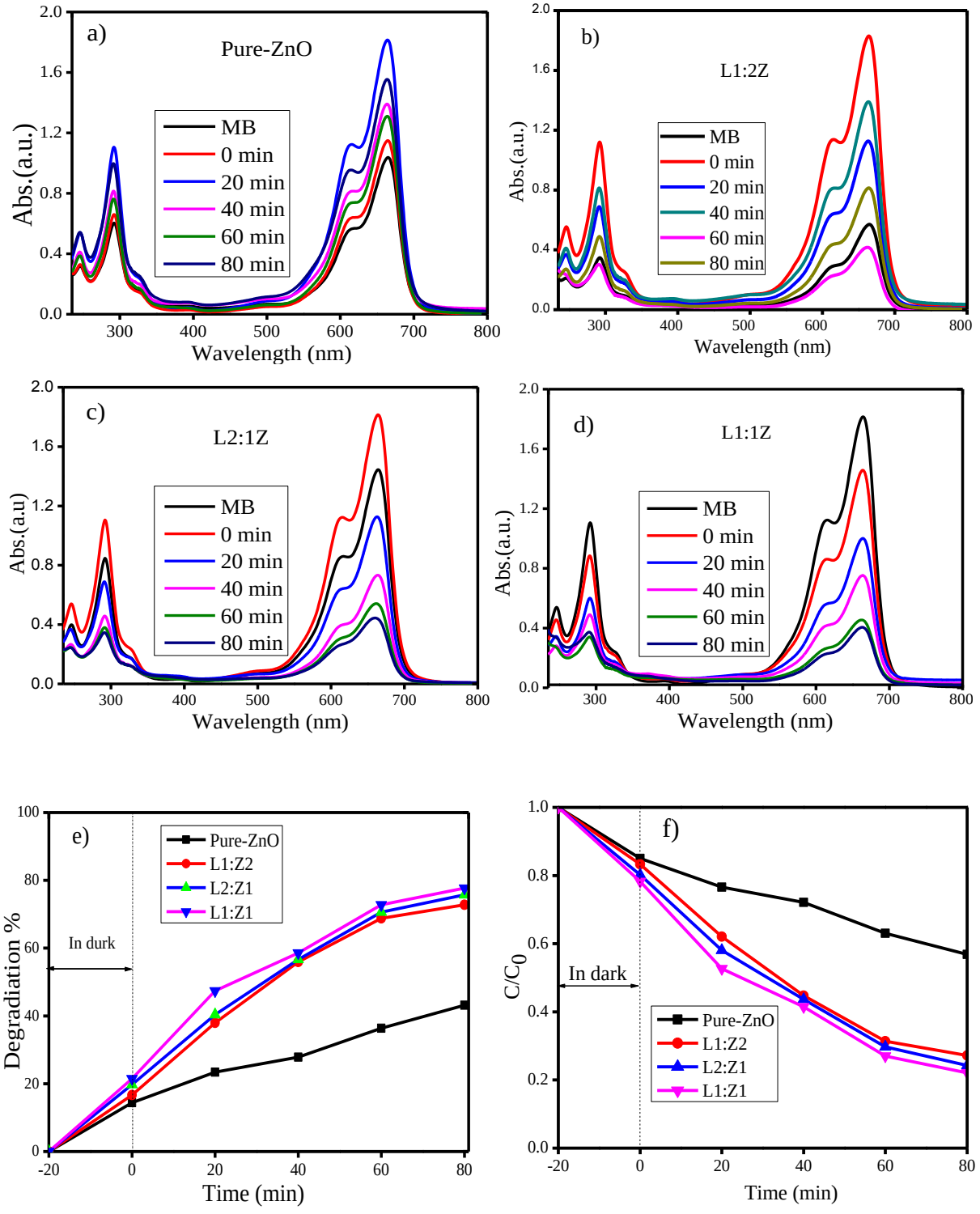

Figure 23 Photocatalytic Activity of a) pure-ZnO, b) L1:Z1, c) L2:Z1, d) L1:Z2 catalysts with different S. abyssinica leaf extract concentration, e) percentage degradation, f) C_t/C_0 of the degradation.

Photocatalytic Activity of all 1NZO, 3NZO, 5NZO, and 7NZO catalyst is done shown in Figure 24 (a-f) and the comparison depend up on the effect of Ni concentration in ZnO lattice are evaluated. It is observed that the 5NZO sample exhibits the highest photocatalytic activity (79.73 %), compared to the pure-ZnO, 1NZO, 3NZO, and 7NZO samples (33.1 %, 72.48 %, 74.12 % and 78.01 %, respectively), during 80 minute reaction time. This may be due to narrowed band gap, creation of electron trap level which prevents recombination, and lowered electron transfer resistance (Gnanamozhi et al., 2020) as compared to 1 % and 3 % of Ni, and due to lower distortion of ZnO lattice as compared to 7 % Ni doped ZnO (Gnanamozhi et al., 2020; Zhao et al., 2011). The photocatalyst was able to improve photogenerated carriers and light absorption by lowering the band gap of 5 percent Ni doped ZnO nanoparticles.

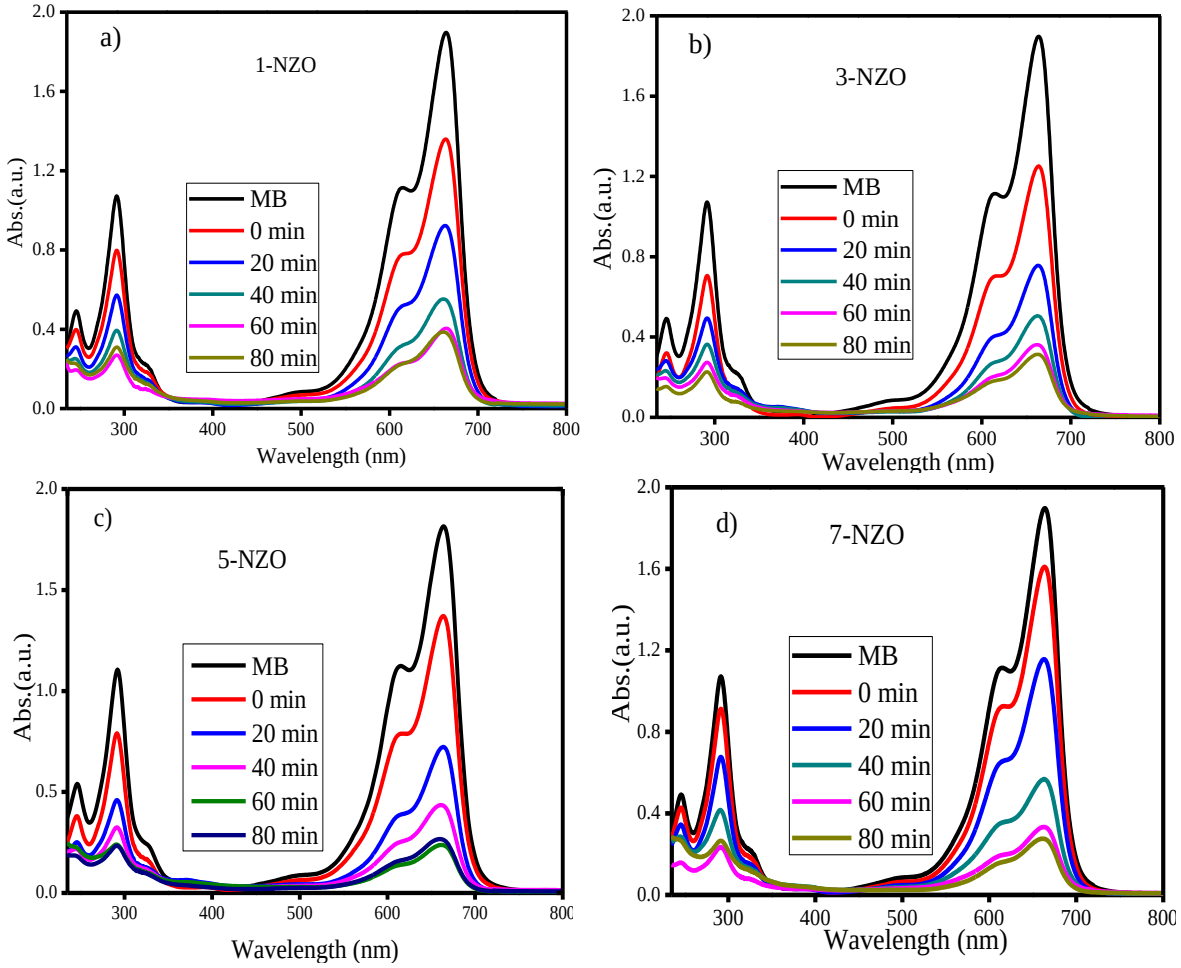

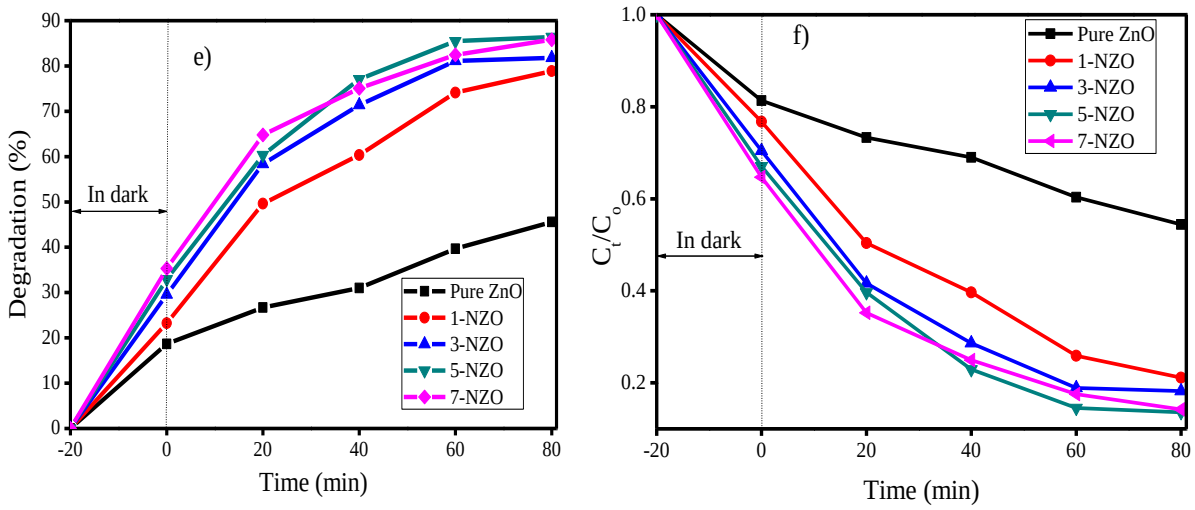

Figure 24 Photocatalytic Activity of a) 1NZO, b) 3NZO, c) 5NZO, d) 7NZO degradation on the effect of Ni concentration e) percentage degradation, f) C_t/C_0 of the degradation.

Photocatalytic Activity of all 5NZO, 2MZO, 1NMZO, 3NMZO, 5NMZO, 5NMZO, and 9NZMO are done as shown in Figure 25 (a-h) and the comparison of all samples as which catalyst have the highest photocatalytic activates due to different effects are evaluated. The rate of degradation usually depends on the stability, morphology, surface area, band gap, charge transferring resistance, photo elimination and crystalline structure of the photo-catalyst (Milenova et al., 2013). When 2 % Mn is doped on ZnO, the degradation efficiency increased from 69 % to 76.6 %. Moreover, when ZnO is co-doped with Mn and Ni- like 1NMZO, 3NMZO, 5NMZO, 7NMZO, and 9NMZO, degradation efficiency highly increased to 84.5 %, 92.8 %, 99.5 %, 97.3 %, and 92.3 % respectively. Hence, the 5NMZO catalyst exhibits the enhanced separation rate of electron-hole pairs; these in turn effectively degrade 99.5 % of MB dye within 60 min under visible light. It is seen that Mn/Ni dual-doped ZnO NP has a modified crystal structure, improved surface area, the band gap is tuned to the visible region, and the recombination is highly reduced, and hence generated more active sites on the photocatalyst surface. As to comparing the previous work to current in Table (9), the photocatalytic degradation of the current work is higher than the previous and S. abyssinica leaf contribution is very high. Even if degrading the methylene blue dyes with in the short period of time as compared to the previous.

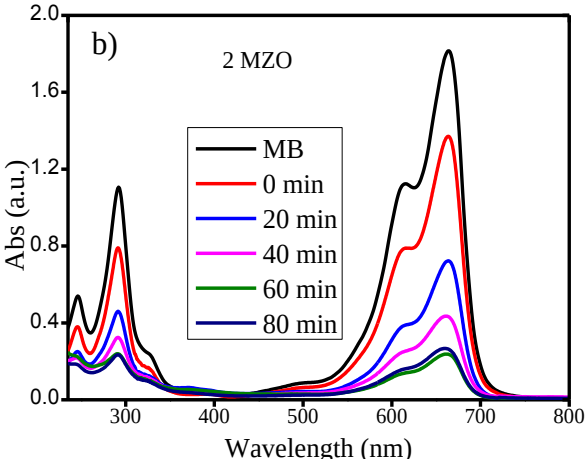
b)
2 MZO
MB
0 min
20 min
40 min
60 min
80 min
Abs (a.u.)
Wavelength (nm)

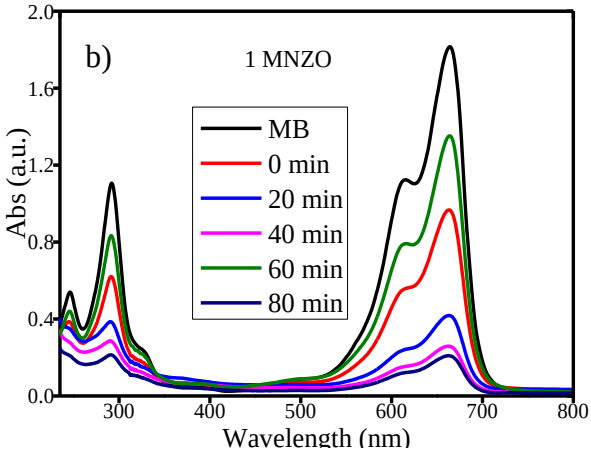
b)
1 MNZO
MB
0 min
20 min
40 min
60 min
80 min
Abs (a.u.)
Wavelength (nm)

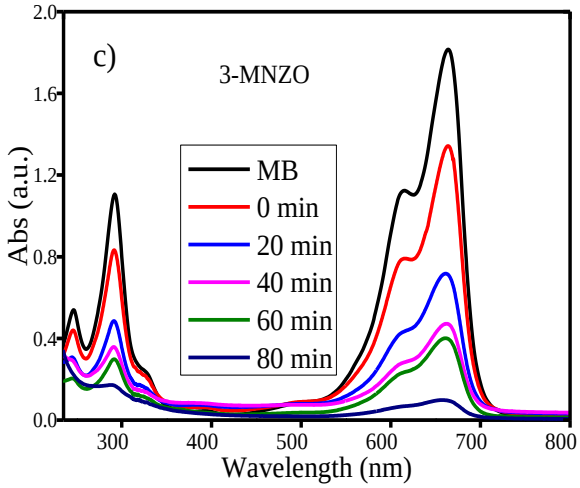
c)
3-MNZO
MB
0 min
20 min
40 min
60 min
80 min
Abs (a.u.)
Wavelength (nm)

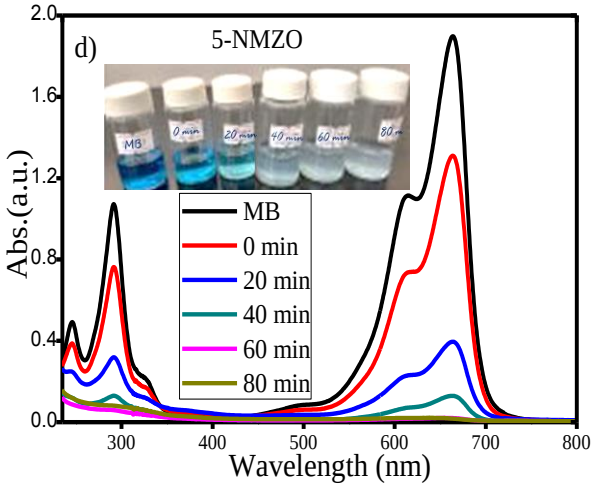
d)
5-NMZO
MB
0 min
20 min
40 min
60 min
80 min
Abs.(a.u.)
Wavelength (nm)

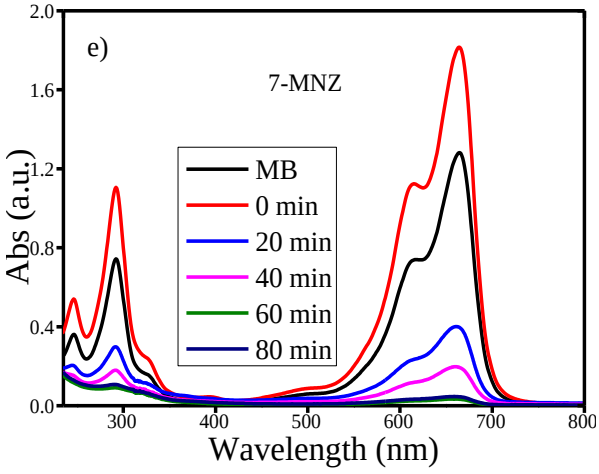
e)
7-MNZ
MB
0 min
20 min
40 min
60 min
80 min
Abs (a.u.)
Wavelength (nm)

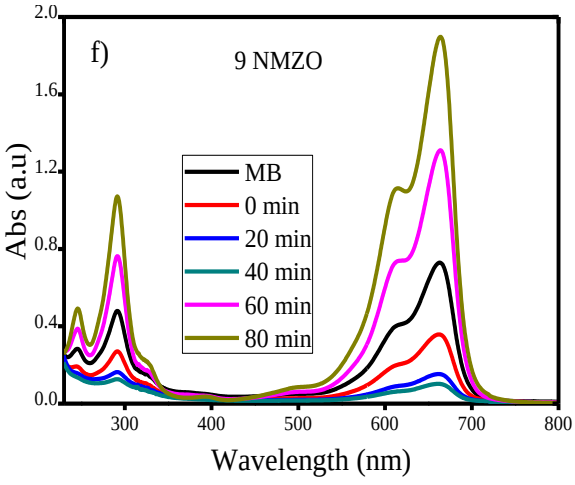
f)
9 NMZO
MB
0 min
20 min
40 min
60 min
80 min
Abs (a.u)
Wavelength (nm)

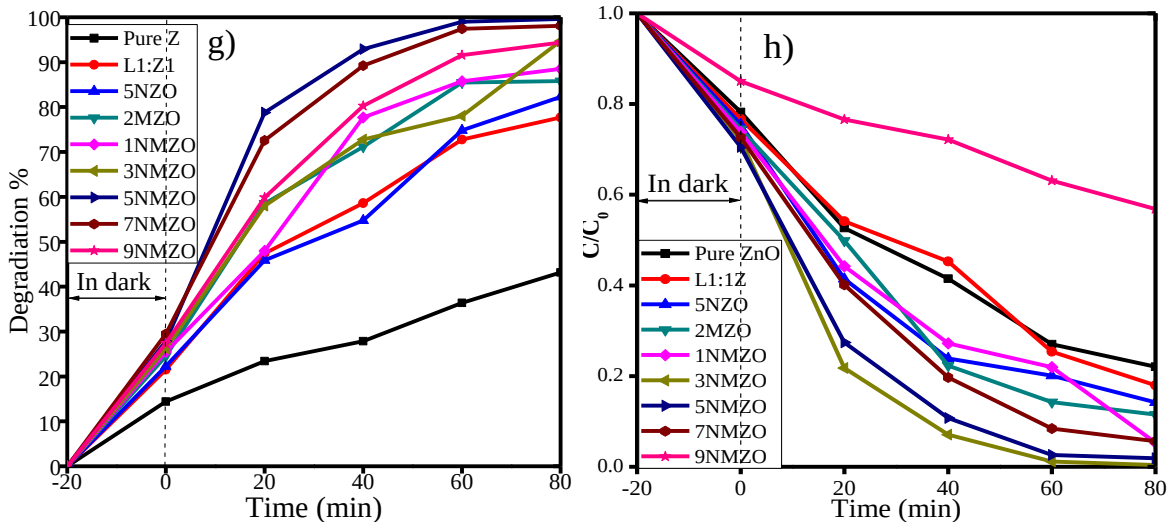

Figure 25 Photocatalytic Activity of a) 5NZO, a) 2MZO, b) 1NMZO, c) 3NMZO, d) 5NMZO, e) 5NMZO, f) 9NZMO degradation catalysts, g) percentage degradation, h) C_t/C_0 of the degradation.

Table 9 comparing the current photocatalytic degradation with previous works

No	Nanocatalysts	Biogenic source	dyes	Efficiency (%)	Time (min)	Reference
1	Cu - ZnO	Vernonia amygdalina	MB	60 %	100	(Okeke et al., 2020)
2	Ag- ZnO	Pedalium murex L.	MB	92.4 %	150	(Nagasundari, Muthu, Kaviyarasu, Al Farraj, & Alkufeidy, 2021)
3	Ag–ZnO	Capparis	MB	87 %	100	(Farooq et al., 2022)
4	Ag- ZnO	Sida rhombifolia	MB	57 %	200	(Babu & Antony, 2019)
5	Ag- ZnO	Pomegranate peel	MB	70 %	60	(Kaviya & Prasad, 2015)
6	Ag/ZnO	Padina gymnospora	MB	98.7 %	150	(Rajaboopathi & Thambidurai, 2018)
7	Mn/Mg - ZnO	Ocimum tenuiflorum	MB	78 %	60	(Subbiah, Muthukumaran, & Raja, 2020)
8	Mn/Mg - ZnO	Centella asiatica	MB	94.1 %	80	(Subbiah, Muthukumaran, & Raja, 2019)
9	ZnO	-	MB	33.1 %	80	The present work
10	ZnO	Stephania abyssinica	MB	72.5 %	80	The present work
11	Mn- ZnO	Stephania abyssinica	MB	76.6 %	80	The present work
12	Ni- ZnO	Stephania abyssinica	MB	79.7 %	80	The present work
13	Mn/Ni - ZnO	Stephania abyssinica	MB	99.5 %	80	The present work

4.12.1. Photodegradation Kinetics

Langmuir Hinshelwood kinetic equations were utilized to determine the kinetics of photodegradation. $lnC = -Kt + lnC_o$ (7)

Rearranging Eq. 7 gives

$ln\ C_o/C = kt$ (8)

Where Co and C are the initial dye concentration (mg L^{-1}) and the dye concentration (mg L^{-1}) at time t, and k is the pseudo-first-order reaction rate constant (min^{-1}), The initial concentration (C_o) and the ratio of dye concentration at time t (C) were plotted versus time.

The slopes were used to determine the degradation rate constants. Figure 26 (a, b) displays the curve fitting of pure-ZnO, L1:Z1, L2:Z1, and L1:Z2 degradation by the pseudo-kinetic equation and the rate constants (k) of those of those samples, and Table 10 shows the Percent Degradation Efficiency (PDE) and kinetic rate constant (k) and correlation coefficients (R^2). When we compared the degradation efficiency and degradation rate constant of pure-ZnO with different leaf concentrations, the Z1:L1 has degradation efficiency (72.5 %) and high degradation rate constant (16.9 x 10^{-3} min^{-1}) due to suitable particle Size and high surface area. The Figure 26 (c, d) shows the kinetic study of pure-ZnO, 1NZO, 3NZO, 5NZO and 7NZO degradation using pseudo-first-order kinetic plot and the rate constants (k) of those of those samples, and Table 11 revels due to the doping of Ni, the 5NZO had the greatest degradation efficiency (79.73 %) and highest degradation rate constant (21.46 x 10^{-3} min^{-1}). The Figure 27(e, f) shows the kinetic study of pure-ZnO, L1:Z1, 5NZO, 2MZO, 1NMZO, 3NMZO, 5NMZO and 9NZMO degradation using pseudo-first-order kinetic plot and the rate constants (k) of those of those samples, and Table 12 revels due to the doping of Mn and Ni, the 5NMZO had the greatest degradation efficiency (99.5 %), highest degradation rate constant (65.27 x 10^{-3} min^{-1}), and correlation coefficients (99.7 %). In comparison to other samples, this is owing to optimum Ni doping, a sufficient bandgap, a lower charge carrier recombination rate, and effective separation of photo-excited electron-hole pairs and oxygen vacancies (Reddy et al., 2020).

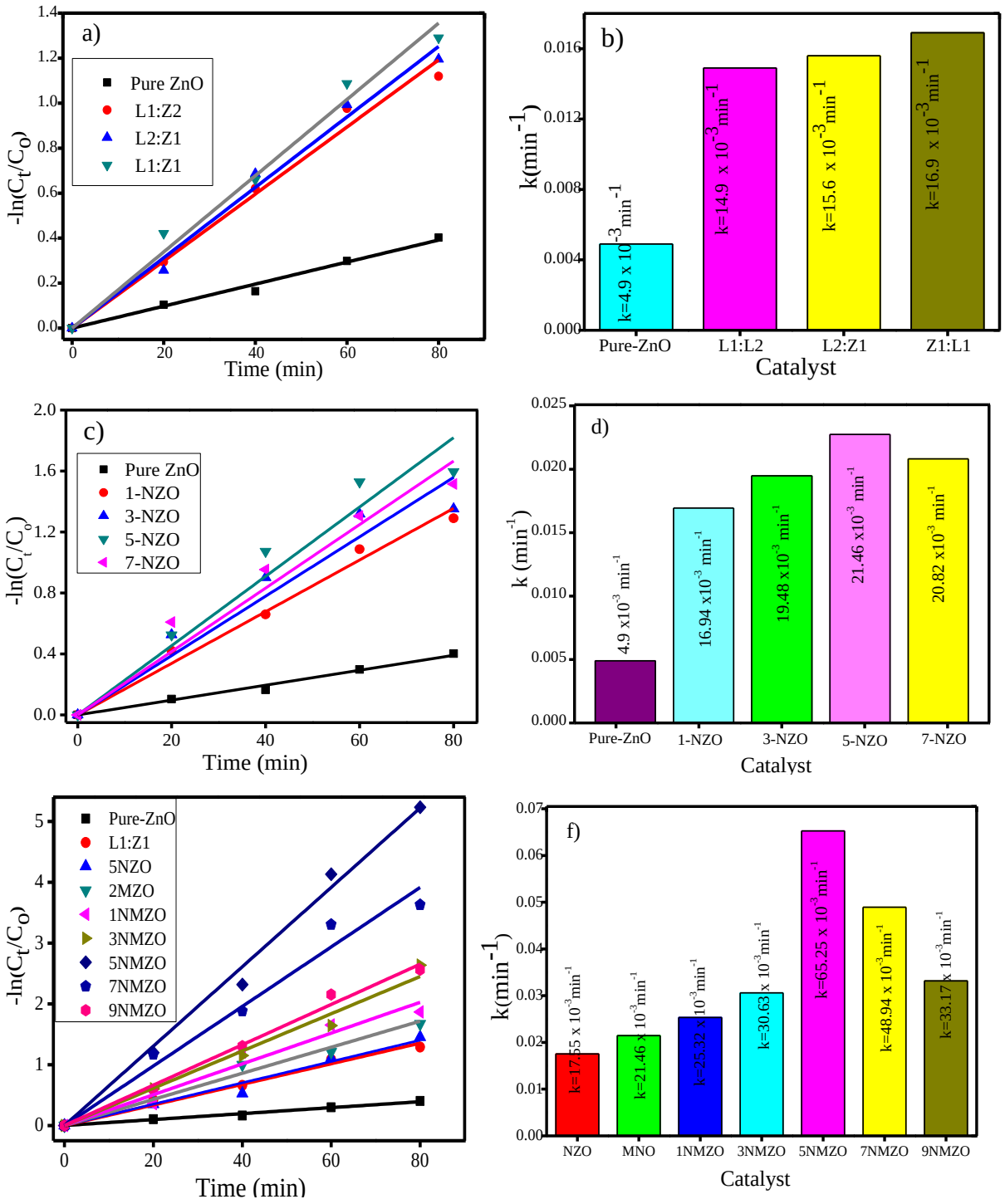

Figure 26 the kinetics study of a) pure-ZnO, L1:Z1, L2:Z1, and L1:Z2 degradation on the effect of leaf extract c) pure-ZnO, 1NZO, 3NZO, 5NZO, 7NZO degradation on the effect of Ni concentration e) pure-ZnO, L1:Z1, 5NZO, 2MZO, 1NMZO, 3NMZO, 5NMZO and 9NZMO degradation using pseudo-first-order kinetic plot, and (b, d, f) the rate constants of those catalysts

Table 10 the percentage degradation efficiency, kinetic rate constant, and correlation coefficients of pure-ZnO sample, and with different leaf concentrations

	Pure-ZnO	L1:L2	L2:Z1	Z1:L1
PDE %	33.12	67.41	69.73	72.54
K(min^{-1})	4.9 x 10^{-3}	14.9 x 10^{-3}	15.6 x 10^{-3}	16.9 x 10^{-3}
R^2	0.995	0.994	0.995	0.994

Table 11 the percentage degradation efficiency, kinetic rate constant, and correlation coefficients of pure-ZnO sample, and with different Ni-doping concentrations

	Pure-ZnO	1-NZO	3-NZO	5-NZO	7-NZO
PDE %	33.1	72.48	74.12	79.73	78.01
K(min^{-1})	4.9 x 10^{-3}	16.94 x 10^{-3}	19.48 x 10^{-3}	21.46 x 10^{-3}	20.82 x 10-3
R^2	0.995	0.994	0.973	0.990	0.982

Table 12 the percentage degradation efficiency, kinetic rate constant, and correlation coefficients of Mn/Ni doped ZnO samples

	2MZO	5NZO	1NMZO	3NMZO	5NMZO	7NMZO	9NMZO
PDE %	76.63	79.73	84.51	92.81	99.53	97.34	92.30
K (min^{-1})	17.55 x 10^{-3}	21.46 x 10^{-3}	25.32 x 10^{-3}	30.63 x 10^{-3}	65.27 x 10^{-3}	48.94 x 10^{-3}	33.17 x 10^{-3}
R^2	0.988	0.990	0.984	0.991	0.997	0.989	0.996

4.12.2. The pH Effect

The pH of the dye solution plays a vital role in photocatalytic decomposition reactions. In the present study, the 5NMZO catalyst test solution was analyzed for both acidic and alkaline pH by adding appropriate amounts of NaOH and HCL solutions. The MB degrading experiment was carried out in acidic media with a pH of 3 and 5, in a neutral with pH of 7 and in basic media with a pH of 9 and 11. As the pH of MB dye solution is increase,

the photocatalytic degrading efficiency of the catalyst increases gradually from acidic to basic as seen in Figure 27. This is because the redox potential of the MB dye is changed due to pH variation and resulted in the interatomic attraction force in between them which increases the catalytic activities (Jyothi & Ravichandran, 2020), the degrading efficiency of the 5NMZO catalyst is higher in basic media. However, in acidic environments, the MB degradation efficiency dropped, which could be connected to the positively charged surface of the catalyst, this is due to the same charge which resulting in a columbic repulsive force between the catalyst and the dye molecules and therefore the catalyst adsorption capacity is minimal (Krishnakumar & Imae, 2014).

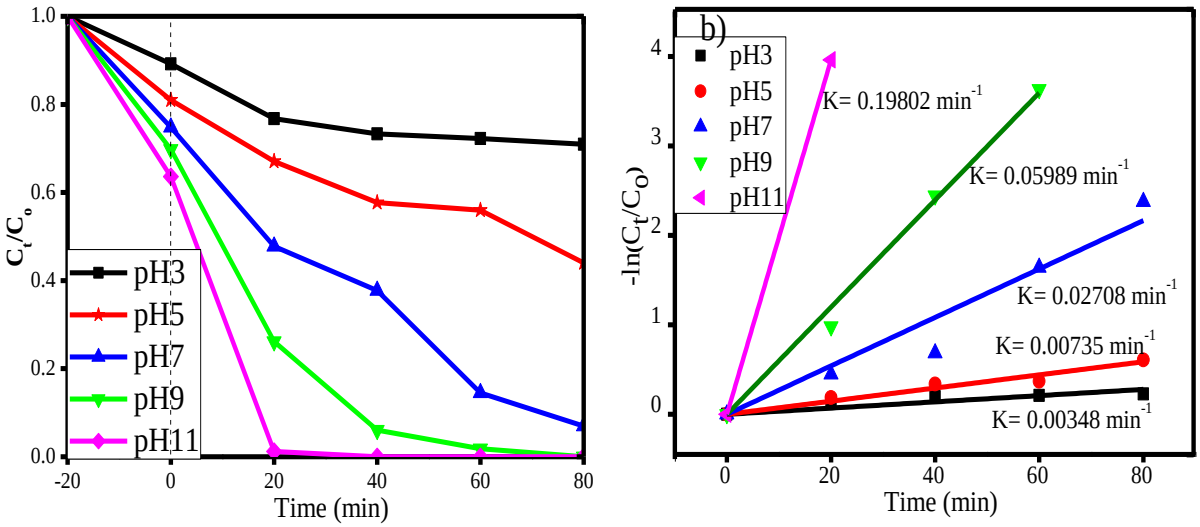

Figure 27 Effect of pH on degradation of Methylene blue at fixed 0.025 mg of 5NMZO catalyst and 10 ppm of MB solution

4.12.3. Effect of Catalytic Dosage on Degradation of MB

In order to evaluate the effect of catalyst dosage on photo degradation of MB, we have performed the experiment by varying the catalyst loading of 5NMZO from 0.1 to 0.5 g/L while other conditions like pH and MB dye concentration remain unchanged as conducted in photocatalytic activity. Figure 28 shows MB percent degradation as a function of catalyst loading where degradation efficiency increases with increasing catalyst dosage from 0.1 to 0.4 g L1 and then decreases when the catalytic dosage reach at 0.5 g/L. The increase in photo degradation of catalyst dosage from 0.1 to 0.4 g/L and maximum degradation efficiency at 0.4 g/L could be attributed due the availability of more active sites and penetration of light, which

could ultimately enhance the photocatalytic activity. At 0.5 g/L, photocatalytic activity is decreased when we compared with 0.4 g/L of catalyst. This may be due to an increase in the turbidity and cloudy or inhibits of the solution and nanoparticle aggregation, which could impede light penetration and lower the active sites of the catalyst (Raha et al., 2021). So, if there is no enough penetration of light, the charge separation between electron and hole will be decrease and the degradation efficiency is decreased.

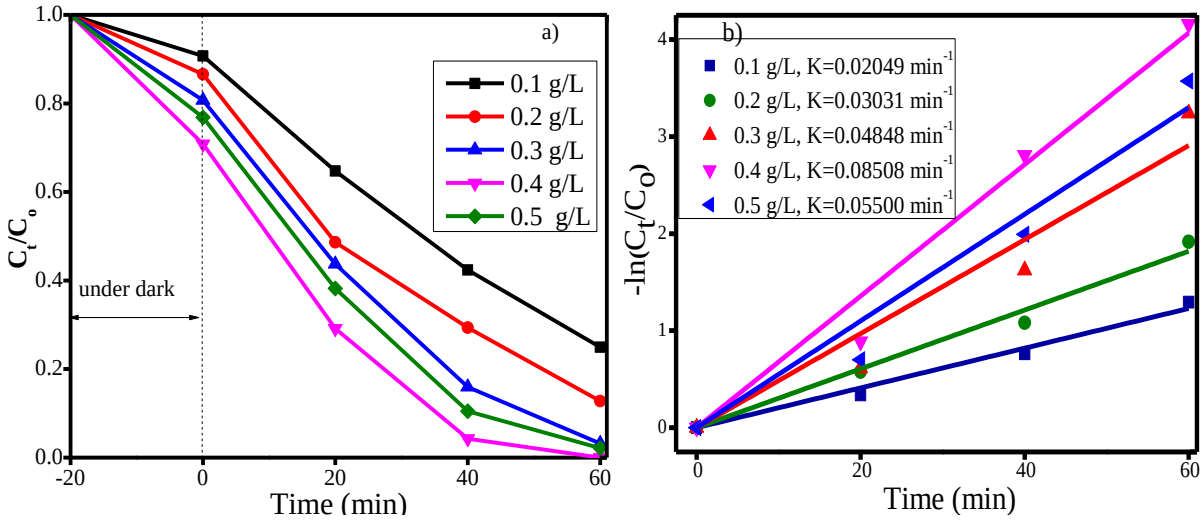

Figure 28 Effect of 5NMZO Catalytic dosage on degradation of Methylene blue at pH 7 and 10 ppm of MB solution

4.12.4. Reusability of Catalyst on Photocatalyst

The photocatalysts long-term stability and recyclability are critical for MB dye degradation as well as large-scale industrial application. The reuse experiment was used to assess the stability of the synthesized photocatalyst. As a result, the reusability of a produced 5NMZO nanocomposite thin film was tested for the degradation of MB dye under visible light illumination for five consecutive cycles, with the findings displayed in Figure 29**.** After each photocatalytic experiment, the catalyst was washed with distilled water and ethanol and collected in a silica crucible, and dried in an oven at 150 °C for 2 h (Magdalane et al., 2017). The obtained dry catalyst sample was subjected to 5 cycles of photocatalysts by maintaining the optimum condition pH 9, 25 mg L^{-1} of catalyst dose, and 10 ppm (mg L^{-1}) of dye solution for the degradation of MB dye under solar radiation. The reusability of the prepared catalyst was efficient up to 5 cycles, and there is small and marginal decrease in photocatalytic efficiency where the percent degradation drops by 5 % at the 5^{th} cycle. This may be because of

a decrease of active sites on catalytic surface and loss of catalyst during the recovery process (Karimi-Shamsabadi, Behpour, Babaheidari, & Saberi, 2017). The manufactured 5NMZO Nano catalyst for photocatalyst is very stable and reusable, based on these findings. Besides, XRD pattern obtained for the recycled photocatalyst showed stability of the characteristic crystallographic planes found in 5NMZO before use and after reuse, and it shows 5NMZO catalyst are more stable or no phase/crystallinity change until reused to five cycle.

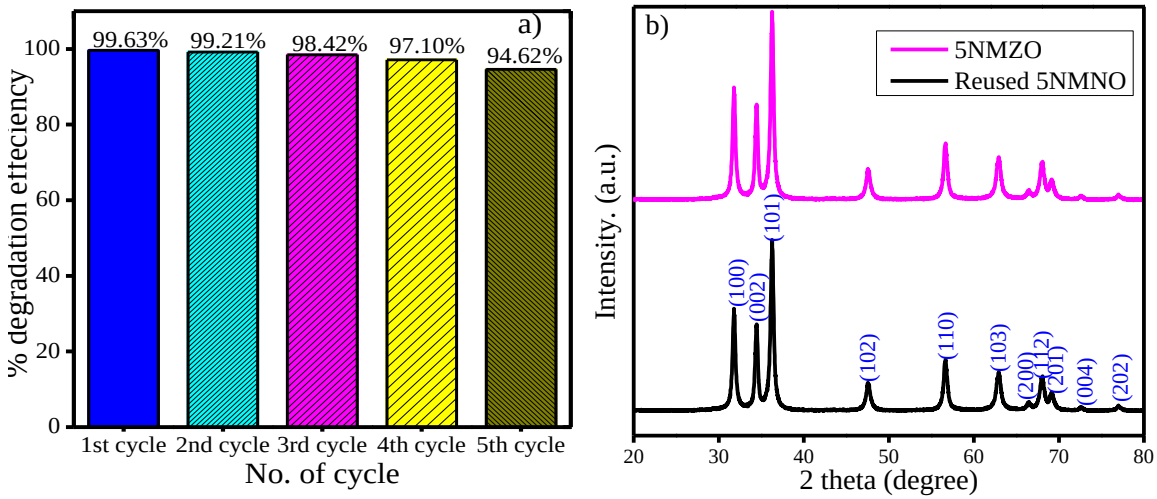

Figure 29 (a) Reusability test 5NMZO catalyst for photocatalytic degradation of Methylene blue under Visible light irradiation (b), XRD pattern obtained for the recycled 5NMZO catalyst

4.12.5 Mechanism of Photodegradation

The possible working mechanism of Ni/Mn co-doped ZnO proposed as following in figure 30. Because ZnO has a high energy bandgap (3.2 eV), direct excitation of electrons from the valance band (VB) to the conduction band (CB) in the presence of visible light is not easily possible. When Ni and Mn ions are added to the lattice, the energy band gap of ZnO is decreased to 2.62 eV. That is due to the development of impurity levels below CB in the bandgap, where electrons can migrate from VB of ZnO to these energy levels. If the energy of photon-induced, the electron-hole pair in the VB is separated and the induced electron travel to Ni and Mn, which can easily transfer the electron to conduction band and operate as an electron buffer, preventing the recombination of electron-hole pairs. The electrons in conduction band reacted with oxygen scavenged from the atmosphere by a catalyst to form

super oxide radicals (-°O_2) and hydroxide radicals (°OH), both of which are extremely responsive to breakdown methylene blues dyes from aqueous solutions. The holes in the catalyst's conduction band reacted with water to produce highly oxidative oxygen species known as °OH radicals. The methylene blue dyes were oxidized by the °OH and holes, resulting in CO_2, H_2O, and non-toxic by-products. This could explain the greater photocatalytic activity of Ni–Mn co-doped ZnO NPs compared to naked ZnO NPs. The reaction of photocatalytic abilities could be best delineated by the following equations:

$$ZnO(e^-_{CB}) + O_2 \rightarrow ZnO + O^{-\cdot}_2 \quad (9)$$

$$h^+_{VB} + H_2O \rightarrow OH^{\cdot} + H^+ \quad (10)$$

$$h^+_{VB} + H_2O \rightarrow H_2O_2 + 2H^+ \quad (11)$$

$$H_2O_2 + e^- \rightarrow OH^{\cdot} + OH^- \quad (12)$$

$$O^{\cdot -}_2 + 2H^+ + e^- \rightarrow H_2O_2 \quad (13)$$

$$H_2O_2 + e^- \rightarrow OH^{\cdot} + OH^- \quad (14)$$

$$O^{\cdot -}_2 / OH^{\cdot} + \text{Methylene Blue} \rightarrow C_2O + H_2O + \text{Intermediates}$$

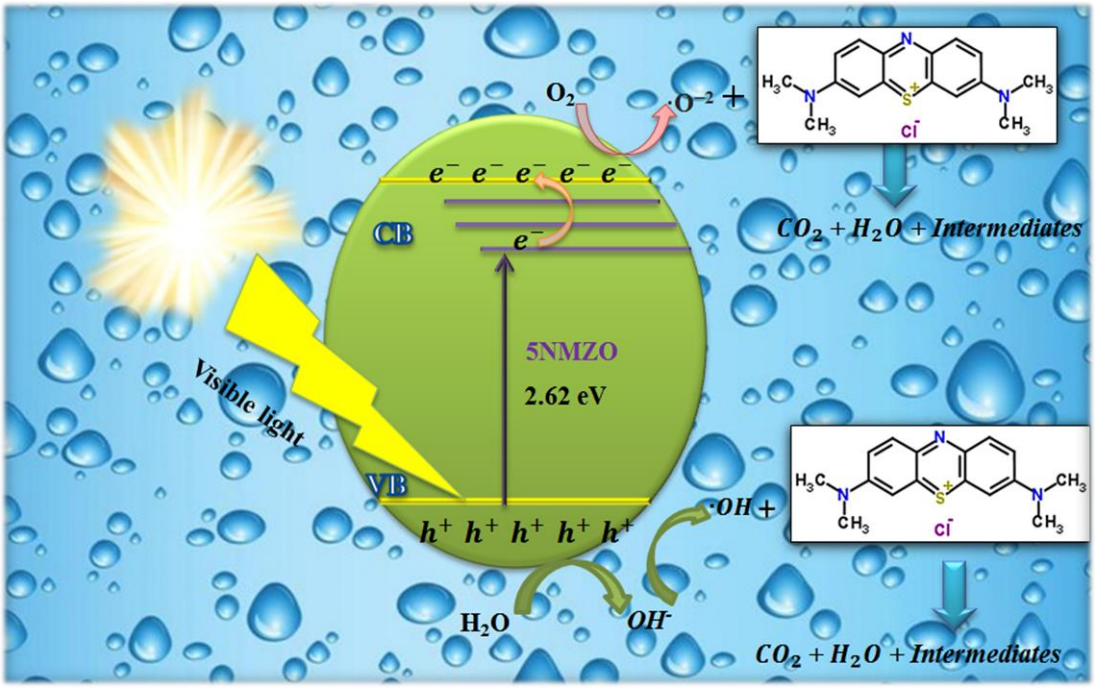

Figure 30 the photo catalysis mechanisms of Ni/Mn co-doped ZnO/leaf extract

5. CONCLUSION AND RECOMMENDATIONS

5.1 Conclusions

The (Mn, Ni) Co-doped ZnO nanostructures using S. abyssinica leaf was synthesized by co-precipitation method. The variation of leaf extract and dopants was done and their names were assigned as ZnO, L1:Z1, L2:Z1, L1:Z2, 1NZO, 3NZO, 5NZO, 7NZO, 2MZO, 1NMZO, 3NMZO, 5NMZO, 7NMZO, and 9NMZO. The composite catalyst was characterized by different techniques. The XRD results confirmed that ZnO is crystalline hexagonal structure with no other impurities peaks and crystalline sizes varied from 36.17 to 17.32 nm due to leaf extract and the dopant concentration, *and* the change in intensities and phase shift due to leaf concentration and Ni/Mi dopants. The thermal properties indicated the co-doping of Ni/Mn on ZnO increases the thermal stability of ZnO. The FT-IR indicated the expected functional groups were well bonded. The morphology indicated that the presence of leaf extract prevents aggregation and controls particle size. The TEM confirmed the particle size and shape which was known in SEM. The HRTEM indicates the d-spacing was well matched with spacing between (002) crystal planes. The presence of Ni^{2+} and Mn^{2+} from XPS indicated that the Ni^{2+} ion and Mn^{2+} have been able to successfully incorporate into the ZnO lattice. Due to doping of Ni/Mn, the tuned band gap tuned from 3.2 eV to 2.62 eV at the 5NMZO catalyst indicated the material was well candidates to ward visible light. The decreased in PL intensity indicated the decreased in recombination rate. The low charge transfer resistance in 5NMZO indicated the charge was easy to transfer. The 99.5 % degradation shows 5NMZO catalyst exhibits highest photocatalytic activities. Those may be due to is due to the low recombination, lower electron transfer resistance, high absorption of visible light, low agglomeration, and high surface area. The highest photocatalytic activity at pH 11 indicates the interatomic attraction force in between negatively charged 5NMZO catalyst and the positively charged MB which to be adsorbed to the surface of the catalyst. The increased in photo degradation efficiency at 0.4 g/L could be attributed to the availability of more active sites and easiness to penetration of light. The reusability of the prepared catalyst up to 5 cycles indicates the catalyst was stable and efficient.

5.2. Recommendations

It can be recommended that many works are used to enhance the photocatalytic performance of ZnO in practical application. The following recommendation can be applied to make the research work completed.

1. The effect of other parameters should be studied in the degradation of different organic and inorganic pollutants.
2. Further characterization like photocurrent is needed to confirm the photoluminescence.
3. It is possible to use for other organic dyes degradation, like methylene orange, Congo red, Naphthol Yellow, etc.
4. Ii is possible to use for various applications such as in acoustic devices, solar cells , piezoelectric devices, medicines, transistors, textiles, rubber products, light emitting diodes, laser diodes, food packaging.
5. It is also nice to use in chemical and biosensors and as an antibacterial, antifungal agent

Reference

Aboulaich, A., Balan, L., Ghanbaja, J., Medjahdi, G., Merlin, C., & Schneider, R. (2011). Aqueous route to biocompatible ZnSe: Mn/ZnO core/shell quantum dots using 1-thioglycerol as stabilizer. *Chemistry of Materials, 23*(16), 3706-3713.

Achouri, F., Corbel, S., Balan, L., Mozet, K., Girot, E., Medjahdi, G., . . . Schneider, R. (2016). Porous Mn-doped ZnO nanoparticles for enhanced solar and visible light photocatalysis. *Materials & Design, 101*, 309-316.

Adeyemi, J. O., Elemike, E. E., & Onwudiwe, D. C. (2019). ZnO nanoparticles mediated by aqueous extracts of Dovyalis caffra fruits and the photocatalytic evaluations. *Materials Research Express, 6*(12), 125091.

Ahmad, K. S., & Jaffri, S. B. (2018). Phytosynthetic Ag doped ZnO nanoparticles: Semiconducting green remediators. *Open Chemistry, 16*(1), 556-570. doi:doi:10.1515/chem-2018-0060

Ahmad, M., Rehman, W., Khan, M. M., Qureshi, M. T., Gul, A., Haq, S., . . . Menaa, F. (2021). Phytogenic fabrication of ZnO and gold decorated ZnO nanoparticles for photocatalytic degradation of Rhodamine B. *Journal of Environmental Chemical Engineering, 9*(1), 104725.

Ajala, F., Lachheb, H., Bouazizi, N., & Houas, A. (2017). Synthesis of Li-doped ZnO via sol–gel process: structural, optical and photocatalytic properties. *Journal of Materials Science: Materials in Electronics, 28*(3), 2817-2825.

Al-Ghafri, B., Bora, T., Sathe, P., Dobrestov, S., & Al-Abri, M. (2018). Photocatalytic microbial removal and degradation of organic contaminants of water using PES fibers. *Applied Catalysis B: Environmental, 233*, 136-142.

Al-Rasheed, R. A. (2005). *Water treatment by heterogeneous photocatalysis an overview*. Paper presented at the Fourth SWCC Acquired Experience Symposium.

Alhefeiti, M. A., Athamneh, K., Vijayan, R., & Ashraf, S. S. (2021). Bioremediation of various aromatic and emerging pollutants by Bacillus cereus sp. isolated from petroleum sludge. *Water Science and Technology, 83*(7), 1535-1547.

Alshehri, A. A., & Malik, M. A. (2019). Biogenic fabrication of ZnO nanoparticles using Trigonella foenum-graecum (Fenugreek) for proficient photocatalytic degradation of methylene blue under UV irradiation. *Journal of Materials Science: Materials in Electronics, 30*(17), 16156-16173.

Aminuzzaman, M., Ying, L. P., Goh, W.-S., & Watanabe, A. (2018). Green synthesis of zinc oxide nanoparticles using aqueous extract of Garcinia mangostana fruit pericarp and their photocatalytic activity. *Bulletin of Materials Science, 41*(2), 1-10.

Anandan, S., & Muthukumaran, S. (2015). Microstructural, crystallographic and optical characterizations of Cu-doped ZnO nanoparticles co-doped with Ni. *Journal of Materials Science: Materials in Electronics, 26*(6), 4298-4307.

Anandan, S., Vinu, A., Lovely, K. S., Gokulakrishnan, N., Srinivasu, P., Mori, T., . . . Ariga, K. (2007). Photocatalytic activity of La-doped ZnO for the degradation of monocrotophos in aqueous suspension. *Journal of Molecular Catalysis A: Chemical, 266*(1-2), 149-157.

Angasa, E., Jamarun, N., & Arief, S. (2020). The effect of Impatiens balsamina L. extract on structural, morphological, optical, and photocatalytic properties of Zn2SnO4. *Journal of Materials Research and Technology, 9*(6), 12917-12925.

Antonopoulou, M., Kosma, C., Albanis, T., & Konstantinou, I. (2020). An overview of homogeneous and heterogeneous photocatalysis applications for the removal of pharmaceutical compounds from real or synthetic hospital wastewaters under lab or pilot scale. *Science of the Total Environment*, 144163.

Aragaw, S. G., Sabir, F. K., Andoshe, D. M., & Zelekew, O. A. (2020). Green synthesis of p-Co3O4/n-ZnO composite catalyst with eichhornia crassipes plant extract mediated for methylene blue degradation under visible light irradiation. *Materials Research Express, 7*(9), 095508.

Archana, B., Manjunath, K., Nagaraju, G., Sekhar, K. C., & Kottam, N. (2017). Enhanced photocatalytic hydrogen generation and photostability of ZnO nanoparticles obtained via green synthesis. *International Journal of Hydrogen Energy, 42*(8), 5125-5131.

Ashokkumar, R., & Ramaswamy, M. (2014). Phytochemical screening by FTIR spectroscopic analysis of leaf extracts of selected Indian medicinal plants. *International journal of Current Microbiology and applied Sciences, 3*(1), 395-406.

Babu, A. T., & Antony, R. (2019). Green synthesis of silver doped nano metal oxides of zinc & copper for antibacterial properties, adsorption, catalytic hydrogenation & photodegradation of aromatics. *Journal of Environmental Chemical Engineering, 7*(1), 102840.

Bai, W., Wu, Z., Mitra, S., & Brown, J. M. (2016). Effects of multiwalled carbon nanotube surface modification and purification on bovine serum albumin binding and biological responses. *Journal of Nanomaterials, 2016*.

Barick, K., Singh, S., Aslam, M., & Bahadur, D. (2010). Porosity and photocatalytic studies of transition metal doped ZnO nanoclusters. *Microporous and Mesoporous Materials, 134*(1-3), 195-202.

Basavalingiah, K., Harishkumar, S., Nagaraju, G., & Rangappa, D. (2019). Highly porous, honeycomb like Ag–ZnO nanomaterials for enhanced photocatalytic and photoluminescence studies: green synthesis using Azadirachta indica gum. *SN Applied Sciences, 1*(8), 1-13.

Becerra-Castro, C., Lopes, A. R., Vaz-Moreira, I., Silva, E. F., Manaia, C. M., & Nunes, O. C. (2015). Wastewater reuse in irrigation: A microbiological perspective on implications in soil fertility and human and environmental health. *Environment international, 75*, 117-135.

Beentje, H. J. (1994). Kenya: trees, shrubs and lianas.

Bhatkhande, D. S., Pangarkar, V. G., & Beenackers, A. A. C. M. (2002). Photocatalytic degradation for environmental applications–a review. *Journal of Chemical Technology & Biotechnology: International Research in Process, Environmental & Clean Technology, 77*(1), 102-116.

Bhuyan, T., Mishra, K., Khanuja, M., Prasad, R., & Varma, A. (2015). Biosynthesis of zinc oxide nanoparticles from Azadirachta indica for antibacterial and photocatalytic applications. *Materials Science in Semiconductor Processing, 32*, 55-61.

Biswas, B. D., Purkayastha, M. D., Tiwari, E., Denrah, S., Sarkar, M., Darbha, G. K., & Majumder, T. P. (2021). Study of the photocatalytic activity of Mn-doped ZnO nanocomposites depending on their morphology and structure with the variation of manganese concentration. *Surfaces and Interfaces, 23*, 100902.

Biswas, R., Banerjee, B., Saha, M., Ahmed, I., Mete, S., Patil, R. A., . . . Haldar, K. K. (2021). Green Approach for the Fabrication of Au/ZnO Nanoflowers: A Catalytic Aspect. *The Journal of Physical Chemistry C, 125*(12), 6619-6631.

Booshehri, A. Y., Goh, S. C.-K., Hong, J., Jiang, R., & Xu, R. (2014). Effect of depositing silver nanoparticles on BiVO 4 in enhancing visible light photocatalytic inactivation of bacteria in water. *Journal of Materials Chemistry A, 2*(17), 6209-6217.

Budianto, E., Yulizar, Y., Saputra, I. S., & Sudirman, S. (2021). *Green synthesis of Au-doped ZnO nanoparticles by in-situ process using Imperata cylindrica L leaf extract.* Paper presented at the AIP Conference Proceedings.

Cao, Y., Yu, Y., Zhang, P., Zhang, L., He, T., & Cao, Y. (2013). An enhanced visible-light photocatalytic activity of TiO2 by nitrogen and nickel–chlorine modification. *Separation and Purification Technology, 104*, 256-262. doi:10.1016/j.seppur.2012.11.030

Castro, L., Blázquez, M. L., Muñoz, J. A., González, F., García-Balboa, C., & Ballester, A. (2011). Biosynthesis of gold nanowires using sugar beet pulp. *Process Biochemistry, 46*(5), 1076-1082.

Chai, H.-Y., Lam, S.-M., & Sin, J.-C. (2019). Green synthesis of magnetic Fe-doped ZnO nanoparticles via Hibiscus rosa-sinensis leaf extracts for boosted photocatalytic, antibacterial and antifungal activities. *Materials Letters, 242*, 103-106.

Challis, J. K., Hanson, M. L., Friesen, K. J., & Wong, C. S. (2014). A critical assessment of the photodegradation of pharmaceuticals in aquatic environments: defining our current understanding and identifying knowledge gaps. *Environmental Science: Processes & Impacts, 16*(4), 672-696.

Chan, Y. Y., Pang, Y. L., Lim, S., Lai, C. W., Abdullah, A. Z., & Chong, W. C. (2019). Biosynthesized Fe-and Ag-doped ZnO nanoparticles using aqueous extract of Clitoria ternatea Linn for enhancement of sonocatalytic degradation of Congo red. *Environmental Science and Pollution Research*, 1-17.

Chang, C.-J., Yang, T.-L., & Weng, Y.-C. (2014). Synthesis and characterization of Cr-doped ZnO nanorod-array photocatalysts with improved activity. *Journal of Solid State Chemistry, 214*, 101-107.

Chang, Y.-C. (2014). Ni-doped ZnO nanotower arrays with enhanced optical and field emission properties. *RSC Advances, 4*(99), 56241-56247.

Chaudhury, S., Mishra, V., & Shah, D. (2019). Highly selective separation of pertechnetate from waste water. *Journal of Water Process Engineering, 31*, 100896.

Chauhan, A., Verma, R., Kumari, S., Sharma, A., Shandilya, P., Li, X., . . . Kumar, R. (2020). Photocatalytic dye degradation and antimicrobial activities of Pure and Ag-doped ZnO using Cannabis sativa leaf extract. *Scientific reports, 10*(1), 1-16.

Chemingui, H., Missaoui, T., Mzali, J. C., Yildiz, T., Konyar, M., Smiri, M., . . . Yatmaz, H. (2019). Facile green synthesis of zinc oxide nanoparticles (ZnO NPs): antibacterial and photocatalytic activities. *Materials Research Express, 6*(10), 1050b1054.

Chiang, M.-Y., & Lin, H.-N. (2015). Enhanced photocatalysis of ZnO nanowires co-modified with cuprous oxide and silver nanoparticles. *Materials Letters, 160*, 440-443.

Crini, G., & Lichtfouse, E. (2019). Advantages and disadvantages of techniques used for wastewater treatment. *Environmental Chemistry Letters, 17*(1), 145-155.

Cuijin, P., Guoping, H., Yan, Z., Hua, Z., Bin, L., Lijuan, C., . . . Sheng, Z. (2016). Superior adsorption performance for triphenylmethane dyes on 3D architectures assembled by ZnO nanosheets as thin as 1.5 nm. *J Hazard Mater, 318*, 732-741.

Dagne, E., Gunatilaka, A. L., Kingston, D. G., & Alemu, M. (1993). 4'-O-methylstephavanine from Stephania abyssinica. *Journal of natural products, 56*(11), 2022-2025.

Das, D., Datta, A. K., Kumbhakar, D. V., Ghosh, B., Pramanik, A., Gupta, S., & Mandal, A. (2017). Assessment of photocatalytic potentiality and determination of ecotoxicity (using plant model for better environmental applicability) of synthesized copper, copper oxide and copper-doped zinc oxide nanoparticles. *PloS one, 12*(8), e0182823.

Dhanalakshmi, A., Natarajan, B., Ramadas, V., Palanimurugan, A., & Thanikaikarasan, S. (2016). Structural, morphological, optical and antibacterial activity of rod-shaped zinc oxide and manganese-doped zinc oxide nanoparticles. *Pramana, 87*(4), 1-9.

Dhivya, A., & Yadav, R. (2021). An Eco-approach synthesis of undoped and Mn doped ZnO nano-photocatalyst for prompt decoloration of methylene blue dye. *Materials Today: Proceedings*.

Dhivya, A., Yadav, R., & Powrnika, S. (2019). Green synthesis of selenium doped zinc oxide nanoparticles using mangifera indica leaf extract and its photodegradation and antibacterial activities. *Journal of Nanoscience and Technology*, 741-744.

Di Fonzo, F., Casari, C. S., Russo, V., Brunella, M. F., Bassi, A. L., & Bottani, C. E. (2008). Hierarchically organized nanostructured TiO2 for photocatalysis applications. *Nanotechnology, 20*(1), 015604.

Di Mauro, A., Fragala, M. E., Privitera, V., & Impellizzeri, G. (2017). ZnO for application in photocatalysis: From thin films to nanostructures. *Materials Science in Semiconductor Processing, 69*, 44-51.

Diallo, A., Kaviyarasu, K., Ndiaye, S., Mothudi, B., Ishaq, A., Rajendran, V., & Maaza, M. (2018). Structural, optical and photocatalytic applications of biosynthesized NiO nanocrystals. *Green Chemistry Letters and Reviews, 11*(2), 166-175.

Diallo, A., Ngom, B., Park, E., & Maaza, M. (2015). Green synthesis of ZnO nanoparticles by Aspalathus linearis: structural & optical properties. *Journal of Alloys and Compounds, 646*, 425-430.

Dreaden, E. C., Alkilany, A. M., Huang, X., Murphy, C. J., & El-Sayed, M. A. (2012). The golden age: gold nanoparticles for biomedicine. *Chemical Society Reviews, 41*(7), 2740-2779.

Du, Y., Chen, R., Yao, J., & Wang, H. (2013). Facile fabrication of porous ZnO by thermal treatment of zeolitic imidazolate framework-8 and its photocatalytic activity. *Journal of Alloys and Compounds, 551*, 125-130.

Duan, J., Liu, X., Han, Q., & Wang, X. (2011). Controlled morphologies and optical properties of ZnO films and their photocatalytic activities. *Journal of Alloys and Compounds, 509*(37), 9255-9263.

Dwivedi, A. K. (2017). Researches in water pollution: A review. *International Research Journal of Natural and Applied Sciences*, *4*(1), 118-142.

Ebadi, A., Soltan Mohammadzadeh, J. S., & Khudiev, A. (2009). What is the correct form of BET isotherm for modeling liquid phase adsorption? *Adsorption, 15*(1), 65-73.

Ebrahimian, J., Mohsennia, M., & Khayatkashani, M. (2021). Catalytic and photocatalytic activity of Urtica dioica-mediated Ud-ZnO nanoparticles. *Optical Materials, 120*, 111404.

El-Khouly, M. E., El-Mohsnawy, E., & Fukuzumi, S. (2017). Solar energy conversion: From natural to artificial photosynthesis. *Journal of photochemistry and photobiology C: Photochemistry Reviews, 31*, 36-83.

Fang, Y. (2017). *Structural parameters (size, defect and doping) of ZnO nanostructures and relations with their optical and electrical properties.* Universitätsbibliothek.

Farooq, M., Shujah, S., Tahir, K., Nazir, S., Khan, A. U., Almarhoon, Z. M., . . . Ullah, A. (2022). Ultra efficient 4-Nitrophenol reduction, dye degradation and Cr (VI) adsorption in the presence of phytochemical synthesized Ag/ZnO nanocomposite: A view towards sustainable chemistry. *Inorganic Chemistry Communications*, 109189.

Fodem, C., Nguelefack-Mbuyo, E. P., Ndjenda II, M. K., Kamanyi, A., & Nguelefack, T. B. (2021). Vasorelaxant-Mediated Antihypertensive Effect of the Leaf Aqueous Extract from Stephania abyssinica (Dillon & A. Rich) Walp (Menispermaceae) in Rat. *BioMed Research International, 2021*.

Fuerte, A., Hernández-Alonso, M. D., Maira, A. J., Martínez-Arias, A., Fernández-García, M., Conesa, J. C., . . . Munuera, G. (2002). Nanosize Ti–W Mixed Oxides: Effect of Doping Level in the Photocatalytic Degradation of Toluene Using Sunlight-Type Excitation. *Journal of Catalysis, 212*(1), 1-9. doi:10.1006/jcat.2002.3760

Ganesh, R. S., Durgadevi, E., Navaneethan, M., Patil, V., Ponnusamy, S., Muthamizhchelvan, C., . . . Hayakawa, Y. (2017). Controlled synthesis of Ni-doped ZnO hexagonal microdiscs and their gas sensing properties at low temperature. *Chemical Physics Letters, 689*, 92-99.

Gayen, R., Majumder, S., Varma, S., & Pal, A. (2010). Vertically aligned Mn-doped zinc oxide nanorods by hybrid wet chemical route. *Materials Chemistry and Physics, 123*(1), 138-146.

Geetha, M., Nagabhushana, H., & Shivananjaiah, H. (2016). Green mediated synthesis and characterization of ZnO nanoparticles using Euphorbia Jatropa latex as reducing agent. *Journal of Science: Advanced Materials and Devices, 1*(3), 301-310.

Giri, P., Bhattacharyya, S., Singh, D. K., Kesavamoorthy, R., Panigrahi, B., & Nair, K. (2007). Correlation between microstructure and optical properties of ZnO nanoparticles synthesized by ball milling. *Journal of Applied Physics, 102*(9), 093515.

Gnanamozhi, P., Renganathan, V., Chen, S.-M., Pandiyan, V., Arockiaraj, M. A., Alharbi, N. S., . . . Alanzi, K. F. (2020). Influence of Nickel concentration on the photocatalytic dye degradation (methylene blue and reactive red 120) and antibacterial activity of ZnO nanoparticles. *Ceramics International, 46*(11), 18322-18330.

Grassi, M., Kaykioglu, G., Belgiorno, V., & Lofrano, G. (2012). Removal of emerging contaminants from water and wastewater by adsorption process *Emerging compounds removal from wastewater* (pp. 15-37): Springer.

Grilli, M. L. (2020). Metal oxides: Multidisciplinary Digital Publishing Institute.

Guo, Y., Cao, X., Lan, X., Zhao, C., Xue, X., & Song, Y. (2008). Solution-based doping of manganese into colloidal ZnO nanorods. *The Journal of Physical Chemistry C, 112*(24), 8832-8838.

Hamid, S. B. A., Teh, S. J., & Lai, C. W. (2017). Photocatalytic water oxidation on ZnO: a review. *Catalysts, 7*(3), 93.

Hojjati-Najafabadi, A., Davar, F., Enteshari, Z., & Hosseini-Koupaei, M. (2021). Antibacterial and photocatalytic behaviour of green synthesis of Zn0. 95Ag0. 05O nanoparticles using herbal medicine extract. *Ceramics International*.

Ibhadon, A. O., & Fitzpatrick, P. (2013). Heterogeneous photocatalysis: recent advances and applications. *Catalysts, 3*(1), 189-218.

Iravani, S. (2011). Green synthesis of metal nanoparticles using plants. *Green Chemistry, 13*(10), 2638-2650.

Ishwarya, R., Vaseeharan, B., Kalyani, S., Banumathi, B., Govindarajan, M., Alharbi, N. S., . . . Benelli, G. (2018). Facile green synthesis of zinc oxide nanoparticles using Ulva

lactuca seaweed extract and evaluation of their photocatalytic, antibiofilm and insecticidal activity. *Journal of Photochemistry and Photobiology B: Biology, 178*, 249-258.

Ismail, A. A., El-Midany, A., Abdel-Aal, E., & El-Shall, H. (2005). Application of statistical design to optimize the preparation of ZnO nanoparticles via hydrothermal technique. *Materials Letters*, *59*(14-15), 1924-1928.

Jan, F. A., Ullah, R., Ullah, N., & Usman, M. (2021). Exploring the environmental and potential therapeutic applications of Myrtus communis L. assisted synthesized zinc oxide (ZnO) and iron doped zinc oxide (Fe-ZnO) nanoparticles. *Journal of Saudi Chemical Society*, *25*(7), 101278.

Javed, R., Rais, F., Fatima, H., ul Haq, I., Kaleem, M., Naz, S. S., & Ao, Q. (2020). Chitosan encapsulated ZnO nanocomposites: Fabrication, characterization, and functionalization of bio-dental approaches. *Materials Science and Engineering: C, 116*, 111184.

Jiang, D., Zhang, Y., & Li, X. (2019). Synergistic effects of CuO and Au nanodomains on Cu2O cubes for improving photocatalytic activity and stability. *Chinese Journal of Catalysis, 40*(1), 105-113. doi:10.1016/s1872-2067(18)63164-x

Ju, D., Xu, H., Qiu, Z., Guo, J., Zhang, J., & Cao, B. (2014). Highly sensitive and selective triethylamine-sensing properties of nanosheets directly grown on ceramic tube by forming NiO/ZnO PN heterojunction. *Sensors and Actuators B: Chemical*, *200*, 288-296.

Jyothi, N. S., & Ravichandran, K. (2020). Optimum pH for effective dye degradation: Mo, Mn, Co and Cu doped ZnO photocatalysts in thin film form. *Ceramics International, 46*(14), 23289-23292.

Kale, A., Bao, Y., Zhou, Z., Prevelige, P. E., & Gupta, A. (2013). Directed self-assembly of CdS quantum dots on bacteriophage P22 coat protein templates. *Nanotechnology, 24*(4), 045603.

Kanchi, S. (2014). Nanotechnology for water treatment. *J. Environ. Anal. Chem, 1*(2), 1-3.

Kant, S., & Kumar, A. (2012). A comparative analysis of structural, optical and photocatalytic properties of ZnO and Ni doped ZnO nanospheres prepared by sol gel method. *Adv Mat Let*, *3*(4), 350-354.

Karimi-Shamsabadi, M., Behpour, M., Babaheidari, A. K., & Saberi, Z. (2017). Efficiently enhancing photocatalytic activity of NiO-ZnO doped onto nanozeoliteX by synergistic effects of pn heterojunction, supporting and zeolite nanoparticles in photo-degradation of Eriochrome Black T and Methyl Orange. *Journal of Photochemistry and Photobiology A: Chemistry, 346*, 133-143.

Karimi, L., Zohoori, S., & Yazdanshenas, M. E. (2014). Photocatalytic degradation of azo dyes in aqueous solutions under UV irradiation using nano-strontium titanate as the nanophotocatalyst. *Journal of Saudi Chemical Society, 18*(5), 581-588. doi:10.1016/j.jscs.2011.11.010

Karthik, K., Raghu, A., Reddy, K. R., Ravishankar, R., Sangeeta, M., Shetti, N. P., & Reddy, C. V. (2022). Green synthesis of Cu-doped ZnO nanoparticles and its application for the photocatalytic degradation of hazardous organic pollutants. *Chemosphere, 287*, 132081.

Kaviya, S., & Prasad, E. (2015). Biogenic synthesis of ZnO–Ag nano custard apples for efficient photocatalytic degradation of methylene blue by sunlight irradiation. *RSC Advances, 5*(22), 17179-17185.

Kavyashree, D., Kumari, R. A., Nagabhushana, H., Sharma, S., Vidya, Y., Anantharaju, K., . . . Rajanaik, H. (2015). Orange red emitting Eu3+ doped zinc oxide nanophosphor material prepared using Guizotia abyssinica seed extract: Structural and photoluminescence studies. *Journal of Luminescence, 167*, 91-100.

Kayani, Z. N., Anjum, M., Riaz, S., Naseem, S., & Zeeshan, T. (2020). Role of Mn in biological, optical, and magnetic properties ZnO nano-particles. *Applied Physics A, 126*(3), 1-17.

Kebebew, M. (2018). Diversity and management of useful homegardens plant species in Arba Minch Town, Southern Ethiopia: Implication for plant diversity conservation and food security. *International Journal of Economic Plants, 5*(3), 137-148.

Khan, M. M., Adil, S. F., & Al-Mayouf, A. (2015). Metal oxides as photocatalysts (Vol. 19, pp. 462-464): Elsevier.

Khan, M. M., Harunsani, M. H., Tan, A. L., Hojamberdiev, M., Azamay, S., & Ahmad, N. (2020). Antibacterial activities of zinc oxide and Mn-doped zinc oxide synthesized using Melastoma malabathricum (L.) leaf extract. *Bioprocess and biosystems engineering, 43*(8), 1499-1508.

Khan, S. A., Noreen, F., Kanwal, S., Iqbal, A., & Hussain, G. (2018). Green synthesis of ZnO and Cu-doped ZnO nanoparticles from leaf extracts of Abutilon indicum, Clerodendrum infortunatum, Clerodendrum inerme and investigation of their biological and photocatalytic activities. *Materials Science and Engineering: C, 82*, 46-59.

Khanizadeh, B., Khosravi, M., Behnajady, M. A., Shamel, A., & Vahid, B. (2020). Mg and La Co-doped ZnO nanoparticles prepared by sol–gel method: synthesis, characterization and photocatalytic activity. *Periodica Polytechnica Chemical Engineering, 64*(1), 61-74.

Kommineni, S., Zoeckler, J., Stocking, A., Liang, P., Flores, A., Rodriguez, R., . . . Brown, A. (2000). 3.0 Advanced oxidation processes. *center for groundwater restoration and protection national water research institute*.

Krishnakumar, B., & Imae, T. (2014). Chemically modified novel PAMAM-ZnO nanocomposite: synthesis, characterization and photocatalytic activity. *Applied Catalysis A: General, 486*, 170-175.

Kumar, A., & Lingfa, P. (2020). Sodium bentonite and kaolin clays: Comparative study on their FT-IR, XRF, and XRD. *Materials Today: Proceedings, 22*, 737-742.

Kumar, K., Chitkara, M., Sandhu, I. S., Mehta, D., & Kumar, S. (2014). Photocatalytic, optical and magnetic properties of Fe-doped ZnO nanoparticles prepared by chemical route. *Journal of Alloys and Compounds, 588*, 681-689.

Kumar, S., Kumar, D., Sahu, M., & Kumar, A. (2020). FTIR Based Pharmacological Validation of Bridelia retusa.

Kumar, S. G., Kavitha, R., & Sushma, C. (2020). Doped zinc oxide nanomaterials: structure–electronic properties and photocatalytic applications *Interface Science and Technology* (Vol. 31, pp. 285-312): Elsevier.

Kupchan, S. M., Liepa, A. J., & Fujita, T. (1973). New phenolic hasubanan alkaloids from Stephania abyssinica. *The Journal of organic chemistry, 38*(1), 151-153.

Lakshmi, K., Mathusalini, S., Arasakumar, T., Kadirvelu, K., & Mohan, P. (2017). Highly reactive lanthanum doped zinc oxide nanofiber photocatalyst for effective decontamination of methyl parathion. *Journal of Materials Science: Materials in Electronics, 28*(17), 12944-12955.

Lam, S.-M., Sin, J.-C., Zeng, H., Lin, H., Li, H., Chai, Y.-Y., . . . Mohamed, A. R. (2021). Green synthesis of Fe-ZnO nanoparticles with improved sunlight photocatalytic performance for polyethylene film deterioration and bacterial inactivation. *Materials Science in Semiconductor Processing, 123*, 105574.

Li, J., Shen, D., Zhang, J., Zhao, D., Li, B., Lu, Y., . . . Fan, X. (2006). Magnetism origin of Mn-doped ZnO nanoclusters. *Journal of magnetism and magnetic materials, 302*(1), 118-121.

Lida, J., & Qingrui, Z. (2020). Heterogeneous fenton catalytic oxidation for water treatment. *Progress in Chemistry, 32*(7), 978.

Liewhiran, C., & Phanichphant, S. (2007). Influence of thickness on ethanol sensing characteristics of doctor-bladed thick film from flame-made ZnO nanoparticles. *Sensors, 7*(2), 185-201.

Lin, H., Chen, Y., & Chen, Y. (2007). Water splitting reaction on NiO/InVO4 under visible light irradiation. *International Journal of Hydrogen Energy, 32*(1), 86-92. doi:10.1016/j.ijhydene.2006.04.007

Lin, L., Zheng, R., Xie, J., Zhu, Y., & Xie, Y. (2007). Synthesis and characterization of phosphor and nitrogen co-doped titania. *Applied Catalysis B: Environmental, 76*(1-2), 196-202.

Lin, Z., Du, C., Yan, B., & Yang, G. (2019). Two-dimensional amorphous CoO photocatalyst for efficient overall water splitting with high stability. *Journal of Catalysis, 372*, 299-310.

Liu, X., Zhong, Q., Guo, W., Zhang, W., Ya, Y., & Xia, Y. (2021). Novel platycladus orientalis–shaped Fe-doped ZnO hierarchical nanoflower decorated with Ag nanoparticles for photocatalytic application. *Journal of Alloys and Compounds*, 160501.

Lou, T., Yan, X., & Wang, X. (2019). Chitosan coated polyacrylonitrile nanofibrous mat for dye adsorption. *International Journal of Biological Macromolecules, 135*, 919-925.

Luo, H., Takata, T., Lee, Y., Zhao, J., Domen, K., & Yan, Y. (2004). Photocatalytic activity enhancing for titanium dioxide by co-doping with bromine and chlorine. *Chemistry of Materials, 16*(5), 846-849.

Lupan, O., Pauporté, T., Viana, B., & Aschehoug, P. (2011). Electrodeposition of Cu-doped ZnO nanowire arrays and heterojunction formation with p-GaN for color tunable light emitting diode applications. *Electrochimica Acta, 56*(28), 10543-10549.

Lv, D., Zheng, L., Zhang, H., & Deng, Y. (2018). Coagulation of colloidal particles with ferrate (vi). *Environmental Science: Water Research & Technology, 4*(5), 701-710.

Lv, W., Wei, B., Xu, L., Zhao, Y., Gao, H., & Liu, J. (2012). Photocatalytic properties of hierarchical ZnO flowers synthesized by a sucrose-assisted hydrothermal method. *Applied Surface Science, 259*, 557-561.

Ma, J., Wang, R., Wang, X., Zhang, H., Zhu, B., Lian, L., & Lou, D. (2019). Drinking water treatment by stepwise flocculation using polysilicate aluminum magnesium and cationic polyacrylamide. *Journal of Environmental Chemical Engineering, 7*(3), 103049.

Ma, S., Li, R., Lv, C., Xu, W., & Gou, X. (2011). Facile synthesis of ZnO nanorod arrays and hierarchical nanostructures for photocatalysis and gas sensor applications. *J Hazard Mater, 192*(2), 730-740. doi:10.1016/j.jhazmat.2011.05.082

Mabe, I., Rapp, C., Bain, M., & Nys, Y. (2003). Supplementation of a corn-soybean meal diet with manganese, copper, and zinc from organic or inorganic sources improves eggshell quality in aged laying hens. *Poultry Science, 82*(12), 1903-1913.

Madathil, A. N. P., Vanaja, K., & Jayaraj, M. (2007). *Synthesis of ZnO nanoparticles by hydrothermal method.* Paper presented at the Nanophotonic materials IV.

Magdalane, C. M., Kaviyarasu, K., Vijaya, J. J., Jayakumar, C., Maaza, M., & Jeyaraj, B. (2017). Photocatalytic degradation effect of malachite green and catalytic hydrogenation by UV–illuminated CeO2/CdO multilayered nanoplatelet arrays: investigation of antifungal and antimicrobial activities. *Journal of Photochemistry and Photobiology B: Biology, 169*, 110-123.

Majumder, A., Saidulu, D., Gupta, A. K., & Ghosal, P. S. (2021). Predicting the trend and utility of different photocatalysts for degradation of pharmaceutically active compounds: A special emphasis on photocatalytic materials, modifications, and performance comparison. *Journal of environmental management, 293*, 112858.

Makarov, V., Love, A., Sinitsyna, O., Makarova, S., Yaminsky, I., Taliansky, M., & Kalinina, N. (2014). "Green" nanotechnologies: synthesis of metal nanoparticles using plants. *Acta Naturae (англоязычная версия), 6*(1 (20)).

Malik, P., Shankar, R., Malik, V., Sharma, N., & Mukherjee, T. K. (2014). Green chemistry based benign routes for nanoparticle synthesis. *Journal of Nanoparticles, 2014*.

Mesfin, F., Demissew, S., & Teklehaymanot, T. (2009). An ethnobotanical study of medicinal plants in Wonago Woreda, SNNPR, Ethiopia. *Journal of Ethnobiology and Ethnomedicine, 5*(1), 1-18.

Milenova, K., Stambolova, I., Blaskov, V., Eliyas, A., Vassilev, S., & Shipochka, M. (2013). The effect of introducing copper dopant on the photocatalytic activity of ZnO nanoparticles. *Journal of chemical technology and metallurgy, 48*(3), 259-264.

Mishra, M., & Chun, D.-M. (2015). α-Fe2O3 as a photocatalytic material: A review. *Applied Catalysis A: General, 498*, 126-141.

Mondal, A., Chouke, P. B., Sonkusre, V., Lambat, T., Abdala, A. A., Mondal, S., & Chaudhary, R. G. (2020). Ni-doped ZnO nanocrystalline material for electrocatalytic oxygen reduction reaction. *Materials Today: Proceedings, 29*, 715-719.

Moritz, M., & Geszke-Moritz, M. (2013). The newest achievements in synthesis, immobilization and practical applications of antibacterial nanoparticles. *Chemical Engineering Journal, 228*, 596-613.

Mullani, S. B., Tawade, A. K., Tayade, S. N., Sharma, K. K. K., Deshmukh, S. P., Mullani, N. B., . . . Delekar, S. D. (2020). Synthesis of Ni 2+ ion doped ZnO–MWCNTs nanocomposites using an in situ sol–gel method: An ultra sensitive non-enzymatic uric acid sensing electrode material. *RSC Advances, 10*(61), 36949-36961.

Murcia Mesa, J. J., Hernández Niño, J. S., González, W., Rojas, H., Hidalgo, M. C., & Navío, J. A. (2021). Photocatalytic Treatment of Stained Wastewater Coming from Handicraft Factories. A Case Study at the Pilot Plant Level. *Water, 13*(19), 2705.

Muthukumar, H., Gire, A., Kumari, M., & Manickam, M. (2017). Biogenic synthesis of nano-biomaterial for toxic naphthalene photocatalytic degradation optimization and kinetics studies. *International Biodeterioration & Biodegradation, 119*, 587-594.

Nagasundari, S. M., Muthu, K., Kaviyarasu, K., Al Farraj, D. A., & Alkufeidy, R. M. (2021). Current trends of Silver doped Zinc oxide nanowires photocatalytic degradation for energy and environmental application. *Surfaces and Interfaces, 23*, 100931.

Nagvenkar, A. P., Deokar, A., Perelshtein, I., & Gedanken, A. (2016). A one-step sonochemical synthesis of stable ZnO–PVA nanocolloid as a potential biocidal agent. *Journal of Materials Chemistry B, 4*(12), 2124-2132.

Nair, M. G., Nirmala, M., Rekha, K., & Anukaliani, A. (2011). Structural, optical, photo catalytic and antibacterial activity of ZnO and Co doped ZnO nanoparticles. *Materials Letters, 65*(12), 1797-1800.

Nakata, K., & Fujishima, A. (2012). TiO2 photocatalysis: Design and applications. *Journal of photochemistry and photobiology C: Photochemistry Reviews, 13*(3), 169-189.

Namini, A. S., Delbari, S. A., Mousavi, M., & Ghasemi, J. B. (2021). Synthesis and characterization of novel ZnO/NiCr2O4 nanocomposite for water purification by degradation of tetracycline and phenol under visible light irradiation. *Materials Research Bulletin, 139*, 111247.

Narayanan, S., Begum, M. S., Manikandan, G., & Yuvashree, M. (2021). Green synthesis strategy for producing doped and undoped ZnO nanoparticles: their photocatalytic studies for industrial dye degradation. *Water Science and Technology*.

Naskar, A., Lee, S., & Kim, K.-s. (2020). Antibacterial potential of Ni-doped zinc oxide nanostructure: Comparatively more effective against Gram-negative bacteria including multi-drug resistant strains. *RSC Advances, 10*(3), 1232-1242.

Nosaka, Y., & Nosaka, A. Y. (2017). Generation and detection of reactive oxygen species in photocatalysis. *Chemical reviews, 117*(17), 11302-11336.

Noukelag, S. K., Razanamahandry, L. C., Ntwampe, S. K., Arendse, C. J., & Maaza, M. (2021). Industrial dye removal using bio-synthesized Ag-doped ZnO nanoparticles. *Environmental Nanotechnology, Monitoring & Management, 16*, 100463.

Nunes, D., Pimentel, A., Santos, L., Barquinha, P., Pereira, L., Fortunato, E., & Martins, R. (2019). Structural, optical, and electronic properties of metal oxide nanostructures. *Met. Oxide Nanostruct*, 59-102.

Okeke, I., Agwu, K., Ubachukwu, A., Maaza, M., & Ezema, F. (2020). Impact of Cu doping on ZnO nanoparticles phyto-chemically synthesized for improved antibacterial and photocatalytic activities. *Journal of Nanoparticle Research, 22*(9), 1-18.

Okeke, I., Agwu, K., Ubachukwu, A., Madiba, I., Maaza, M., Whyte, G., & Ezema, F. (2021). Impact of particle size and surface defects on antibacterial and photocatalytic activities of undoped and Mg-doped ZnO nanoparticles, biosynthesized using one-step simple process. *Vacuum, 187*, 110110.

Oudhia, A., Kulkarni, P., & Sharma, S. (2015). Green synthesis of ZnO nanotubes for bioapplications. *Int J Curr Eng Technol, 1*, 280-281.

Pandey, A. K., Kumar, R., Maurya, D., & Singh, V. P. (2015). Bionanoparticles: a green nanochemical approach. *PharmaTutor, 3*(9), 28-35.

Pandey, G., Singh, S., & Hitkari, G. (2018). Synthesis and characterization of polyvinyl pyrrolidone (PVP)-coated Fe 3 O 4 nanoparticles by chemical co-precipitation method and removal of Congo red dye by adsorption process. *International Nano Letters, 8*(2), 111-121.

Parsons, S. (2004). *Advanced oxidation processes for water and wastewater treatment*: IWA publishing.

Parveen, K., Banse, V., & Ledwani, L. (2016). *Green synthesis of nanoparticles: their advantages and disadvantages.* Paper presented at the AIP conference proceedings.

Pathania, D., Sharma, A., Kumar, S., Srivastava, A. K., Kumar, A., & Singh, L. (2021). Bio-synthesized Cu–ZnO hetro-nanostructure for catalytic degradation of organophosphate chlorpyrifos under solar illumination. *Chemosphere, 277*, 130315.

Patil, A. B., Patil, K. R., & Pardeshi, S. K. (2010). Ecofriendly synthesis and solar photocatalytic activity of S-doped ZnO. *Journal of Hazardous Materials, 183*(1-3), 315-323.

Patil, S. S., Mali, M. G., Tamboli, M. S., Patil, D. R., Kulkarni, M. V., Yoon, H., . . . Kolekar, S. S. (2016). Green approach for hierarchical nanostructured Ag-ZnO and their photocatalytic performance under sunlight. *Catalysis Today, 260*, 126-134.

Patterson, J. W. (1985). Industrial wastewater treatment technology.

Paulos, A. (2020). *Synthesis of Cu2O/ZnO/kaolinite composite for the degradation of methylene blue under visible light.* ASTU.

Pei, C., Han, G., Zhao, Y., Zhao, H., Liu, B., Cheng, L., . . . Liu, S. (2016). Superior adsorption performance for triphenylmethane dyes on 3D architectures assembled by ZnO nanosheets as thin as∼ 1.5 nm. *Journal of Hazardous Materials, 318*, 732-741.

Pera-Titus, M., García-Molina, V., Baños, M. A., Giménez, J., & Esplugas, S. (2004). Degradation of chlorophenols by means of advanced oxidation processes: a general review. *Applied Catalysis B: Environmental, 47*(4), 219-256.

Pirkanniemi, K., & Sillanpää, M. (2002). Heterogeneous water phase catalysis as an environmental application: a review. *Chemosphere, 48*(10), 1047-1060.

Podporska-Carroll, J., Myles, A., Quilty, B., McCormack, D. E., Fagan, R., Hinder, S. J., . . . Pillai, S. C. (2017). Antibacterial properties of F-doped ZnO visible light photocatalyst. *Journal of Hazardous Materials, 324*, 39-47.

Prabhakar, R. R., Mathews, N., Jinesh, K., Karthik, K., Pramana, S. S., Varghese, B., . . . Mhaisalkar, S. (2012). Efficient multispectral photodetection using Mn doped ZnO nanowires. *Journal of Materials Chemistry, 22*(19), 9678-9683.

Prasse, C., Stalter, D., Schulte-Oehlmann, U., Oehlmann, J., & Ternes, T. A. (2015). Spoilt for choice: A critical review on the chemical and biological assessment of current wastewater treatment technologies. *Water research, 87*, 237-270.

Qiao, R., Wu, W., Zhu, X., Yin, Q., Tan, L., & Ke, X. (2020). Synthesis of heteroatom-doped ZnO nanoparticles as an efficient visible light photocatalyst and its photoelectrochemical performance. *Indian Journal of Chemistry-Section A (IJCA), 55*(5), 566-570.

Raha, S., Mohanta, D., & Ahmaruzzaman, M. (2021). Novel CuO/Mn3O4/ZnO nanocomposite with superior photocatalytic activity for removal of Rabeprazole from water. *Scientific reports, 11*(1), 1-19.

Rahman, A., Harunsani, M. H., Tan, A. L., Ahmad, N., Min, B.-K., & Khan, M. M. (2021). Influence of Mg and Cu dual-doping on phytogenic synthesized ZnO for light induced antibacterial and radical scavenging activities. *Materials Science in Semiconductor Processing, 128*, 105761.

Rahman, A., Tan, A. L., Harunsani, M. H., Ahmad, N., Hojamberdiev, M., & Khan, M. M. (2021). Visible light induced antibacterial and antioxidant studies of ZnO and Cu-doped ZnO fabricated using aqueous leaf extract of Ziziphus mauritiana Lam. *Journal of Environmental Chemical Engineering, 9*(4), 105481.

Raizada, P., Sudhaik, A., Patial, S., Hasija, V., Khan, A. A. P., Singh, P., . . . Nguyen, V.-H. (2020). Engineering nanostructures of CuO-based photocatalysts for water treatment:

current progress and future challenges. *Arabian Journal of Chemistry, 13*(11), 8424-8457.

Rajabi, H. R., Khani, O., Shamsipur, M., & Vatanpour, V. (2013). High-performance pure and Fe3+-ion doped ZnS quantum dots as green nanophotocatalysts for the removal of malachite green under UV-light irradiation. *J Hazard Mater, 250-251*, 370-378. doi:10.1016/j.jhazmat.2013.02.007

Rajaboopathi, S., & Thambidurai, S. (2018). Enhanced photocatalytic activity of Ag-ZnO nanoparticles synthesized by using Padina gymnospora seaweed extract. *Journal of Molecular Liquids, 262*, 148-160.

Rajeshwar, K., Osugi, M., Chanmanee, W., Chenthamarakshan, C., Zanoni, M. V. B., Kajitvichyanukul, P., & Krishnan-Ayer, R. (2008). Heterogeneous photocatalytic treatment of organic dyes in air and aqueous media. *Journal of photochemistry and photobiology C: Photochemistry Reviews, 9*(4), 171-192.

Rajrana, K., Gupta, A., Mir, R. A., & Pandey, O. (2019). Facile sono-chemical synthesis of nanocrystalline MnO2 for catalytic and capacitive applications. *Physica B: Condensed Matter, 564*, 179-185.

Ramesh, P., Rajendran, A., & Meenakshisundaram, M. (2014). Green syntheis of zinc oxide nanoparticles using flower extract cassia auriculata. *Journal of nanoscience and nanotechnology, 2*(1), 41-45.

Ramesh, P., Rajendran, A., & Subramanian, A. (2014). Synthesis of zinc oxide nanoparticle from fruit of Citrus aurantifolia by chemical and green method. *Asian J. Phytomed. Clin. Res, 2*, 189-195.

Rana, S., & Singh, R. P. (2016). Investigation of structural, optical, magnetic properties and antibacterial activity of Ni-doped zinc oxide nanoparticles. *Journal of Materials Science: Materials in Electronics, 27*(9), 9346-9355.

Ranjitha, R., Meghana, K., Kumar, V. D., Bhatt, A. S., Jayanna, B., Ravikumar, C., . . . Sakai, K. (2021). Rapid photocatalytic degradation of cationic organic dyes using Li-doped Ni/NiO nanocomposites and their electrochemical performance. *New Journal of Chemistry, 45*(2), 796-809.

Rathnasamy, R., Thangasamy, P., Thangamuthu, R., Sampath, S., & Alagan, V. (2017). Green synthesis of ZnO nanoparticles using Carica papaya leaf extracts for photocatalytic and photovoltaic applications. *Journal of Materials Science: Materials in Electronics, 28*(14), 10374-10381.

Rauf, M., & Ashraf, S. S. (2009). Fundamental principles and application of heterogeneous photocatalytic degradation of dyes in solution. *Chemical Engineering Journal, 151*(1-3), 10-18.

Reddy, I. N., Reddy, C. V., Shim, J., Akkinepally, B., Cho, M., Yoo, K., & Kim, D. (2020). Excellent visible-light driven photocatalyst of (Al, Ni) co-doped ZnO structures for organic dye degradation. *Catalysis Today, 340*, 277-285.

Reza, K. M., Kurny, A., & Gulshan, F. (2017). Parameters affecting the photocatalytic degradation of dyes using TiO 2: a review. *Applied Water Science, 7*(4), 1569-1578.

Rodríguez-González, V., Zanella, R., del Angel, G., & Gómez, R. (2008). MTBE visible-light photocatalytic decomposition over Au/TiO2 and Au/TiO2–Al2O3 sol–gel prepared catalysts. *Journal of Molecular Catalysis A: Chemical, 281*(1-2), 93-98. doi:10.1016/j.molcata.2007.07.009

RR, M. C., & Rajalaxshmi, A. Green Synthesis, Characterization of ZnO nanoparticles and Ceion doped ZnO nanoparticles assisted Sesbania Grandiflora for photocatalytic

application. *Research Journal of Material Sciences E-ISSN, 2320*, 6055.

Sadiq, H., Sher, F., Sehar, S., Lima, E. C., Zhang, S., Iqbal, H. M., . . . Nuhanović, M. (2021). Green synthesis of ZnO nanoparticles from Syzygium Cumini leaves extract with robust photocatalysis applications. *Journal of Molecular Liquids, 335*, 116567.

Sagar, P., Shishodia, P., Mehra, R., Okada, H., Wakahara, A., & Yoshida, A. (2007). Photoluminescence and absorption in sol–gel-derived ZnO films. *Journal of Luminescence, 126*(2), 800-806.

Saleh, R., & Djaja, N. F. (2014a). Transition-metal-doped ZnO nanoparticles: synthesis, characterization and photocatalytic activity under UV light. *Spectrochimica Acta Part A: Molecular and Biomolecular Spectroscopy, 130*, 581-590.

Saleh, R., & Djaja, N. F. (2014b). UV light photocatalytic degradation of organic dyes with Fe-doped ZnO nanoparticles. *Superlattices and Microstructures, 74*, 217-233.

Samanta, A., Goswami, M., & Mahapatra, P. (2018a). Magnetic and electric properties of Ni-doped ZnO nanoparticles exhibit diluted magnetic semiconductor in nature. *Journal of Alloys and Compounds, 730*, 399-407.

Samanta, A., Goswami, M., & Mahapatra, P. (2018b). Optical properties and enhanced photocatalytic activity of Mg-doped ZnO nanoparticles. *Physica E: Low-dimensional Systems and Nanostructures, 104*, 254-260.

Sangeetha, G., Rajeshwari, S., & Venckatesh, R. (2011). Green synthesis of zinc oxide nanoparticles by aloe barbadensis miller leaf extract: Structure and optical properties. *Materials Research Bulletin, 46*(12), 2560-2566.

Sangeetha, R., Muthukumaran, S., & Ashokkumar, M. (2015). Structural, optical, dielectric and antibacterial studies of Mn doped Zn0. 96Cu0. 04O nanoparticles. *Spectrochimica Acta Part A: Molecular and Biomolecular Spectroscopy, 144*, 1-7.

Saravanadevi, K., Kavitha, M., Karpagavinayagam, P., Saminathan, K., & Vedhi, C. (2020). Biosynthesis of ZnO and Ag doped ZnO nanoparticles from Vitis vinifera leaf for antibacterial, photocatalytic application. *Materials Today: Proceedings*.

Sathishkumar, P., Mangalaraja, R. V., Anandan, S., & Ashokkumar, M. (2013). CoFe2O4/TiO2 nanocatalysts for the photocatalytic degradation of Reactive Red 120 in aqueous solutions in the presence and absence of electron acceptors. *Chemical Engineering Journal, 220*, 302-310. doi:10.1016/j.cej.2013.01.036

Sathishkumar, P., Pugazhenthiran, N., Mangalaraja, R. V., Asiri, A. M., & Anandan, S. (2013). ZnO supported CoFe2O4 nanophotocatalysts for the mineralization of Direct Blue 71 in aqueous environments. *J Hazard Mater, 252-253*, 171-179. doi:10.1016/j.jhazmat.2013.02.030

Schmelzer, G. H., & Gurib-Fakim, A. (2008). *Medicinal plants* (Vol. 11): Prota.

Senol, S., Ozugurlu, E., & Arda, L. (2020). Synthesis, structure and optical properties of (Mn/Cu) co-doped ZnO nanoparticles. *Journal of Alloys and Compounds, 822*, 153514.

Senthilkumar, S., & Sivakumar, T. (2014). Green tea (Camellia sinensis) mediated synthesis of zinc oxide (ZnO) nanoparticles and studies on their antimicrobial activities. *Int J Pharm Pharm Sci, 6*(6), 461-465.

Shah, N. I., Jabeen, N., Irum, S., Ahmad, K. S., Tauseef, I., Khan, T. F., . . . Mehmood, A. (2021). Environmentally benign and economical bio-fabrication of ZnO and Cr-doped

ZnO nanoparticles using leaf extract of Citrus reticulata for biological activities. *Materials Today Communications, 27*, 102383.

Shie, J. L., Lee, C. H., Chiou, C. S., Chang, C. T., Chang, C. C., & Chang, C. Y. (2008). Photodegradation kinetics of formaldehyde using light sources of UVA, UVC and UVLED in the presence of composed silver titanium oxide photocatalyst. *J Hazard Mater, 155*(1-2), 164-172. doi:10.1016/j.jhazmat.2007.11.043

Shifu, C., Wei, Z., Wei, L., Huaye, Z., & Xiaoling, Y. (2009). Preparation, characterization and activity evaluation of p–n junction photocatalyst p-CaFe2O4/n-ZnO. *Chemical Engineering Journal, 155*(1-2), 466-473. doi:10.1016/j.cej.2009.07.009

Siddhapara, K., & Shah, D. (2014). Study of photocatalytic activity and properties of transition metal ions doped nanocrystalline TiO2 prepared by sol-gel method. *Advances in Materials Science and Engineering, 2014*.

Singh, J., Sharma, S., Soni, S., Sharma, S., & Singh, R. C. (2019). Influence of different milling media on structural, morphological and optical properties of the ZnO nanoparticles synthesized by ball milling process. *Materials Science in Semiconductor Processing, 98*, 29-38.

Singh, R., Barman, P., & Sharma, D. (2017). Synthesis, structural and optical properties of Ag doped ZnO nanoparticles with enhanced photocatalytic properties by photo degradation of organic dyes. *Journal of Materials Science: Materials in Electronics, 28*(8), 5705-5717.

Singh, R. P., Shukla, V. K., Yadav, R. S., Sharma, P. K., Singh, P. K., & Pandey, A. C. (2011). Biological approach of zinc oxide nanoparticles formation and its characterization. *Adv. Mater. Lett, 2*(4), 313-317.

Siripireddy, B., & Mandal, B. K. (2017). Facile green synthesis of zinc oxide nanoparticles by Eucalyptus globulus and their photocatalytic and antioxidant activity. *Advanced Powder Technology, 28*(3), 785-797.

Sobana, N., & Swaminathan, M. (2007). The effect of operational parameters on the photocatalytic degradation of acid red 18 by ZnO. *Separation and Purification Technology, 56*(1), 101-107. doi:10.1016/j.seppur.2007.01.032

Sohrabnezhad, S., & Seifi, A. (2016). The green synthesis of Ag/ZnO in montmorillonite with enhanced photocatalytic activity. *Applied Surface Science, 386*, 33-40.

Sonune, A., & Ghate, R. (2004). Developments in wastewater treatment methods. *Desalination, 167*, 55-63.

Sorbiun, M., Mehr, E. S., Ramazani, A., & Fardood, S. T. (2018). Biosynthesis of Ag, ZnO and bimetallic Ag/ZnO alloy nanoparticles by aqueous extract of oak fruit hull (Jaft) and investigation of photocatalytic activity of ZnO and bimetallic Ag/ZnO for degradation of basic violet 3 dye. *Journal of Materials Science: Materials in Electronics, 29*(4), 2806-2814.

Sotiriou, G. A., Watson, C., Murdaugh, K. M., Darrah, T. H., Pyrgiotakis, G., Elder, A., . . . Demokritou, P. (2014). Engineering safer-by-design silica-coated ZnO nanorods with reduced DNA damage potential. *Environmental Science: Nano, 1*(2), 144-153.

Soto-Robles, C., Luque, P., Gómez-Gutiérrez, C., Nava, O., Vilchis-Nestor, A., Lugo-Medina, E., . . . Castro-Beltrán, A. (2019). Study on the effect of the concentration of Hibiscus sabdariffa extract on the green synthesis of ZnO nanoparticles. *Results in Physics, 15*, 102807.

Squadrone, S., Ciccotelli, V., Prearo, M., Favaro, L., Scanzio, T., Foglini, C., & Abete, M. (2015). Perfluorooctane sulfonate (PFOS) and perfluorooctanoic acid (PFOA):

emerging contaminants of increasing concern in fish from Lake Varese, Italy. *Environmental monitoring and assessment, 187*(7), 1-7.

Srimathi, K., Hussain, T., Panigrahi, P., Subramaniam, N. G., & Ahuja, R. (2020). Influence of Sodium Iodide doped polypyrrole on green synthesized aluminum doped ZnO for the enhanced charge separation at the interface. *Optical Materials, 99*, 109568.

Su, J., Xue, H., Gu, M., Xia, H., & Pan, F. (2014). Synthesis of spherical Cr2O3 nanoparticles by a microwave refluxing method and their photocatalytic properties. *Ceramics International, 40*(9), 15051-15055.

Subbiah, R., Muthukumaran, S., & Raja, V. (2019). Fine-tuning of energy gap, FTIR, photoluminescence and photocatalytic behavior of Centella asiatica extract mediated Mn/Mg doped ZnO nanostructure. *Journal of Materials Science: Materials in Electronics, 30*(18), 17066-17077.

Subbiah, R., Muthukumaran, S., & Raja, V. (2020). Biosynthesis, structural, photoluminescence and photocatalytic performance of Mn/Mg dual doped ZnO nanostructures using Ocimum tenuiflorum leaf extract. *Optik, 208*, 164556.

Subbiah, R., Muthukumaran, S., & Raja, V. (2021). Phyto-assisted Synthesis of Mn and Mg Co-doped ZnO Nanostructures Using Carica papaya Leaf Extract for Photocatalytic Applications. *BioNanoScience, 11*(4), 1127-1141.

Suganya, S., & Vivekanandhan, S. (2019). Neem (Azadirachta indica) gum assisted sol–gel synthesis and characterization of ZnO nanoparticles for photocatalytic application. *Journal of the Australian Ceramic Society, 55*(2), 433-442.

Suresh, D., Shobharani, R., Nethravathi, P., Kumar, M. P., Nagabhushana, H., & Sharma, S. (2015). Artocarpus gomezianus aided green synthesis of ZnO nanoparticles: luminescence, photocatalytic and antioxidant properties. *Spectrochimica Acta Part A: Molecular and Biomolecular Spectroscopy, 141*, 128-134.

Sweeney, R. Y., Mao, C., Gao, X., Burt, J. L., Belcher, A. M., Georgiou, G., & Iverson, B. L. (2004). Bacterial biosynthesis of cadmium sulfide nanocrystals. *Chemistry & biology, 11*(11), 1553-1559.

Sze, S., & Ng, K. (2007). Physics of Semiconductor Devices 3rd ed Wiley. *New York*.

Tefera, B. N., & Kim, Y.-D. (2019). Ethnobotanical study of medicinal plants in the Hawassa Zuria District, Sidama zone, Southern Ethiopia. *Journal of Ethnobiology and Ethnomedicine, 15*(1), 1-21.

Thema, F., Manikandan, E., Dhlamini, M., & Maaza, M. (2015). Green synthesis of ZnO nanoparticles via Agathosma betulina natural extract. *Materials Letters, 161*, 124-127.

Tun, P., Wang, K., Naing, H., Wang, J., & Zhang, G. (2019). Facile preparation of visible-light-responsive kaolin-supported Ag@ AgBr composites and their enhanced photocatalytic properties. *Applied Clay Science, 175*, 76-85.

Uddin, M. T., Nicolas, Y., Olivier, C., Toupance, T., Servant, L., Muller, M. M., . . . Jaegermann, W. (2012). Nanostructured SnO2–ZnO heterojunction photocatalysts showing enhanced photocatalytic activity for the degradation of organic dyes. *Inorganic chemistry, 51*(14), 7764-7773.

Vaishnav, A., Pal, B., & Prakash, N. T. (2018). *Biosynthesized Selenium co-catalyst for Improved Photocatalytic activity of Se-ZnO Nanocomposites.*

Vanalakar, S., Agawane, G., Shin, S., Suryawanshi, M., Gurav, K., Jeon, K., . . . Kim, J. (2015). A review on pulsed laser deposited CZTS thin films for solar cell applications. *Journal of Alloys and Compounds, 619*, 109-121.

Vidya, C., Hiremath, S., Chandraprabha, M., Antonyraj, M. L., Gopal, I. V., Jain, A., & Bansal, K. (2013). Green synthesis of ZnO nanoparticles by Calotropis gigantea. *Int J Curr Eng Technol, 1*(1), 118-120.

Vishwakarma, K. (2013). *Green synthesis of ZnO nanoparticles using Abrus precatorius seeds extract and their characterization.*

Wahab, R., Hwang, I. H., Kim, Y.-S., Musarrat, J., Siddiqui, M. A., Seo, H.-K., . . . Shin, H.-S. (2011). Non-hydrolytic synthesis and photo-catalytic studies of ZnO nanoparticles. *Chemical Engineering Journal, 175*, 450-457. doi:10.1016/j.cej.2011.09.055

Wang, H., Qiu, X., Zhong, R., Fu, F., Qian, Y., & Yang, D. (2017). One-pot in-situ preparation of a lignin-based carbon/ZnO nanocomposite with excellent photocatalytic performance. *Materials Chemistry and Physics, 199*, 193-202.

Wang, L.-w., Xu, Z., Zhang, F.-j., Zhao, S.-l., & Lu, L.-f. (2010). Structure, optical, and magnetic properties of Mn-doped ZnO films prepared by sputtering. *International Journal of Minerals, Metallurgy, and Materials, 17*(4), 475-480.

Wang, Q., & Yang, Z. (2016). Industrial water pollution, water environment treatment, and health risks in China. *Environmental pollution, 218*, 358-365.

Waste, H. (2010). World Water Quality Facts and Statistics.

Wiśniewski, M., Bieniek, A., Bolibok, P., Koter, S., Bryk, P., Kowalczyk, P., & Terzyk, A. P. (2019). Mechanistic aspects of water adsorption-desorption in porphyrin containing MOFs. *Microporous and Mesoporous Materials, 290*, 109649.

Wu, C., Shen, L., Yu, H., Huang, Q., & Zhang, Y. C. (2011). Synthesis of Sn-doped ZnO nanorods and their photocatalytic properties. *Materials Research Bulletin, 46*(7), 1107-1112.

Wu, Y., Xing, M., Tian, B., Zhang, J., & Chen, F. (2010). Preparation of nitrogen and fluorine co-doped mesoporous TiO2 microsphere and photodegradation of acid orange 7 under visible light. *Chemical Engineering Journal, 162*(2), 710-717. doi:10.1016/j.cej.2010.06.030

Xiao, Q., & Ouyang, L. (2009). Photocatalytic photodegradation of xanthate over Zn1−xMnxO under visible light irradiation. *Journal of Alloys and Compounds, 479*(1-2), L4-L7.

Xie, J., Deng, H., Xu, Z., Li, Y., & Huang, J. (2006). Growth of ZnO photonic crystals by self-assembly. *Journal of Crystal Growth, 292*(2), 227-229.

Yadav, L. R., Raghavendra, M., Manjunath, K., & Nagaraju, G. (2018). Photocatalytic, biodiesel, electrochemical sensing properties and formylation reactions of ZnO nanoparticles synthesized via eco-friendly green synthesis method. *Journal of Materials Science: Materials in Electronics, 29*(10), 8747-8759.

Yang, Y., Li, X.-j., Chen, J.-t., & Wang, L.-y. (2004). Effect of doping mode on the photocatalytic activities of Mo/TiO2. *Journal of Photochemistry and Photobiology A: Chemistry, 163*(3), 517-522.

Yin, Z., Chen, N., Yang, F., Song, S., Chai, C., Zhong, J., . . . Ibrahim, K. (2005). Structural, magnetic properties and photoemission study of Ni-doped ZnO. *Solid state communications, 135*(7), 430-433.

Yousefi, A., Allahverdi, A., & Hejazi, P. (2013). Effective dispersion of nano-TiO2 powder for enhancement of photocatalytic properties in cement mixes. *Construction and Building Materials, 41*, 224-230. doi:10.1016/j.conbuildmat.2012.11.057

Yu, C., Yang, K., Shu, Q., Yu, J. C., Cao, F., Li, X., & Zhou, X. (2012). Preparation, characterization and photocatalytic performance of Mo-doped ZnO photocatalysts. *Science china chemistry, 55*(9), 1802-1810.

Yu, W., Yang, L., Teng, X., Zhang, J., Zhang, Z., Zhang, L., & Fu, G. (2008). Influence of structure characteristics on room temperature ferromagnetism of Ni-doped ZnO thin films. *Journal of Applied Physics, 103*(9), 093901.

Zelekew, O. A., Aragaw, S. G., Sabir, F. K., Andoshe, D. M., Duma, A. D., Kuo, D.-H., . . . Feyisa, G. B. (2021). Green synthesis of Co-doped ZnO via the accumulation of cobalt ion onto Eichhornia crassipes plant tissue and the photocatalytic degradation efficiency under visible light. *Materials Research Express, 8*(2), 025010.

Zhang, F., Chao, D., Cui, H., Zhang, W., & Zhang, W. (2015). Electronic structure and magnetism of Mn-Doped ZnO nanowires. *Nanomaterials, 5*(2), 885-894.

Zhang, L., Ding, Y., Povey, M., & York, D. (2008). ZnO nanofluids–A potential antibacterial agent. *Progress in Natural Science, 18*(8), 939-944.

Zhang, Z., Meng, G., Wu, Q., Hu, Z., Chen, J., Xu, Q., & Zhou, F. (2014). Enhanced cold field emission of large-area arrays of vertically aligned ZnO-nanotapers via sharpening: experiment and theory. *Scientific reports, 4*(1), 1-7.

Zhao, J., Wang, L., Yan, X., Yang, Y., Lei, Y., Zhou, J., . . . Zhang, Y. (2011). Structure and photocatalytic activity of Ni-doped ZnO nanorods. *Materials Research Bulletin, 46*(8), 1207-1210.

Zheng, Y., Fu, L., Han, F., Wang, A., Cai, W., Yu, J., . . . Peng, F. (2015). Green biosynthesis and characterization of zinc oxide nanoparticles using Corymbia citriodora leaf extract and their photocatalytic activity. *Green Chemistry Letters and Reviews, 8*(2), 59-63.

Zhou, L., Wang, W., Xu, H., Sun, S., & Shang, M. (2009). Bi2O3 hierarchical nanostructures: controllable synthesis, growth mechanism, and their application in photocatalysis. *Chemistry–A European Journal, 15*(7), 1776-1782.

Research Fund Acknowledgement

This research thesis was funded by Adama Science and Technology University under the grant number of ASTU/SM-R/434/22, Adama, Ethiopia.